UNIVERSITY OF TWENTE.

Faculty of Engineering Technology.

Water Engineering Group.

Improving Suspended Sediment Transport Models for Breaking Wave Conditions

Minfei He

M.Sc Thesis

August.2017

Supervisors:

Dr. ir. J. Ribberink

Dr. ir. J. Van der Werf

Dr. ir. J. Van der Zanden

Preface

First of all, I would like to express my sincere gratitude to my supervisor Dr. ir. Jan, Ribberink in University of Twente for the continuous support for my research. The inspiring and insightful discussions with him contributed a lot to my work in the field of sediment transport modelling. His strict requirements also have motivated me all the time.

I also want to express my deepest thanks to Dr. ir. Jebbe, Van der Werf in Deltares and Dr. ir. Joep, Van der Zanden in University of Twente. The excellent routine guidance and inspiring discussions from Joep have brought me many ideas. The valuable suggestions and comments from Jebbe have widened my horizon and made me work on the model more efficiently.

Furthermore, I would like to thank several other staff in Deltares, who kindly helped and inspired me in terms of compiling the source code of Delft3D: Kees Nederhoff, Adri Mourits and Qinghua Ye.

Finally, I would like to thank my parents for the unconditional support and thank my friends for the company during my studies at University of Twente

Abstract

In coastal regions, the prediction of erosion or accretion of beaches is a critical issue to society. However, current models like Delft3D do not predict suspended sediment transport under breaking wave conditions very well. Generally, the current-related suspended sediment transport is largely influenced by the sediment mixing coefficient and reference concentration. In this project, the reference concentration model in Delft3D was improved on the basis of measurements in SINBAD wave flume experiment. Potential reference concentration models were firstly stand-alone tested with Matlab. Then, Hsu and Liu(2004)'s adaption for the default model in Delft3D and Van der Zanden, et al.(2017)'s reference concentration model were selected to be implemented into Delft3D environment.

In order to ensure an accurate hydrodynamic input for the implemented models, the Delft3D hydrodynamic model of SINBAD wave flume experiment was investigated and re-calibrated on the basis of a sensitivity analysis. According to the hydrodynamic re-calibration, the wave height prediction, undertow prediction and turbulent kinetic energy cannot be well-modelled at the same time. Considering the turbulent kinetic energy cannot be directly calibrated well, the wave height and undertow predictions were prior to be calibrated. Later on, an additional adaption in Delft3D source code, which increases the turbulence injection depth and decreases the near-surface turbulence production, was implemented for improving near-bed turbulent kinetic energy prediction under regular wave conditions. Moreover, the modelled breaking point was shifted shoreward by 2 m in order to improve the mismatch between the maximum predicted near bed turbulent kinetic energy and the measurement, which sacrifices the well-predicted wave height.

After the hydrodynamic validation of Delft3D model under the regular wave condition, Hsu & Liu(2004)'s adaption and Van der Zanden, et al.(2017)'s model were tested against SINBAD measurements. Both models improve the reference concentration prediction to a certain extent in the breaking region. In terms of offshore-directed suspended sediment transport, these implemented models give better predictions at the breaker bar, while they underestimates the offshore-directed suspended load transport at the bar trough.

In order to test these implemented models under irregular wave conditions, LIP 1B case was selected for the test as it is more similar to SINBAD wave flume experiment due to strong waves and undertow. Both implemented models generally improve, but overestimate the reference concentration in the breaking region. Under this circumstance, the offshore-directed suspended sediment transport is overestimated as well. Furthermore, due to the overestimated near-bed undertow and suspended sediment concentration at a secondary breaker bar, the suspended sediment transport is significantly overestimated.

Key words: Reference concentration, Hydrodynamic validation, Suspended sediment transport

Table of Contents

Chapter 1 Introduction

In this chapter, an introduction of the thesis is given, which includes research background, problem statement, research questions, research approach and outline of the project.

1.1. Research background

Coastal regions are often densely populated and offer various services to society(Van der Zanden, 2017b). The dynamics of coastal area is a very important issue to many industries and public services, including harbors, drinking water supply, tourism, aquaculture and ecology(Giardino, et al., 2011). In order to understand these dynamics, morphological models are used to predict the evolution of coastal area to contribute to the protection strategy. However, sediment transport under breaking wave conditions is not very well understood and modelled.

To improve the performance of this prediction, high resolution sediment transport process measurements during experiments in the large-scale CIEM wave flume at the Universitat Politecnica de Catalunya, Barcelona was done by Van der Zanden et al. in 2014. The detailed physical mechanisms of sediment transport and morphodynamics in the wave breaking region were carefully investigated and measured.

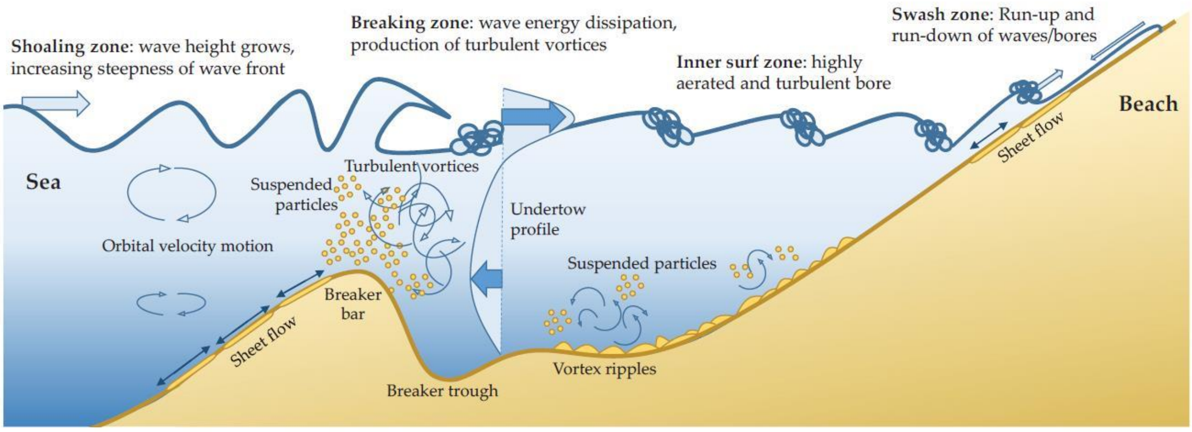

Figure 1 Conceptual drawing of cross-shore sediment transport processes in the near shore region, adopted from Van der Zanden(2016)

From Figure 1, with waves approaching to the shore, the wave height increases while the wave celerity decreases in shoaling zone. During the shoaling process, non-linear effect would become increasingly important as energy transfers from the primary wave components to their higher harmonics(Phillips and Miles, 1960). The non-linear effect results in skewed waves, which are with high short-duration crests and long-duration flat troughs. Eventually, the increasing wave asymmetry leads to the wave breaking. Four breaking types, plunging, spilling, surging and collapsing, are defined, according to wave and bed profile characteristics(Battjes, 1974).

When waves break, turbulence is generated by a moving fluid's internal shear stress. Additionally, the bed friction is a source of generating turbulence(Feddersen and Williams, 2007). The turbulence is commonly described as turbulent kinetic energy (TKE). The turbulent kinetic energy is not fully locally determined, because in horizontal and vertical direction, advection and diffusion of turbulence exists(Ting and Kirby, 1995). Turbulent kinetic energy can stir up sediments from sea bed into suspension, and thus has a critical influence on sediment transport under breaking waves, which suggests turbulence and sediment concentration near bed shows a self-similar process(Yoon and Cox, 2012).

With waves continue approaching the shore, outer-flow net currents are generated, which are generally offshore-directed in the lower half of the water column as they compensate for the onshore mass flux (Stokes drift) that occurs especially above wave trough level(Van der Zanden, 2017b). This time-averaged return current is termed undertow, which would contribute to offshore-directed sediment transport, especially for the current related suspended sediment transport.

In this experiment, Van der Zanden(2016) particularly focused on the TKE in the complete water column induced by breaking waves. From the experiment, time-averaged reference concentrations correlate poorly with periodic and time-averaged near bed velocities, but correlate significantly with near-bed time-averaged turbulence kinetic energy(Van der Zanden, 2017b). It indicates that the effects of breaking-generated turbulence an important driver for the sediment pick-up. The current-related suspended sediment transport is offshore-directed at outer-flow elevations due to undertow. The wave related suspended transport is onshore-directed and is generally confined to the wave bottom boundary layer(Van der Zanden, 2017b). Suspended particles travel back and forth between the breaking and shoaling zones following the orbital motion, leading to local intra-wave concentration changes. In this project, only the current-related suspended sediment transport was looked into and the wave-related suspended sediment transport is out of the scope of this research.

1.2. Problem statement

In this research project, the process-based engineering morphological model Delft3D was used, comprising hydrodynamics, sediment transport and bed level evolution in three dimensions(J. Van der Werf, 2013). Schnitzler(2015) built a 2DV Delft3D model against SINBAD wave flume experiment. According to his modelling, hydrodynamics and bedload sediment transport were predicted fairly well, while the suspended sediment transport needs further improvements. As discussed above, the suspended sediment transport is closely related to undertow and suspended sediment concentration in the water column.

In order to successfully describe the equilibrium vertical distribution of suspended sediment concentration and amount of suspended sediment transport, the near-bed reference concentration at reference level is defined as a boundary condition(Drake and Cacchione, 1989). Sediment transport is defined as bed-load transport beneath the reference level and suspended load transport above the reference level.

In default Delft3D model, the reference concentration is mainly controlled by the combined effect of wave orbital velocity and current velocity, which is seen to perform well for non-breaking waves(Van Rijn 2007b). However, in the wave breaking region, the measured near-bed suspended sediment concentration is sensitive to breaking induced turbulent kinetic energy(Van der Zanden, 2017b), which is not well modelled in Delft3D.

Therefore, compared to latest measurements of SINBAD wave flume experiment, the modelled suspended sediment transport can be further improved on the basis of a better prediction of reference concentration in the wave breaking region.

1.3. Research questions

RQ 1) With input of SINBAD measurements, how well do existing models predict reference concentrations in the wave breaking region.

With input of high resolution measurements in SINBAD wave flume experiment, errors induced by poor hydrodynamic input can be excluded. Therefore, it is essential to find out how well the existing models predict reference concentrations in the wave breaking region.

RQ 2) How well are the hydrodynamics of regular plunging breaking waves simulated by Delft3D and how could it be improved?

In order to ensure the well-predicted hydrodynamic input for the implemented models in Delft3D environment, the hydrodynamics of regular plunging breaking waves simulated by Delft3D was investigated. It is critical to understand how well the hydrodynamics of regular plunging breaking waves simulated by Delft3D are and how it could be improved.

RQ 3) To what extent do the implemented reference concentration models into Delft3D contribute to better simulations of suspended sediment concentrations and transport in the surf zone?

After the implementation of selected reference concentration models into Delft3D, the suspended sediment concentration and transport in the surf zone should be improved. However, it is important to understand that to what extent the implemented models contribute to a better prediction and how it could be further improved.

1.4. Research approach

Firstly, eight existing reference concentration models were stand-alone tested with Matlab and compared in order to find applicable models that give better predictions. Most of the input for the stand-alone tested models is taken from measurements in SINBAD wave flume experiment. Only part of the input is generated from Delft3D hydrodynamic model.

Secondly, the Delft3D hydrodynamic model was investigated and improved in order to ensure an accurate input for implemented reference concentration models. The improvements of Delft3D hydrodynamic model include re-calibration of user input parameters and re-formulation of near-surface turbulent kinetic energy production. Noticeably, the adjustments in Delft3D hydrodynamic model can only be applied under regular wave conditions.

Last but not least, selected models were implemented into Delft3D environment and tested against measurements of SINBAD and LIP 1B wave flume experiments. In SINBAD wave flume experiment, regular plunging breaking waves were generated, while irregular spilling breaking waves were generated in LIP 1B wave flume experiment. Under this circumstance, it is clear whether these implemented reference concentration models perform well in various conditions.

1.5. Outline

In this thesis, the first chapter is an introduction of the project, containing a brief research background, problem statement, research questions, research approach and the thesis outline. The second chapter documents the general methodology used in this project, which contains descriptions of SINBAD wave flume experiment, and Delft3D hydrodynamic and morphodynamic models. The third chapter is about stand-alone tested reference concentration models, including different assumptions and formulas in these models and their modelled results. The fourth chapter is the hydrodynamic validation of Delft3D model under regular wave conditions, where the wave height, undertow and turbulent kinetic energy predictions are investigated and validated. The fifth chapter is the implementation and validation of selected reference concentration models within Delft3D, which contains tests against measurements of SINBAD and LIP 1B wave flume experiments. Discussions are in the sixth chapter and the last chapter is about conclusions and recommendations.

Chapter 2 Methodology

In this chapter, descriptions of the SINBAD wave flume experiment and Delft3D hydrodynamic and morphodynamic models are given.

2.1. Description of SINBAD experiment

The SINBAD experimental set-up and bed profile are shown in Figure 2. The experiment was conducted in the 100m long, 3m wide and 4.5m deep CIEM wave flume in Barcelona, done by Van der Zanden et al. in 2014.

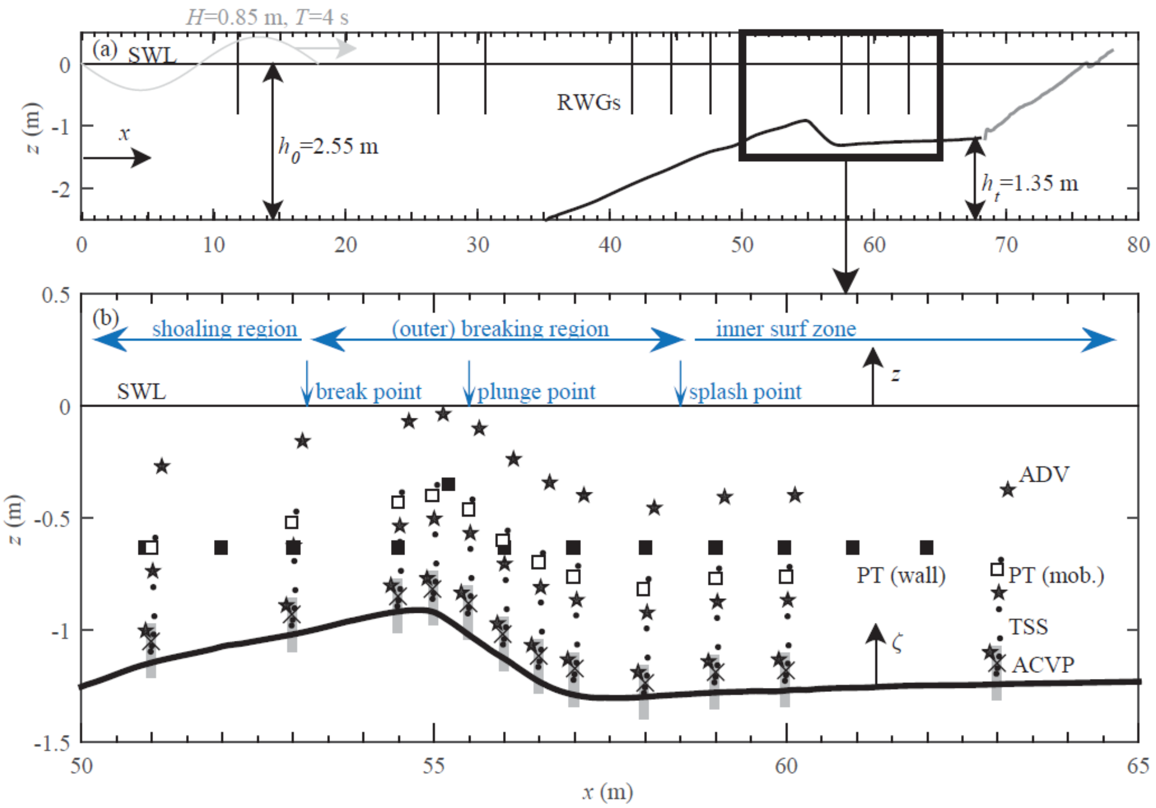

Figure 2 SINBAD experimental set-up and locations of the measurement. a). Initial bed profile [black line] and fixed beach [grey line], and locations of resistive wave gauges [RWGs, vertical black lines];b). Measurement positions of ADVs [star symbols], mobile-frame Pressure Transducers [PT, white squares], well-deployed PTs [black squares], Transverse Suction System nozzles [TSS, black dots], Optical Backscatter Sensor [black crosses], and measuring range of mobile-frame ACVP [grey boxes], taken from Van der Zanden(2016).

The bed consisted of an 1:10 offshore slope, and a breaker bar through configuration. The bar was composed of well sorted medium sand with median sand diameter D_{50}=0.24 mm. Regular waves were generated with the wave period T=4.0 s and the wave height H=0.85 m at the wave paddle. The breaking wave were of the plunging breaking type(Van der Zanden, 2016).

The outer flow velocities were measured by Acoustic Doppler Velocimeters (ADVs) with an acoustic frequency of 10 MHz, which measured three velocity-components (cross-shore, lateral and vertical velocity) at a rate of 100 Hz. Near bed data were measured using a downward-looking high-resolution Acoustic Concentration and Velocity Profiler (ACVP), which operated at an acoustic frequency of 1 MHz. Those ACVPs measured the simultaneous horizontal and vertical velocities and sediment mass concentration. Water surface elevation were measured at 40 Hz using resistive wave gauges (RWGs) and pressure transducers (PTs) along the flume, where linear wave theory was used to convert the dynamic pressure measurements into water surface elevations(Van der Zanden, 2016). Noticeably, this conversion could be applied up to a frequency of 0.33 Hz, which in the SINBAD wave flume experiment includes the primary wave frequency (0.25 Hz) but not the higher harmonics(Van der Zanden, 2016). Therefore, the actual wave height is underestimated by approximately 10%. Bed profile measurements were obtained along two transects, using echo sounders deployed from a second mobile carriage, at a horizontal resolution of 2 cm and with an estimated bed measurement accuracy of +/- 1 cm(Van der Zanden, 2016). Time-averaged sediment concentrations were obtaine9d with a six-nozzle Transverse Suction System (TSS), consisting of six stainless-steel nozzles, each connected through plastic tubing to a peristaltic pump on top of the wave flume(Van der Zanden, 2017b).

The experiment was run for 90 minutes of waves, comprising of six 15 minutes runs, during which the bed further evolved. The bed profile was measured at the start of each experiment and after every second run, i.e., at 0, 30, 60, and 90 minutes(Van der Zanden, 2017b). Therefore, at 12 cross-shore measurement locations, measurements in 6 runs were gained.

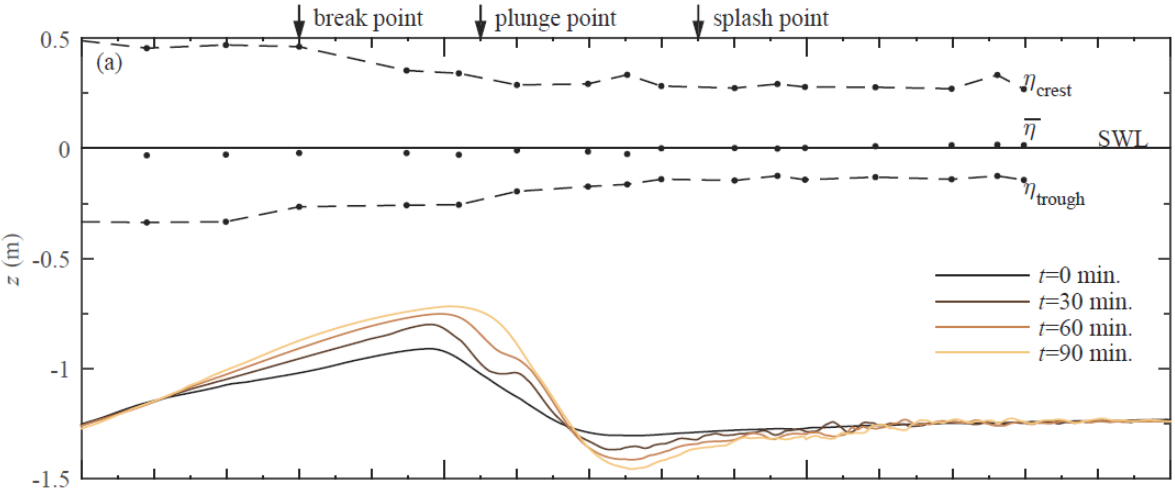

Figure 3 Bed profile evolution [Solid lines, with each line representing the mean value over all experimental days], and water levels for t=0-15 mins [dots and dashed line], taken for Van der Zanden(2017b).

In Figure 3, the bar crest grows and migrates slightly onshore during 90 min, leading to increases in the bar's offshore and onshore slope. Meanwhile, the bar trough deepens, resulting in a steepening of the shoreward-facing slope(Van der Zanden, 2017b). Noticeably, from 30 min to 60 min, a quasi-2D bed form (Quasi-uniform in long shore direction) was identified(Van der Zanden, 2017b), which would lead to more near bed turbulence produced by bed friction.

Besides, according to Van der Zanden(2017b), the near-bed reference concentration is significantly correlated to breaking induced turbulent kinetic energy. Both the measured near bed suspended sediment concentration and turbulent kinetic energy increased along the shoaling region and reached their maximum value around the plunging point. Then they decreased along the inner surf zone.

The detailed measurements of SINBAD wave flume experiment in the wave breaking region were used for stand-alone tests of existing reference concentration models with Matlab.

2.2. Description of hydrodynamic and morphodynamic models in Delft3D

Delft3D is a process based morphodynamic modelling system comprising coupled, wave-averaged equations of hydrodynamic (waves and mean currents), sediment transport and bed level evolution in three dimensions(Lesser, et al., 2004). In the system, Delft3D-Wave and Delft3D-Flow work together. In Flow Module, which is based on shallow water assumption, the water level, flow velocity, sand concentrations, net sand transport rate and bed level changes are calculated(Lesser *et al.*, 2004; Van der Werf, 2013). Only flow module was used for modelling within this project.

2.2.1. Wave model in Delft3D

In Delft3D, the short wave energy is defined as

$$E_w = \frac{1}{8}\rho_w g H_{rms}^2 \qquad (2\text{-}1)$$

With water density ρ_w, gravitational acceleration g and significant wave height H_{rms}. The short wave energy is computed in Delft3D using the so-called roller model which shows the energy balance between short wave energy and roller energy. In Delft3D, the wave energy balance depends on energy change over two horizontal direction, while it only applies in cross-shore direction within a stationary roller model in the case of SINBAD wave flume experiment, which can be simplified to,

$$\frac{\partial(E_w c_g)}{\partial x} = -D_f - D_w \tag{2-2}$$

$$\frac{\partial(2E_r c)}{\partial x} = D_w - D_r \tag{2-3}$$

Equation (2-2) expresses the short wave energy E_w dissipates due to bottom friction D_f and wave breaking D_w. The latter equation shows the short wave energy is transformed into roller energy E_r due to roller energy dissipation term D_r.

The roller energy is defined as a body of water that moves with the wave in front of the wave crest. The roller transports mass, momentum and energy, contributing to undertow and wave set-up (J.Van der Werf, 2013).

$$E_r = \frac{1}{2}\rho V_r c^2 \tag{2-4}$$

Where V_r is roller volume, c is roller velocity and c_g is the wave group velocity.

As Delft3D was developed for irregular wave conditions, default wave model the wave energy dissipation is given by a parameterization model as below(Baldock *et al.*, 1998).

$$D_w = \frac{1}{4}\alpha_{rol}\rho_w g f_p exp\left(-\frac{H_{max}^2}{H_{rms}^2}\right)(H_{max}^2 + H_{rms}^2) \tag{2-5}$$

With a manually defined roller dissipation coefficient α_{rol}, peak wave angular frequency f_p and the maximum wave height H_{max}.

Regarding the dissipation term due to the bottom friction, it is defined by,

$$D_f = f_w \frac{\rho_w}{\sqrt{\pi}} u_{orb}^3 \tag{2-6}$$

Where f_w is a manually defined bottom friction parameter and u_{orb} is the wave orbital velocity.

The roller energy dissipation is given by,

$$D_r = 2\beta_{rol} g \frac{E_r}{c_p} \tag{2-7}$$

The parameter β_{rol} is manually defined, which is important for determining the undertow prediction(Schnitzler, 2015).

Additionally, a breaker delay concept was proposed by Walstra *et al.*(2012), which account for the fact that short waves require some time to react the local change in the bathmetry. The weighting function is given by,

$$W(x') = \left(\lambda\frac{2\pi}{k_x} - x'\right) \tag{2-8}$$

With local cross-shore coordinate *x'*, breaker delay parameter λ and the wave number in cross-shore direction k_x.

$$H = \frac{\int_{x-\lambda\frac{2\pi}{k_x}}^{x} W(x-x\prime)h(x)dx}{\int_{x-\lambda\frac{2\pi}{k_x}}^{x} W(x-x\prime)dx} \tag{2-9}$$

Where H is water depth, influenced by the linear weighting function $\mathrm{W(x')}$ in the seaward direction.

2.2.2. Flow model in Delft3D

In order to compensate for wave-induced onshore mass flux near the right closed boundary of SINBAD wave flume, an offshore-directed current is generated in the lower parts of the water column. As waves only propagate in the cross-shore direction in SINBAD wave flume experiment, the lateral terms have been removed in Delft3D flow model.

$$\int_{-d}^{\bar{\zeta}} \rho_w u dz = \frac{E_w}{f\omega} k_x \tag{2-10}$$

With short wave energy E_w derived from Equation (2-1). f_ω is wave angular frequency. $\bar{\zeta}$ is mean water surface level, *d* is water depth and z denotes the vertical coordinate. The model generates the undertow profile u from the bed to the water surface.

The boundary condition for the flow model in the case of SINBAD wave flume experiment is discussed below.

For the vertical boundary conditions on the bottom and at the water surface, they are defined as,

$$\omega|_{\sigma=0\ and -1} = 0 \tag{2-11}$$

ω is the vertical flow velocity. It means no flow went through the boundaries.

For the bed or free surface boundary condition, it is defined as,

$$\frac{\nu_V}{H}|_{\sigma=-1\ or\ 0} = \frac{1}{\rho_w}\tau_{bs} \tag{2-12}$$

ν_V is the vertical eddy viscosity, H is total water depth $(\bar{\zeta} + d)$ and τ_{bs} is shear stress derived from Chèzy coefficient on the bottom or wind stress at the water surface.

When shear stress is zero, it is a free slip boundary condition, while it is a partial slip boundary condition with non-zero shear stress. As no wind was in SINBAD wave flume experiment, it is a free slip boundary condition at the water surface.

For the boundary condition at the right end of the flume, it is defined as,

$$u = 0 \tag{2-13}$$

It means no flow went through the right boundary of the flume.

2.2.3. Turbulence model in Delft3D

In model of SINBAD wave flume experiment, ***k-ε*** turbulence model was applied, in which ***k*** is turbulent kinetic energy and ***ε*** is turbulent kinetic energy dissipation. Similarly, the alongshore-direction was neglected in this model.

The transport equations for ***k*** and ***ε*** are non-linearly coupled by means of their eddy diffusivity D_k, D_ε and the dissipation terms(Deltares, 2014). As stationary turbulence model was used, time derivative terms have been removed in Equation (2-14) and (2-15).

The transport equations are given by,

$$u\frac{\partial k}{\partial x} + \frac{\omega}{d+\delta}\frac{\partial k}{\partial \delta} = \frac{1}{(d+\delta)^2}\frac{\partial}{\partial \sigma}\left(D_k\frac{\partial k}{\partial \sigma}\right) + P_k + P_{k\omega} + B_k - \varepsilon \tag{2-14}$$

$$u\frac{\partial \varepsilon}{\partial \delta} + \frac{\omega}{d+\delta}\frac{\partial \varepsilon}{\partial \sigma} = \frac{1}{(d+\delta)^2}\frac{\partial}{\partial \sigma}\left(D_\varepsilon\frac{\partial \varepsilon}{\partial \sigma}\right) + P_\varepsilon + P_{\varepsilon\omega} + B_\varepsilon - c_{2\varepsilon}\frac{\varepsilon^2}{k} \tag{2-15}$$

With

$$D_k = \frac{v_{mol}}{\sigma_{mol}} + \frac{v_{3D}}{\sigma_k} \text{ and } D_\varepsilon = \frac{v_{3D}}{\sigma_\varepsilon} \tag{2-16}$$

u and *ω* are flow velocities in cross-shore direction and in vertical-direction (δ-direction). δ denotes the vertical coordinate in this model and *d* is the water depth below horizontal plane. From Equation (2-14) and (2-15) in the ***k-ε*** turbulence closure model, the advection terms of turbulence, which are on the left side of equations, are only controlled by the velocities in two dimensions. The turbulent kinetic energy and the energy dissipation only diffuse vertically.

The production term of turbulence P_k is defined by Walstra, et al.(2001), the production of turbulence kinetic energy at the water surface is related to the wave energy dissipation of in the wave model.

$$P_k = \frac{4D_W}{H_{rms}}\left(1 - \frac{2z'}{H_{rms}}\right) \qquad for\ z' \le \frac{1}{2}H_{rms} \tag{2-17}$$

Where *z'* is the depth to water surface. It is assumed that the production term of turbulent kinetic energy linearly distributed over the thickness of half significant wave height to mean water surface(Walstra, et al., 2001). On the other hand, the turbulent kinetic energy generated by bed friction is given by,

$$P_k = \frac{4D_f}{\delta_w}\left(1 - \frac{z' - h}{\delta_w}\right) \qquad for\ h \le z' \le (h - \delta_w) \tag{2-18}$$

With thickness of wave boundary layer δ_w, vertical coordinate *z'* with its origin at mean water surface level and positive downwards(Walstra, et al., 2001).

The buoyancy flux B_k is defined by:

$$B_k = \frac{\nu_V}{\rho_w \sigma_\rho} \frac{g}{H} \frac{\partial \rho_w}{\partial \sigma} \tag{2-19}$$

With the Prandtl-Schmidt number $\sigma_\rho = 0.7$ for salinity and temperature and $\sigma_\rho = 1.0$ for suspended sediments.

The production term of energy dissipation P_ε and buoyancy flux B_ε are given by:

$$P_\varepsilon = c_{1\varepsilon} \frac{\varepsilon}{k} P_k \tag{2-20}$$

$$B_\varepsilon = c_{1\varepsilon} \frac{\varepsilon}{k} (1 - c_{3\varepsilon}) B_k \tag{2-21}$$

The calibration constants were defined by *Rodi, et al.(1984)*. $c_{1\varepsilon} = 1.44$, $c_{2\varepsilon} = 1.92$ and $c_{3\varepsilon} = 0$ in unstable stratification conditions and $c_{3\varepsilon} = 1$ in stable stratification conditions.

In ***k-ε*** turbulence closure model, the boundary conditios for the turbulent kinetic energy ***k*** follow Dirichlet boundary condition, as below,

$$k|_{\sigma=-1} = \frac{u_{*b}^2}{c_\mu} \tag{2-22}$$

With the bed shear velocity u_{*b}, and a calibration constant $c_\mu$which is 0.1112 in the Delft3D default model. In absence of wind in SINBAD wave flume experiment, the turbulent kinetic energy at the water surface was set to 0.

At the bottom, the turbulent kinetic energy is computed on the basis of bed shear stress. Noticeably, this turbulent kinetic energy at the bottom has no horizontal advection.

$$k(z) = \frac{u_{*b}^2}{\sqrt{c_\mu}}\left(1 - \frac{z + d}{H}\right) \tag{2-23}$$

Where z denotes the vertical coordinate.

For energy dissipation ***ε***, the bed boundary condition is prescribed by,

$$\varepsilon|_{\sigma=-1} = \frac{u_{*b}^3}{\kappa z_0} \tag{2-24}$$

With the bed roughness length z_0 and von Karman constant κ. Similarly, in case of no wind, the energy dissipation ***ε*** was set to zero at the free surface.

At open boundaries at the bed and at the free surface, the dissipation is computed by Equation (2-25), without horizontal advection.

$$\varepsilon(z) = \frac{u_{*b}^3}{\kappa(z + d)} \tag{2-25}$$

2.2.4. Current-related suspended sediment transport model in Delft3D

Suspended sediment concentrations in Delft3D are calculated with three-dimensional advection diffusion equation. Similarly, it is only applied in the cross-shore and vertical directions within a stationary morphodynamic model in the case of SINBAD wave flume experiment.

$$\frac{\partial uc}{\partial x} + (w_l - w_s)\frac{\partial c}{\partial z} - \frac{\partial}{\partial x}\left(\epsilon_{s,x}\frac{\partial c}{\partial x}\right) - \frac{\partial}{\partial z}\left(\epsilon_{s,z}\frac{\partial c}{\partial z}\right) = 0 \tag{2-26}$$

In Equation (2-26), the last two terms are the diffusion in two applied directions, where $\epsilon_{s,x}$ and $\epsilon_{s,z}$ are the sediment diffusivities in each direction. Note that for the advection term of z direction, the difference between lifting velocity w_l and settling velocity w_s is taken into account. It indicates the suspended sediment concentration can advect and diffuse in both cross-shore and vertical directions.

Current-related suspended sediment is transported by the mean current including the effect of wave stirring on the sediment load(Van Rijn, 2007b). The current-related suspended sediment is calculated by,

$$q_{sc} = \int_a^h ucdz \tag{2-27}$$

Where u is the velocity vector and c is the suspended sediment concentration profile in the water column from reference level a to the water surface.

The reference concentration model and the reference level are discussed in next chapter. The wave-related suspended sediment transport is not discussed here as it is out of the scope of this project.

For the current-related suspended sediment transport model, the water level boundary condition is,

$$-w_s c - \varepsilon_{s,z}\frac{\partial c}{\partial z} = 0 \qquad at\ z = \zeta \tag{2-28}$$

Where $\varepsilon_{s,z}$ is the sediment vertical mixing coefficient at the water surface.

The bed boundary condition is prescribed by,

$$-w_s c - \varepsilon_{s,z}\frac{\partial c}{\partial z} = D - E \qquad at\ z = z_b \tag{2-29}$$

With sediment deposition rate D of sediment fraction and sediment erosion rate E of sediment fraction.

At the right end of the flume, no sediment flux went through the closed boundary. At the open boundary of left side, an ‘equilibrium’ concentration profile is simulated, leading to a zero concentration gradient at the open boundary.

Chapter 3 Validation of existing reference concentration models with Matlab

In order to improve the reference concentration predicted by Delft3D, eight parameterization models or process-based models were stand-alone tested with Matlab for investigating the feasibility of implementation into Delft3D environment. Note that part of inputs for these reference concentration models are the modelled terms in Delft3D instead of measurements in SINBAD wave flume experiment.

3.1. Introduction of stand-alone tested reference concentration models

The reference concentration is a conceptual boundary condition to compute suspended sediment concentration profile. Generally assumptions of the stand-alone tests are listed below.

• The measurement input of free-stream velocity, wave orbital velocity and turbulent kinetic energy for stand-alone tested reference concentration models were taken at the level of 2 cm above the bottom, which is the approximate level of wave boundary layer. In wave boundary layer, bottom friction leads to strong rotational wave-frequency flows(Henderson and Allen, 2004) and near-bed stream. These effects in wave boundary layer should be excluded for accurate hydrodynamic inputs in these stand-alone tests. In this case, the wave boundary layer is simplified to 2 cm above the bed along the entire surf zone, neglecting effects of ripples' heights.

• The measured suspended sediment concentration is comparable only at the same level as the modelled reference concentration. In SINBAD wave flume experiment, due to the appearance of ripples, the reference level may vary at different cross-shore locations.

In the following stand-alone tested reference concentration models, generic variables used in all of them are listed below for reference.

Table 1 Generic variables used in all tested stand-along Matlab models

Regular Variables	Data Input
Sediment density ρ_s	2650 [kg/m^3]
Water density ρ_w	1000 [kg/m^3]
Relative density s	2.65 [-]
Eddy viscosity v	10^{-6} [m^2/s]
Gravitational acceleration g	9.8 [m/s^2]
Wave period T_w	4 [s]
Grain size d_{50} and d_{90}	local measurements [m]

In this chapter, formulas and assumptions in eight existing reference concentration are introduced and described in Section 3.2. Then, these modelled results are compared to measured reference concentrations in SINBAD wave flume experiment in Section 3.3 to find the applicable models for Delft3D implementation. At last, these stand-alone tests are summarized in Section 3.4.

3.2. Descriptions of stand-alone tested reference concentration models

In this section, formulas and assumptions in these eight existing reference concentration models are described below.

3.2.1. Van Rijn(2007b)'s reference concentration model (default model)

The Van Rijn(2007b)'s reference concentration model is widely used and is the default model in Delft3D. The reference concentration at a certain elevation a near the bed is based on free-stream near-bed current and wave orbital velocity.

In order to implement the Van Rijn(2007b)'s model in stand-alone Matlab, the following assumptions were made,

• In SINBAD wave flume experiment, as only ripples appeared in the inner surf zone, the bed roughness related to mega-ripples and dunes are not discussed here. Therefore, the bed roughness depends on effects of ripples and sediment grain size.

• According to Van Rijn(2007b), the wave-related bed roughness value $k_{s,w,r}$ is same as the current-related bed roughness value $k_{s,c,r}$.

In the model, the reference level depends on the current- and wave-related bed roughness value. Generally, the bed roughness value is computed on the basis of effects of ripples, with a minimum value of 1 cm.

$$a = min\left[0.2h, max\left(\frac{1}{2}k_{s,c,r}, 0.01\right)\right] \tag{3-1}$$

$$C_a = 0.015\frac{d_{50}}{a}\frac{T^{1.5}}{D_*^{0.3}} \tag{3-2}$$

The current-related bed roughness value is estimated from sediment median grain size d_{50}, which is the size in which 50% of the mixture is finer.

$$k_{s,c,r} = 150f_{cs}d_{50} \qquad for\ \Psi \leq 50 \tag{3-3}$$

$$k_{s,c,r} = 20f_{cs}d_{50} \qquad for\ \Psi \geq 250 \tag{3-4}$$

$$k_{s,c,r} = (182.5 - 0.652\Psi)f_{cs}d_{50} \qquad for\ 50 < \Psi < 250 \tag{3-5}$$

Where,

$$f_{cs} = \left(0.25d_{gravel}/d_{50}\right)^{1.5} \qquad for\ d_{50} > d_{gravel} = 0.002m \tag{3-6}$$

$$f_{cs} = 1 \qquad for\ d_{50} \leq d_{gravel} = 0.002m \tag{3-7}$$

In Van Rijn(2007b)'s reference concentration model, the dimensionless grain size D_* and the dimensionless mobility parameter Ψ are given by,

$$D_* = d_{50}\left[\frac{(s-1)g}{\nu^2}\right]^{1/3} \tag{3-8}$$

$$\psi = U_{wc}^2/[(s-1)gd_{50}] \tag{3-9}$$

Where U_{wc} is velocity parameter for combined wave-current conditions.

$$U_{wc} = \sqrt{U_w^2 + u_c^2} \tag{3-10}$$

The u_c is the time-averaged current velocity and wave orbital velocity is calculated from $U_w = \sqrt{2}u_{rms}$, where u_{rms} is the measured root-mean-square wave orbital velocity at the level of 2 cm above the bed.

The dimensionless bed-shear stress *T* is given by,

$$T = \frac{(\tau'_{b,cw} - \tau_{b,cr})}{\tau_{b,cr}} \tag{3-11}$$

Where $\tau'_{b,cw}$ is the current- and wave-related bed shear stress and $\tau_{b,cr}$ is critical bed shear stress.

$$\tau'_{b,cw} = \tau'_{b,c} + \tau'_{b,w} \tag{3-12}$$

With

$$\tau'_{b,c} = \mu_c\alpha_{cw}\tau_{bc} \tag{3-13}$$

$$\tau'_{b,w} = \mu_w\tau_{b,w} \tag{3-14}$$

μ_c is current-related efficiency factor.

$$\mu_c = \frac{f'_c}{f_c} \tag{3-15}$$

f'_c is the grain-related friction coefficient based on d_{90}, f_c is the current-related friction coefficient based on predicted bed roughness values(Van Rijn, 2007b).

$$f_c = \frac{0.24g}{\left(log_{10}\left(\frac{12h}{k_{scr}}\right)\right)^2} \tag{3-16}$$

$$f_c' = \frac{0.24g}{\left(log_{10}\left(\frac{12h}{3d_{90}}\right)\right)^2} \tag{3-17}$$

With water depth h and d_{90} that is the grain size in which 90% of the mixture is finer.

α_{cw} is a wave-current interaction factor according to *Van Rijn and Kroon(1992).*

$$\alpha_{cw} = \left[\frac{ln(90\delta_w/k_a)}{ln(90\delta_w/k_{scr})}\right]^2 \left[\frac{-1+ln(30h/k_{scr})}{-1+ln(30h/k_a)}\right]^2 \tag{3-18}$$

With maximum thickness of wave boundary layer δ_w and apparent roughness related to wave-current interaction k_a.

$$k_a = min(10k_{scr}, k_{scr}\, exp\left[\frac{\gamma U_W}{u_c}\right]) \tag{3-19}$$

Where $\gamma = 0.8 + \varphi - 0.3\varphi^2$. φ is angle between current and wave direction, which is 180^{o} in this model according to the strong undertow compensating for mass flux of waves(Van Rijn, 1984).

$$\delta_w = 0.072A_\delta(A_\delta/k_{scr}) \tag{3-20}$$

And A_δ is wave-induced water semi-excursion, which is given by,

$$A_\delta = T_w \cdot U_w/2\pi \tag{3-21}$$

T_w is the period of the wave.

Regarding of the effective wave-related bed shear stress with wave-related efficiency factor μ_w, it is given by,

$$\mu_w = \frac{0.7}{D_*} \tag{3-22}$$

In the condition that $\mu_{w,min} = 0.14$ for $D_* \geq 5$ and $\mu_{w,max} = 0.35$ for $D_* \leq 5$.

The wave- and current-related bed shear stress is calculated by,

$$\tau_{bw} = \frac{1}{4}\rho_w U_w^2 f_w \tag{3-23}$$

$$\tau_{bc} = \frac{1}{8}0.5\rho_w u_c^2 f_c \tag{3-24}$$

Where f_w wave-related friction factor is given by,

$$f_w = exp[-6 + 5.2(A_\delta/k_{scr})^{-0.19}] \tag{3-25}$$

The critical bed shear stress is calculated from the critical Shields parameter θ.

$$\theta_{cr} = 0.115D_*^{-0.5} \qquad for\ D_* < 4 \tag{3-26}$$

$$\theta_{cr} = 0.14D_*^{-0.64} \qquad for\ 4 < D_* < 10 \tag{3-27}$$

$$\tau_{cr} = \rho_w\theta_{cr}(s-1)gd_{50} \tag{3-28}$$

The measurement input for Van Rijn(2007b)'s reference concentration model is listed in Table 2.

Table 2 Data input for Van Rijn(2007b) reference concentration model(default)

Variables	Data Input
Water depth h	local measurements [m]
Root mean squared wave orbital velocity u_{rms}	local measurements at 2 cm above the bed. [m/s](ACVP)
Time-averaged current velocity u_c	local measurements at 2 cm above the bed. [m/s](ACVP)

3.2.2. Nielsen(1986)'s reference concentration model

Nielsen(1986)'s model relates the reference concentration to the Shields parameter. Shields parameter θ is a dimensionless number which is to express the initiation of motion of sediment.

$$a = 0\ m \tag{3-29}$$

$$C_a = 0.005\rho_s\theta^3 \tag{3-30}$$

The Shields parameter is given by,

$$\theta = \frac{\tau}{\rho_w(s-1)gd_{50}} \tag{3-31}$$

Where τ is the bed shear stress.

Using Jonsson(1966)'s definition of the wave friction factor, the bed shear stress is given by Nielsen(1986),

$$\tau = 0.5\rho_w f'(A_\delta f_\omega)^2 \tag{3-32}$$

With the expression of $U_w = A_\delta \mathrm{f}_\omega$, the bed shear stress is rewritten to,

$$\tau = 0.5\rho_w f' U_w^2 \tag{3-33}$$

In SINBAD wave flume experiment, the shear velocity is influenced by both the current and waves. Therefore, the wave orbital velocity was replaced by velocity parameter U_{wc} for the combined wave-current condition, derived from Equation (3-10).

Where A_δ is the wave-induced water semi-excursion just outside the boundary layer, *f'* is the friction factor and f_ω is the wave angular frequency $2\pi/T_w$.

The friction factor *f'* is calculated from,

$$f' = exp\left(5.213\left(\frac{r}{A_\delta}\right)^{0.194} - 5.977\right) \tag{3-34}$$

Due to the Swart(1974) and following Engelund & Hansen(1967), the hydraulic roughness r is given by Nielsen (1986),

$$r = 2.5d_{50} \tag{3-35}$$

According to measurements by Du Toit & Sleath(1981), ripples enhance the bed shear stress near the ripple crest(Nielsen, 1986). In the SINBAD wave flume experiment, ripples (height 0.05 m, length 0.4 m) appeared in the inner surf zone. Thus, the estimation of enhanced Shields parameter over a ripple bed is described by,

$$\theta_r = \frac{\theta}{(1-\pi\eta/\lambda)^2} \tag{3-36}$$

With the ripple height η and ripple length λ. Thus, the reference concentration is transformed to,

$$C_a = 0.005\rho_s\theta_r^3 \tag{3-37}$$

The measurement input for Nielsen(1986)'s reference concentration model is listed in Table 3.

Table 3 Data input for Nielsen (1986) reference concentration model

Variables	Data input
Root mean squared wave orbital velocity u_{rms}	local measurements at 2 cm above the bed. [m/s] (ACVP)
Time-averaged current velocity u_c	local measurements at 2 cm above the bed. [m/s] (ACVP)
Ripple height η	0.05 [m]
Ripple length λ	0.4 [m]

3.2.3. Mocke and Smith(1992)'s reference concentration model

Mocke and Smith(1992)'s reference concentration model is another empirical model, which is relevant to wave height H, water depth h and Shields parameter θ.

In this model, the reference level is at the outer boundary of viscous layer(Mocke and Smith, 1992), which is practically at the bottom.

$$a \approx 0 \tag{3-38}$$

With the eddy viscosity ν and the frequency of oscillation f_ω $(2\pi/T_w)$, the reference concentration is given by,

$$C_a = \rho_s K^{-0.92}(H/h)^{3.32}(H^3/hT)^{-0.92}\theta^{0.37} \tag{3-39}$$

In this case, $K = 1.51 \times 10^3 \quad sm^{-2}$, which is a proportionality constant related to energy dissipation term.

Shields parameter is given by,

$$\theta = \frac{\bar{u}^2}{(s-1)gd_{50}} \tag{3-40}$$

The bed shear velocity is rewritten to the mean velocity $\bar{u}$(Mocke and Smith, 1992), which is estimated from water depth h in shallow water conditions(Stive, 1980).

$$\bar{u} = 0.1c \tag{3-41}$$

$$c = \sqrt{gh} \tag{3-42}$$

The measurement input for Mocke and Smith(1992)'s reference concentration model is listed in Table 4.

Table 4 Data input for Mocke and Smith(1992)'s reference concentration model

Variables	Data Input
Wave height H	local measurements [m](PTs)
Water depth h	local measurements [m]

3.2.4. Okayasu(2009)'s adaption combined with default model

Okayasu(2009) developed an improved Shields parameter, taking turbulent kinetic energy into account. In current project, the adapted Shields parameter is implemented into Van Rijn(2007b)'s model in the way of implementing adapted effective bed shear stress into Equation (3-11) to calculate dimensionless bed shear stress *T*. Rewriting Equation (3-31) to,

$$\tau'_{b,cw} = \rho_w(s-1)g\theta d_{50} \tag{3-43}$$

The effective bed shear stress $\tau'_{b,cw}$ can be derived from this improved Shields parameter. Additionally, the reference level a is at the same level in Van Rijn(2007b)'s model.

$$\theta = \frac{F_D+F_I}{W-F_L} \tag{3-44}$$

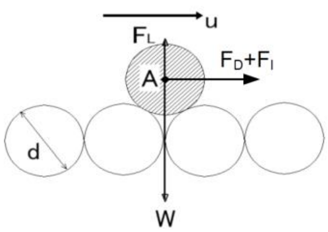

Figure 4 Forces for picking up or moving sediment, taken from Okayasu(2009)

Where F_D is the drag force, F_I the inertia force, W the gravitational force and F_L the lifting force acting on a sediment particle including effect of turbulence. In Figure 4, the initial motion of a sand particle is influenced by these forces.

$$F_D = \frac{1}{2} C_D \rho_s \frac{\pi d_{50}^2}{4} u_{bt}^2 \tag{3-45}$$

Where C_D is drag coefficient and given by,

$$C_D = \frac{24}{Re}(1 + 0.15Re^{0.687}) \quad for\ Re < 1000 \tag{3-46}$$

With the particle Reynolds number *Re*.

$$Re = \frac{d_{50} U_w}{\nu} \tag{3-47}$$

u_{bt} is the bottom shear velocity including the turbulence component.

$$u_{bt} = \frac{\kappa}{ln\left(\frac{30.1h}{d_{50}}\right)}(U_{wc} + 1.41u'_{rms}) \tag{3-48}$$

Where u'_{rms} the root-mean-square turbulence in SINBAD experimental measurements. The factor 1.41 is derived under the assumption of isotropic turbulence in the horizontal 2-D plane. U_{wc} is the combined wave- and current-related velocity and κ is von Karman constant 0.4(Okayasu, 2009).

$$F_I = C_I \rho_s \frac{\pi d_{50}^3}{6} \frac{du_b}{dt} \tag{3-49}$$

Where C_I is the inertia coefficient and was taken to be 1.5 for this case. The time derivatives of velocity is estimated from,

$$\frac{du_b}{dt} = u_b \frac{\varepsilon}{0.09 f_\mu K} \tag{3-50}$$

With the bottom shear velocity u_b, the energy dissipation rate of turbulence ε and the turbulence kinetic energy K. This method is obtained for the ***k-ε*** model at low Reynolds number(Jones and Launder, 1972).

$$\varepsilon = f_e K \tag{3-51}$$

$$f_\mu = exp\left(\frac{-2.5}{1 + K^2/50\nu\varepsilon}\right) \tag{3-52}$$

$$f_e = St \frac{U_{wc}}{d_s} \tag{3-53}$$

Where ν is eddy viscosity, f_e is the representative frequency of eddies, *St* is Strouhal number 0.2 and d_s is the representative length of turbulence generating objects, which is set as 0.1m in current study.

Furthermore, the gravitational force and lifting force are calculated by,

$$W = g(\rho_s - \rho_w) \frac{\pi d_{50}^3}{6} \tag{3-54}$$

$$F_L = \frac{1}{2} C_L \rho_s \frac{\pi d_{50}^2}{4} u_{bt}^2 \tag{3-55}$$

Where C_L is assumed to be 0.2 for the present study.

Note that the experiment conducted by Okayasu(2009) for developing this adaption is significantly different from SINBAD wave flume experiment. In Okayasu(2009)'s experiment, only flow is generated and turbulence is produced by irregular structures in the flow flume, while turbulence is produced by waves breaking in SINBAD wave flume experiment.

The measurement input for Okayasu(2009)'s reference concentration model is listed in Table 5.

Table 5 Data input for Okayasu(2009)'s reference concentration model

Variables	Data Input
Van Karman constant	0.4 [-]
Inertia coefficient C_I	1.5 [-]
Manual defined parameter C_μ	0.09 [-]
Strouhal number *St*	0.2 [-]
The representative length of turbulence generating objects	0.2 [m]
Lifting coefficient C_L	0.2 [-]
Water depth *h*	local measurements [m]
Root mean squared wave orbital velocity $\mathrm{u_{rms}}$	local measurements at 2 cm above the bed. [m/s] (ACVP)
Time-averaged current velocity u_c	local measurements at 2 cm above the bed. [m/s] (ACVP)
Root mean squared turbulence velocity $u_{rms}{}'$	local measurements at 2 cm above the bed. [m/s] (ACVP)
Time-averaged turbulence kinetic energy *TKE*	local measurements at 2 cm above the bed. [m^2/s^2] (ACVP)
Elevation above the bed ζ	local measurements [m]

3.2.5. Hsu and Liu(2004)'s adaptation combined with default model

According to Hsu and Liu(2004), the near-bed sediment pickup in the wave breaking region was adjusted in the way of taking effects of turbulence induced by waves breaking into account. In their research, the model was developed and calibrated on the basis of intra-wave measurements.

Therefore, the adapted Shields parameter proposed by Hsu and Liu(2004) was implemented into the default model as in Equation (3-43). As mentioned before, the Van Rijn(2007b)'s model was developed for the free-stream conditions, without accounting for effects of the turbulent kinetic energy. After implementing this adaptation, the reference concentration can increase due to near-bed turbulence.

Apparently, the reference level is the same as in Van Rijn(2007b)'s model.

The adapted Shields parameter and effective bed shear stress is given by,

$$\theta = \frac{\tau'_{b,cw} + \rho_s e_k TKE}{\rho_s (s-1) g d} \tag{3-56}$$

$$\tau'_{b,cwt} = \tau'_{b,c} + \tau'_{b,w} + \rho_w e_k k \tag{3-57}$$

With e_k being a numerical coefficient, it determines the sediment suspension efficiency(Hsu and Liu, 2004). In this test, it is set to 0.05, based on Hsu and Liu(2004)'s calibration against intra-wave measurements.

Therefore, the adapted bed shear stress given by Equation (3-57) was implemented into Equation (3-11). The measurement input for Hsu and Liu(2004)'s reference concentration model is listed in Table 6.

Table 6 Data input for Hsu & Liu(2004)'s reference concentration model

Variables	Data Input
Water depth *h*	local measurements [m]
Root mean squared wave orbital velocity u_{rms}	local measurements at 2 cm above the bed. [m/s](ACVP)
Time-averaged current velocity u_c	local measurements at 2 cm above the bed. [m/s] (ACVP)
Sediment suspension efficiency e_k	0.05[-]
Time-averaged turbulence kinetic energy *k*	local measurements at 2 cm above the bed. [m^2/s^2](ACVP)

3.2.6. Van der Zanden, et al.(2017)'s model of reference concentration

Van der Zanden, et al.(2017) developed a reference concentration model, which is calibrated against SINBAD measurements. The model is based on Van Rijn(2007b)'s model, which was extended to account for effects of turbulent kinetic energy, see Equation (3-58)

$$\tau'_{b,cw} = 0.3\rho_w k \tag{3-58}$$

w_s is the measured settling velocity.

The reference level a is same as in Van Rijn(2007b)'s model.

In Equation (3-11), in order to compute the dimensionless bed shear stress T, the critical shear stress is needed. In this model, the critical shear stress was modified to,

$$\tau_{b,cr} = \rho_w \left(\frac{4w_s}{D^*}\right)^2 \qquad for \quad 1 < D^* < 10 \tag{3-59}$$

Therefore, by implementing Equation (3-58) and (3-59) into Equation (3-11), this model gives different reference concentration predictions. Noticeably, Van der Zanden, et al.(2017) calibrated the model on the basis of intra-wave measurements in SINBAD wave flume experiment.

The measurement input for Van der Zanden, et al.(2017)'s reference concentration model is listed in Table 7.

Table 7 Data input for Van der Zanden, et al.(2017)'s reference concentration model

Variables	Data Input
Time-averaged turbulence kinetic energy k	local kinetic turbulence energy at 2 cm above the bed. [m/s] (ACVP)
Elevation above the bed ζ	local measurements [m]
Settling velocity w_s	Measured velocity - 0.034 [m/s]

3.2.7. Spielmann, et al.(2004b)'s reference concentration model

Spielmann, et al.(2004b)'s reference concentration model is based on the roller energy dissipation estimated by Delft3D. It is noted that the roller energy is a modelled term in Delft3D instead of a physical term. Thus, it cannot be measured from the SINBAD wave flume experiment. The reference concentration is given by,

$$C_a = \alpha_c \rho_s \left[\frac{D_r}{(\rho_s - \rho_w) g d_{50} C_\varphi}\right]^3 \tag{3-60}$$

The reference level is taken as 1 cm above the bed.

$$a = 0.01\ [m] \tag{3-61}$$

Where α_c is dimensionless calibration coefficient, taken as 1×10^{-6}(Spielmann, et al., 2004). D_r is the roller energy dissipation predicted by Delft3D and C_φ is the wave celerity.

As the dissipation of roller energy and wave celerity cannot be read directly from Delft3D, they are estimated by,

$$D_r = 2\beta g \frac{E_r}{C_\varphi} \tag{3-62}$$

$$C_\varphi = \sqrt{gh} \tag{3-63}$$

With roller energy E_r and coefficient β, which is related to the wave steepness (usually β=0.1) (Spielmann, et al., 2004). As the SINBAD experiment was conducted in shallow water region, the wave celerity is calculated only based on water depth h in this case.

The modelled input for Spielmann, et al.(2004b)'s reference concentration model is listed in Table 8. In this test, in order to be comparable with measured reference concentration in SINBAD wave flume experiment, the dimensionless calibration coefficient α_c was roughly re-calibrated to 4×10^{-5}.

Table 8 Data input for Spielmann, et al.(2004b)'s reference concentration model

Variables	Data Input
Non-dimensional calibrated coefficient α_c	1×10^{-6} [-] / Recalibrated 4×10^{-5} [-]
Non-dimensional coefficient related to wave steepness β	0.1 [-]
Water depth h	output from Delft3D [m]
Roller energy E_r	output from Delft3D [J/m^2]

3.2.8. Steetzel(1993)'s model of reference concentration

In Steetzel(1993)'s model, the reference concentration is related to both the intensity of breaking and the way of breaking (spilling or plunging), which is given by,

$$C_a = \rho_s K_c F_D \left(\frac{\rho_w}{\tau_{cr}}\right)^{\frac{3}{2}} F_k(\gamma|\alpha_k)^{\frac{3}{2}} \left(\frac{D_t}{\rho_w}\right) \tag{3-64}$$

The reference level in this model is assumed at 1 cm above the bed.

$$a = 0.01\ [m] \tag{3-65}$$

In Equation (3-64), τ_{cr} is the critical shear stress and D_t is the turbulent kinetic energy dissipation.

The critical shear stress is defined by,

$$\tau_{cr} = \theta_{cr}(\Delta - 1)\rho_w g d_{50} \tag{3-66}$$

In current study, the critical Shields parameter amounts to 0.05(Steetzel, 1993).

F_D is a dimensionless correction coefficient based on sediment diameter and estimated by,

$$F_D = \left(\frac{0.000225}{D_{50}}\right)^{\alpha_D} \tag{3-67}$$

According to the calibration conducted by Steetzel(1993)'s in his research, the α_D is taken as 1.2.

F_K is a dimensionless coefficient which describes the effect of the way waves break. It is calculated from,

$$F_k(\gamma|\alpha_k) = \left[\alpha_k\gamma\left(exp\left(\frac{1}{\alpha_k\gamma}\right) - 1\right)\right]^{-1} \tag{3-68}$$

Where α_k is a dimensionless constant and γ is significant wave height over water depth H_{rms}/h. In Figure 5, it shows the behaviours of this breaking function.

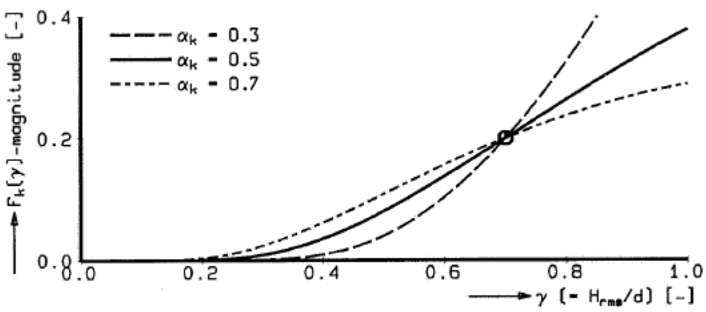

Figure 5 Behaviours of breaking function. This figure is taken from Steetzel(1993)

D_t is turbulent kinetic energy dissipation, which is calculated from

$$D_t = \rho_w \overline{K}^{\frac{3}{2}} \tag{3-69}$$

$\overline{K}$ is depth-averaged turbulent kinetic energy.

According to the SINBAD wave flume experimental set-up, turbulent kinetic energy was only measured by ADVs at three vertical levels in the water column. Based on the assumed distribution of turbulent kinetic energy, these three measurements was fit to an exponential distribution, in which case the depth-averaged turbulent kinetic energy is estimated by,

$$\bar{K} = \frac{1}{h}\int_0^h K \tag{3-70}$$

The measurement and modelled input for Steetzel(1993)'s reference concentration model is listed in Table 9.

Table 9 Data input for Steetzel(1993)'s reference concentration model

Variables	Data Input
Dimensionless calibration factor K_c	1.2×10^{-6} [-]
Critical Shields parameter θ_{cr}	0.05 [-]
Dimensionless factor α_D	1.2 [-]
Non-dimensional calibrated coefficient α_k	0.5 [-]
Water depth h	local measurements /Output from Delft3D [m]
Significant wave height H_{rms}	local measurements /Output from Delft3D [m]
Depth-averaged turbulence kinetic energy $\bar{K}$	Estimations of local measurements /Output from Delft3D [m^2/s^2]

3.3. Results of stand-alone tested reference concentration models

In this section, reference concentration predictions of eight stand-alone tested models are shown and discussed in order to decide which ones are feasible to be implemented into Delft3D environment. In these tests with measurements input, the dimensionless Root-Mean-Square-Error [RMSE] was calculated to indicate the absolute difference between modelled reference concentration and measurements, which is given by,

$$RMSE = \sqrt{mean\left[\left(\frac{C_p - C_m}{\mu_m}\right)^2\right]} \tag{3-71}$$

With predicted reference concentration C_p, measured reference concentration C_m and mean measured reference concentration μ_m. Besides, the Pearson correlation coefficient r was computed as well in order to see how similar the trend of modelled reference concentration is with measurements.

$$r = \frac{1}{N-1}\sum_{i=1}^{N}\left(\frac{C_p - \mu_p}{\sigma_p}\right)\left(\frac{C_m - \mu_m}{\sigma_m}\right) \tag{3-72}$$

Therefore, how well the tested reference concentration models perform can be quantified with these two parameters.

3.3.1. Van Rijn(2007b)'s reference concentration model (default)

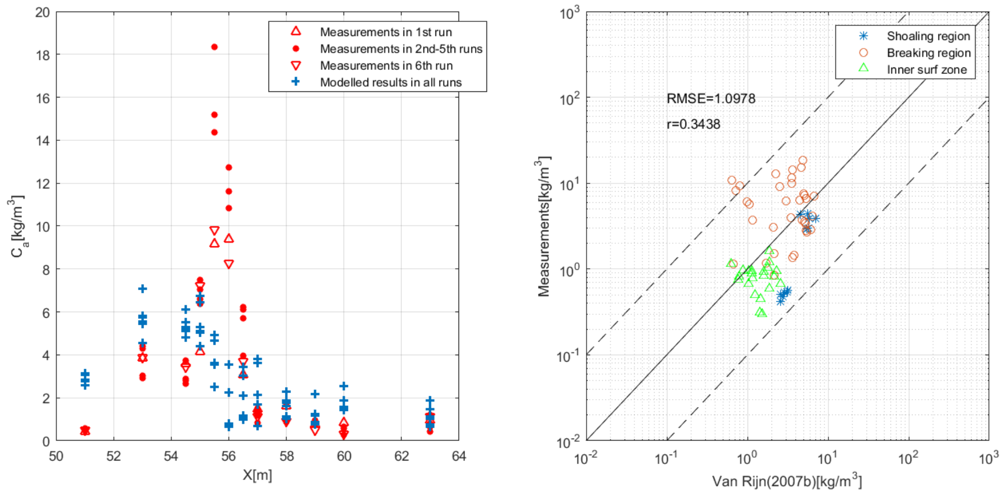

Figure 6 a).Reference concentration comparison between Van Rijn(2007b)'s modelled results and measurements at the reference level. b). Scatter plot of the comparison in shoaling region, breaking region and inner surf zone, with a confidence level of a factor 10.

As mentioned in Section 2.1, the SINBAD wave flume experiment had 6 runs in order to investigate the evolution of bed profile. In Figure 6a, the modelled reference concentrations are compared to SINBAD measurements at the reference level for all 6 runs. The measurements in 1st and 6th runs are highlighted as upward-pointing or downward pointing triangles to see the time-dependency in different runs, i.e., for 0-15 minutes, 15-30 minutes, 30-45 minutes, 45-60 minutes, 60-75 minutes and 75-90 minutes. Each run gives similar measurements except around the plunging point, where measured reference concentrations are relatively low in the 1st and 6th runs. From 2nd run to 5th run, the measured reference concentration increases with a factor of 2. According to the bar evolution in Figure 3, the quasi-2D bed form was identified between 1st and 6th run, which induced more near bed turbulence produced by the bed friction. As near bed reference concentration is significantly correlates with near-bed turbulent kinetic energy(Van der Zanden 2016), it explains the time-dependency of the measured reference concentration in the breaking region.

From Figure 6, in shoaling region (X=50 m-53 m), the Van Rijn(2007b)'s model overestimates the reference concentration with factors from 2 to 8. It is because the wave orbital velocity increases on the bar's offshore slope. In breaking region (X=53 m-58 m), the model significantly underestimates the reference concentration, especially near the plunging point (X=55.5 m). It is explained that the wave orbital velocity is weak at the bar trough due to the deep water. At plunging point (X=55.5 m), measured reference concentrations are higher than modelled concentrations with a factor of 10 as the near-bed sediment is stirred up by strong breaking induced turbulence(Van der Zanden 2016), while the model fails to predict it. In the inner surf zone (X=58 m-63 m), the model overestimates the reference concentration with a factor 5 due to strong undertow compensating for wave-induced onshore mass flux.

In this test, the dimensionless Root-Mean-Square-Error [RMSE] is 1.0978 and the Pearson correlation coefficient *r* is 0.3438, which will be compared to other tests in order to find applicable models to be implemented into Delft3D environment.

3.3.2. Nielsen(1986)'s reference concentration model

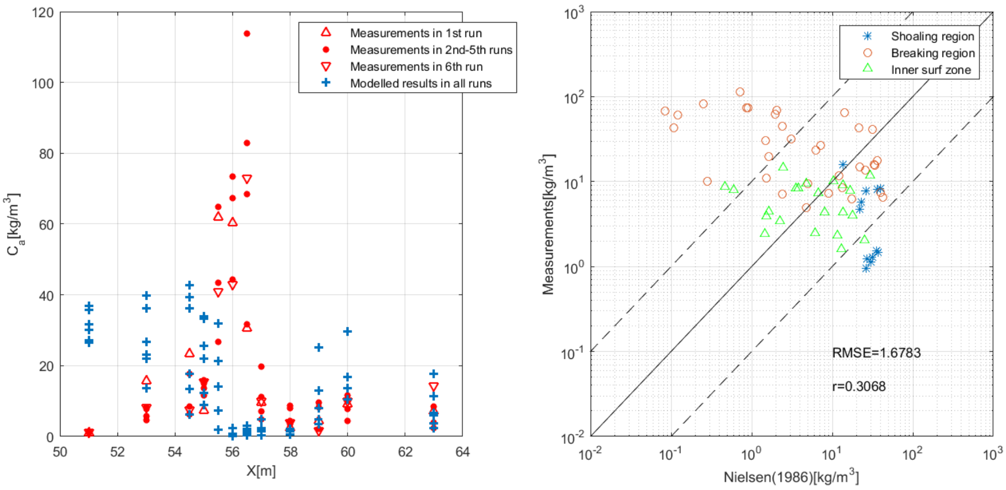

Figure 7 a).Reference concentration comparison between Nielsen(1986)'s modelled results and measurements at the reference level. b). Scatter plot of the comparison in shoaling region, breaking region and inner surf zone, with a confidence level of a factor 10.

As the reference level in Nielsen(1986)'s model is on the bottom, the measured reference concentrations are much higher than in the test of Van Rijn(2007b)'s model with a factor of 5, which indicates the measured near-bed reference concentration is quite sensitive to the reference level. The measurement shows strong time dependency in 6 runs within the breaking region, which can be similarly explained as in the test of Van Rijn(2007b)'s model.

In terms of the comparison between modelled reference concentrations and measurements in Figure 7, in shoaling region (X=50 m-53 m), Nielsen(1986)'s model overestimates the reference concentrations with factors from 5 to 15. It is because the wave orbital velocity increases with the decreasing water depth on the bar's offshore slope. In breaking region (X=53 m-58 m), the model significantly underestimates the reference concentration with a minimum factor of 0.001, which is a very poor prediction. In the inner surf zone (X=58 m-63 m), the model gives both underestimations and overestimations, mostly with factors from 0.1 to 10.

Nielsen(1986) developed this model only based on the wave orbital velocity, while in this test, the combined wave-current related velocity was taken into account. It explains the overestimation in shoaling region, where offshore-directed current velocity was included for calculating reference concentrations. In the breaking region, the relatively low wave orbital velocity due to large water depth and low offshore-directed current velocity result in low predicted reference concentrations, while in the SINBAD experiment, near-bed sediment was stirred up by strong breaking induced turbulence. It explains the significant mismatch between predictions and measurements in the breaking region.

In this test, the dimensionless Root-Mean-Square-Error [RMSE] is 1.6783 and the Pearson correlation coefficient *r* is 0.3068.

3.3.3. Mocke and Smith(1992)'s reference concentration model

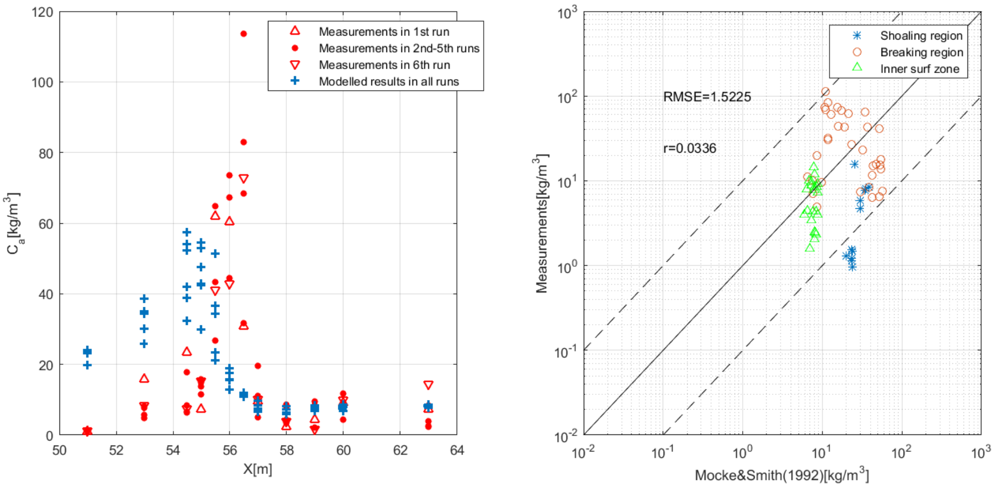

Figure 8 a).Reference concentration comparison between Mocke and Smith(1992)'s modelled results and measurements at the reference level. b). Scatter plot of the comparison in shoaling region, breaking region and inner surf zone, with a confidence level of a factor 10.

Similarly with Nielsen(1986)'s model, the reference level in Mocke and Smith(1992)'s reference concentration model is practically at the bottom. Therefore, the measurement shows the same time dependency as in Nielsen(1986)'s model.

In terms of modelled results in Figure 8, Mocke and Smith(1992)'s model shows a slightly similar trend with measurements but overestimates the reference concentration with a factor of 15 in shoaling region (X=50 m-53 m). In breaking region (X=53 m-58 m), the model gives both underestimations and overestimations with factors from 0.1 to 10. Moreover, the maximum modelled reference concentration in the breaking region is slightly shifted offshore-ward by 0.5 m compared to measurements. In the inner surf zone (X=58 m-63 m), the modelled reference concentration agrees with measurements well.

According to Equation (3-39), the maximum modelled reference concentration is at bar crest, where the wave height is largest. In SINBAD measurements, the maximum measured reference concentration occurs at the plunging point, where the breaking induced turbulent kinetic energy is largest. It explains the mismatch.

In this test, the dimensionless Root-Mean-Square-Error [RMSE] is 1.5225 and the Pearson correlation coefficient r is 0.0336.

3.3.4. Okayasu(2009)'s adaption combined with default model

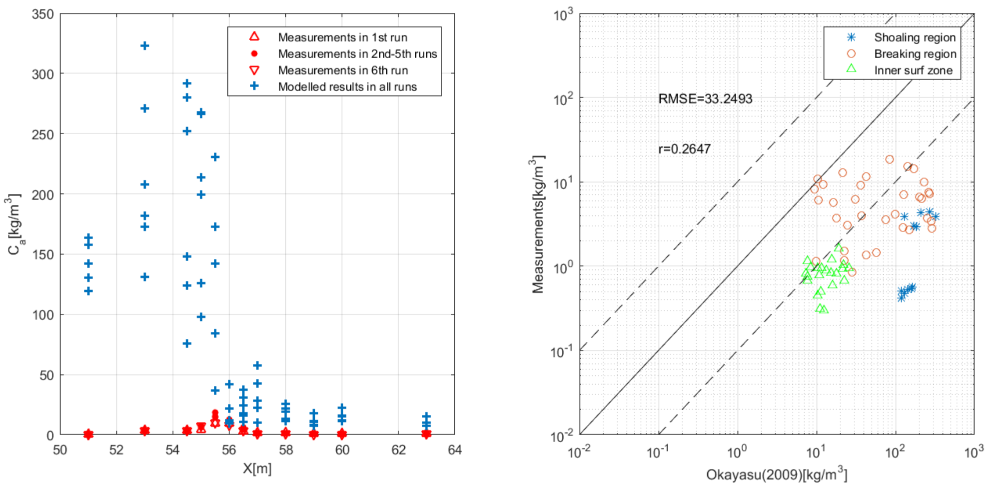

Figure 9 a).Reference concentration comparison between Okayasu(2009)'s modelled results and measurements at the reference level. b). Scatter plot of the comparison in shoaling region, breaking region and inner surf zone, with a confidence level of a factor 10.

The reference level in Okayasu(2009)'s modified reference concentration model is same as in Van Rijn(2007b)'s model. Therefore, measurements in this test have the same time dependency as in Van Rijn(2007b)'s model.

According to Figure 9, it can be concluded that the Okayasu(2009)'s adaption highly overestimates the reference concentration with factors from 10 to 500, especially in shoaling region and breaking region. As mentioned above, the Okayasu(2009)'s experiment was conducted in a flow flume, where turbulence is generated only by irregular structures in the flume, in which circumstance, only flow velocity and turbulent kinetic energy is taken into account by Okayasu(2009). However, in this test, the drag force in Equation (3-45) includes the combined wave- and current-related velocity and turbulent kinetic energy, which leads to the significant overestimation.

In this test, the dimensionless Root-Mean-Square-Error [RMSE] is 33.2493 and the Pearson correlation coefficient *r* is 0.2647.

3.3.5. Hsu and Liu(2004)'s adaption combined with default model

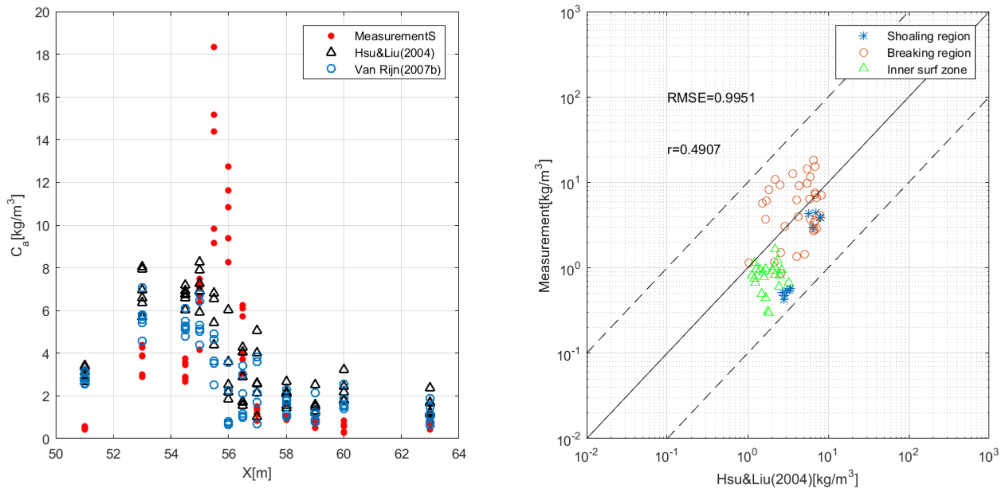

Figure 10 a).Reference concentration comparison between Hsu and Liu(2004)'s modelled results and measurements at the reference level. b). Scatter plot of the comparison in shoaling region, breaking region and inner surf zone, with a confidence level of a factor 10.

In order to compare reference concentration predicted by Hsu and Liu(2004)'s adaption in default model, both of them are shown in Figure 10a.

The reference level in Hsu and Liu(2004)'s modified reference concentration model is same as in Van Rijn(2007b)'s model. Therefore, measurements in this test have the same time-dependency as in Van Rijn(2007b)'s model. For a better readability of Figure 10, measurements in 1st and 6th runs are not highlighted in this case.

From Figure 10, in shoaling region (X=50 m-53 m), the model with Hsu and Liu(2004)'s adaption overestimates the reference concentration with a factor of 8. This overestimation is even higher than in Van Rijn(2007b)'s model. In breaking region (X=53 m-58 m), Hsu and Liu(2004)'s adaption slightly improves the prediction of Van Rijn(2007b)'s model. The model with Hsu and Liu(2004)'s adaption underestimates the reference concentration with a factor of 7, while Van Rijn(2007b)'s model underestimates it with a factor of 11. In the inner surf zone (X=58 m-63 m), the model overestimates the reference concentration with a factor of 7.

In this adaption, Hsu and Liu(2004) took the near bed turbulent kinetic energy into account with a calibration coefficient e_k=0.05, which explains the improvements. However, in Van Rijn(2007b)'s model, the wave orbital velocity and near bed current velocity were already taken into account directly, while in Hsu and Liu(2004)'s adaption, the near-bed turbulence could be generated by the wave orbital velocity and current velocity as well. It leads to the potential risk of double counting the combined wave-current effects.

In this test, the dimensionless Root-Mean-Square-Error [RMSE] is 0.9951 and the Pearson correlation coefficient *r* is 0.4907.

3.3.6. Van der Zanden, et al.(2017)'s reference concentration model

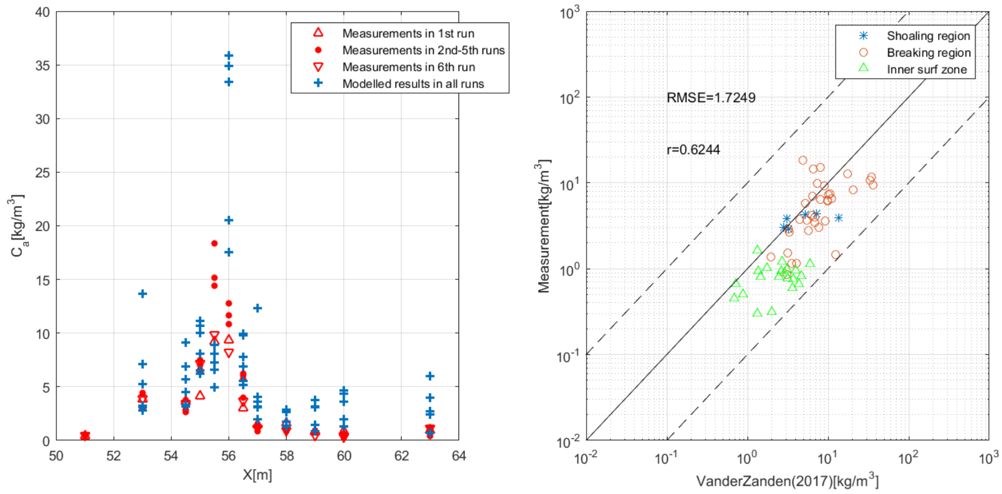

Figure 11 a).Reference concentration comparison between Van der Zanden, et al.(2017)'s modelled results and measurements at the reference level. b). Scatter plot of the comparison in shoaling region, breaking region and inner surf zone, with a confidence level of a factor 10.

As Van der Zanden, et al.(2017)'s reference concentration model was developed on the basis of Van Rijn(2007b)'s model, the reference level in this model is same as in Van Rijn(2007b)'s model. Therefore, measurements in this test have the same time-dependency as in Van Rijn(2007b)'s model.

From Figure 11, in shoaling region (X=50 m-53 m), Van der Zanden, et al.(2017)'s model overestimates the reference concentration with a factor of 5. In breaking region (X=53 m-58 m), it overestimates the reference concentration with a factor of 10, especially at the plunging point. In the inner surf zone (X=58 m-63 m), the model overestimates the reference concentration with a factor of 10 as well.

It has been shown in the research of Van der Zanden(2016) that near bed turbulence is dominant for transporting the suspended sediment in the breaking wave region. Additionally, the model still contains wave-current interaction as near bed turbulent kinetic energy is produced by wave orbital velocity and current velocity as well, which indicates the model can be applied to non-breaking region.

According to Van der Zanden, et al.(2017), the reference concentration scales non-linearly to turbulent kinetic energy, $C_0 \sim k_b^{3/2}$. With a wave-averaged k_b forcing the model, the distribution of k_b is negatively skewed, resulting in a significantly lower reference concentration by 15%(Van der Zanden, et al., 2017). Considering the overestimation already occurred at the plunging point, the model performs slightly worse than the default model in terms of absolute differences between predictions and measurements, which is proved by the dimensionless Root-Mean-Square-Error [RMSE] 1.7249. However, the cross-shore trend of predictions is modelled well compared to measurements, supported by the Pearson correlation coefficient r 0.6244.

3.3.7. Spielmann, et al.(2004b)'s reference concentration model

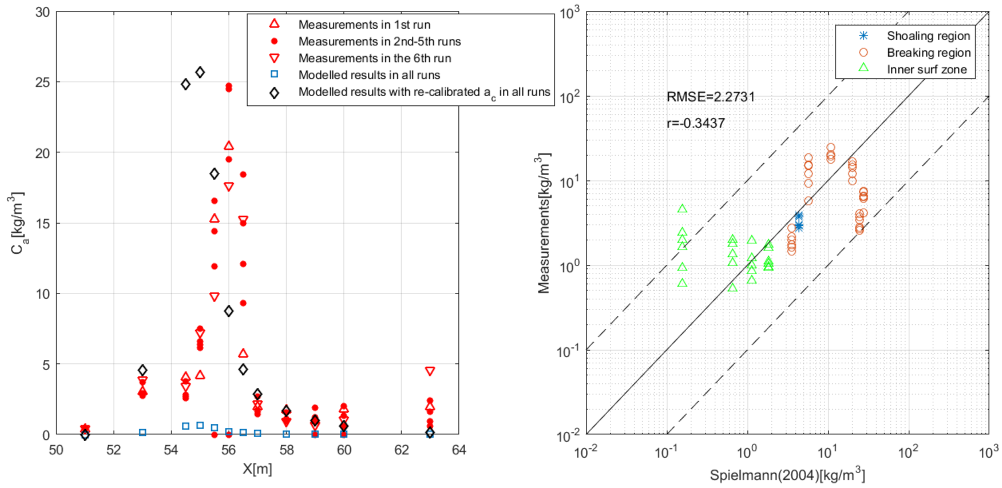

Figure 12. Reference concentration comparison between Spielmann, et al.(2004b)'s modelled results and measurements at the reference level. b). Scatter plot of the comparison in shoaling region, breaking region and inner surf zone, with a confidence level of a factor 10.

Spielmann, et al.(2004b)'s reference concentration model was tested with the roller energy input predicted by Delft3D. Therefore, the number of measurements does not agree the number of predicted reference concentrations at each cross-shore location. After a simple interpolation, the modelled results was interpolated at different measured locations in order to compute dimensionless Root-Mean-Square-Error [RMSE] and Pearson correlation coefficient.

In Spielmann, et al.(2004b)'s reference concentration model, the reference level is set to 1 cm above the bed along the entire surf zone. From Figure 12, the higher measured reference concentration between 2nd to 5th runs in the breaking region can be explained by the quasi-2D bed form between 2nd to 5th runs.

With the default value of calibration coefficient a_c, the model significantly underestimates the reference concentration along the entire surf zone. Due to this significant underestimation, the dimensionless RMSE and Pearson correlation coefficient were not given in this case.

Therefore, after a simple re-calibration of non-dimensional coefficient a_c, the model gives better predictions, which has the same order of magnitude as measurements. In shoaling region (X=50 m-53 m), the predicted reference concentration remains zero as no roller energy is produced with no wave breaking. At the breaking point (X=53 m), the modelled reference concentration agrees with measurements accurately well accidentally. In the model, the reference concentration increases with the increasing roller energy produced by waves breaking, while the relatively high measured reference concentration at the breaking point is induced by advection and diffusion from high reference concentration around the plunging point. In the breaking region and inner surf zone (X=53 m-63 m), the model shows a similar trend with measurements, while an 1 m offshore shift occurs at the maximum predicted reference concentration compared to measurements. As roller energy is a modelled term, which is impossible to be calibrated against measurements. In this case, it is difficult to improve the mismatch between predictions and measurements.

In this test, the dimensionless Root-Mean-Square-Error [RMSE] is 2.2731 and the Pearson correlation coefficient r is 0.3437 in re-calibrated model.

3.3.8. Steetzel(1993)'s reference concentration model

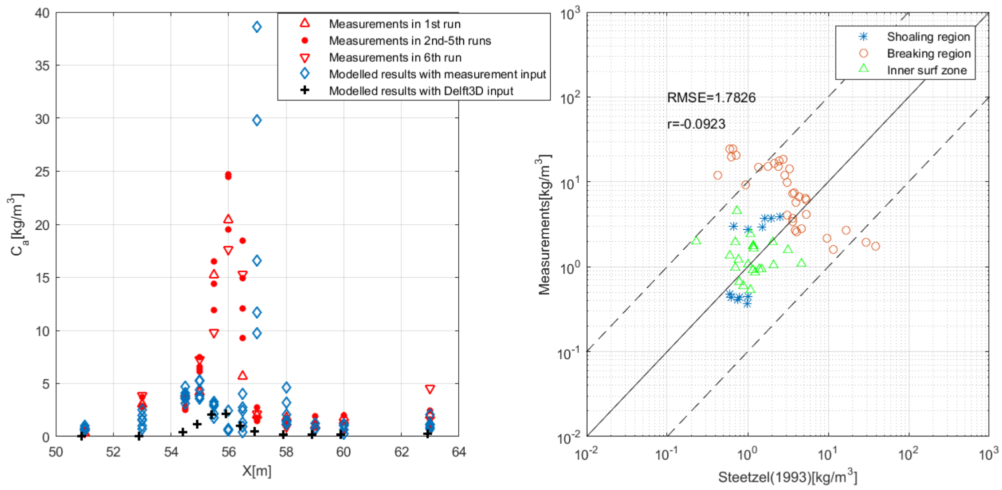

Figure 13 a).Reference concentration comparison between Steetzel(1993)'s modelled results and measurements at reference level. b). Scatter plot of the comparison in shoaling region, breaking region and inner surf zone, with a confidence level of a factor 10.

In Steetzel(1993)'s reference concentration model, the reference level is set to 1 cm above the bed along the entire surf zone. Therefore, the measurements shows the same time-dependency as in Spielmann, et al.(2004b)'s model.

In Figure 13, both the reference concentration predicted by models with measurements input and Delft3D input are shown. In terms of prediction of the model with Delft3D input, the model significantly underestimates the reference concentration with a factor of 10. Due to this significant underestimation, the modelled results were not interpolated to compute the dimensionless Root-Mean-Square-Error [RMSE] and the Pearson correlation coefficient.

In terms of prediction of the model with measurements input, in shoaling region (X=50 m-53 m), the model shows both underestimations and overestimations with factors from 0.4 to 6. In breaking region (X=53 m-58 m), the model underestimates the reference concentration with a factor of 0.0167. Noticeably, at locations of X=57 m, predicted reference concentrations are very high, which can be explained that the near surface measurement of ADV at location of X=57 m was contaminated and abandoned. In this case, the exponential fit only agrees with two measurements in the lower half of water column, leading to extremely high estimations of depth averaged turbulence. In the inner surf zone (X=58 m-63 m), the predicted reference concentration agrees with measurements well.

In this test with measurement input, the dimensionless Root-Mean-Square-Error [RMSE] is 1.7313 and the Pearson correlation coefficient *r* is 0.0899.

3.4. Summary of stand-alone tests

Table 10 Summary of the dimensionless Root-Mean-Square-Error and correlation coefficient r for stand-alone tested models

Stand-alone Models	**[RMSE]**	**Correlation *r***	**Implementation**
Van Rijn(2007b)'s reference concentration model (default)	1.0978	0.3438	
Nielsen(1986)'s reference concentration model	1.6783	0.3068	
Mocke and Smith(1992)'s reference concentration model	1.5225	0.0336	
Okayasu(2009)'s adaption combined with default model	33.2493	0.2647	
Hsu and Liu(2004)'s adaption combined with default model	0.9951	0.4907	✓
Van der Zanden, et al.(2017)'s reference concentration model	1.7249	0.6244	✓
Spielmann, et al.(2004b)'s reference concentration model	2.2731	0.3437	
Steetzel(1993)'s reference concentration model	1.7313	0.0899	

In Table 10, the dimensionless RMSE and the Pearson correlation coefficient *r* for stand-alone tested models are summarized.

Compared to Van Rijn(2007b)'s reference concentration model, Okayasu(2009)'s adaption combined with default model performs poorly due to the extremely high overestimation in shoaling region, which is proved by the very large dimensionless RMSE. Nielsen(1986)'s model significantly underestimates the reference concentration in the breaking region, in which case the large RMSE and smaller Pearson correlation coefficient *r* are given. Mocke and Smith(1992)'s model and Steetzel(1993)'s model with measurements input are weakly correlated with Van Rijn(2007b)'s reference concentration model, which is supported by small Pearson correlation coefficient. In terms of Steetzel(1993)'s model with Delft3D input, it gives worse predictions than Steetzel(1993)'s model with measurements input in the breaking region. In the test of Spielmann, et al.(2004b)'s model, the mismatch between the maximum predicted reference concentration and the measurement needs further improvements. Therefore, all of these models will not be implemented into Delft3D environment.

In terms of Hsu and Liu(2004)'s adaption combined with default model, it gives the best dimensionless RMSE and significantly improves the Pearson correlation coefficient *r* compared to Van Rijn(2007b)'s model. Although Van der Zanden, et al.(2017)'s model overestimates the reference concentration around the plunging point, resulting in a worse dimensionless RMSE, it is closely correlated with measured reference concentration. Therefore, these two models are implemented into Delft3D environment.

Chapter 4 Hydrodynamic validation of Delft3D model

In last chapter, two models were selected to be implemented into Delft3D environment. Different from the stand-alone tests with Matlab, these implementations require hydrodynamic inputs from Delft3D. Therefore, the Delft3D hydrodynamic model was validated in this chapter in order to ensure an accurate input for implemented models.

4.1. Introduction of hydrodynamic validation of Delft3D model

In this section, the general procedure of hydrodynamic validation of Delft3D model is introduced.

First, the SINBAD model set-up by Schnitzler(2015) is briefly mentioned in Section 4.2. It includes the grid set-up, initial condition, boundary conditions, model settings and an adapted formula for the regular wave height prediction.

Then, a hydrodynamic re-calibration of this model will be discussed in Section 4.3 on the basis of a sensitivity analysis. The sensitivity study was conducted in terms of wave height, undertow and turbulent kinetic energy predictions. In Schnitzler(2015)'s set-up model, the wave height is shifted offshore-ward by 2 m and undertow is well modelled. Besides, the turbulent kinetic energy near the water surface is significantly overestimated and near-bed turbulence is underestimated by Schnitzler(2015)'s set-up model. Therefore, the model was re-calibrated empirically, on the basis of insights obtained from the sensitivity study. The hydrodynamic re-calibration significantly improves the wave height prediction and slightly improves the undertow, while turbulent kinetic energy prediction is worse predicted.

After the hydrodynamic re-calibration, an additional adaption for regular wave conditions regarding the near-surface turbulence production in Delft3D source code was implemented. The adaption significantly improves the near-surface and near-bed turbulence prediction, while it slightly worsens the undertow prediction. It is discussed in Section 4.4.

Last but not least, a mismatch between the maximum predicted near-bed cross-shore turbulence and measurements remains in the re-calibrated and adapted model. In this case, the breaking point was shifted shoreward by another 2 m in order to improve the mismatch as the near-bed turbulence is directly taken as input by implemented models.

The hydrodynamic validation of Delft3D is summarized in Section 4.5.

4.2. SINBAD model set-up

The model of SINBAD wave flume experiment was set-up by *Schnitzler(2015)*. The grid, initial conditions, boundary conditions and model setting are discussed in this section.

4.2.1. Grid set-up

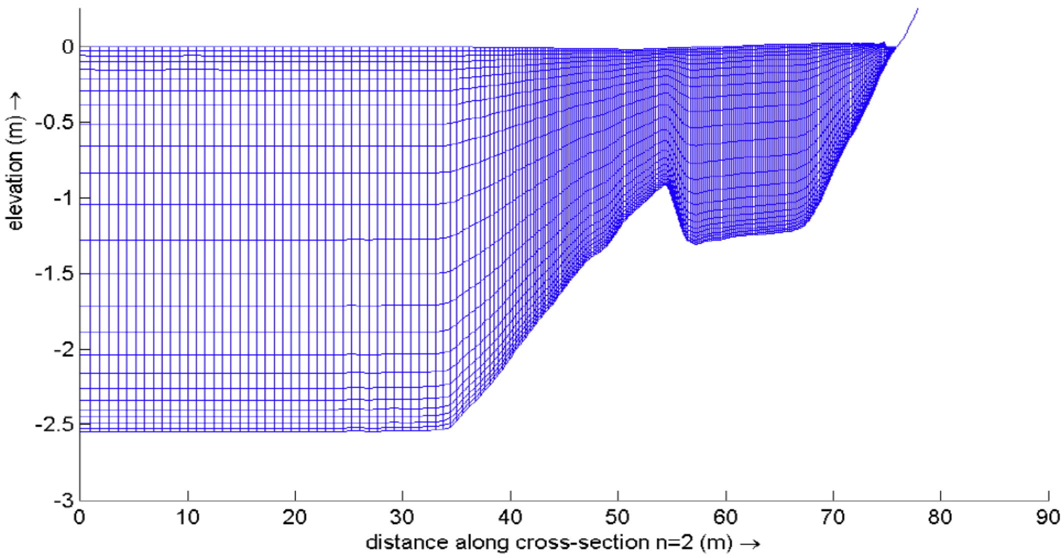

Figure 14 Grid dimensions in Delft3d model of SINBAD wave flume experiment, taken from Schnitzler(2015).

In reference of Figure 14, the model grid consists of 263 cross-shore grid locations, one grid cell in the alongshore direction and 24 vertical layers(Schnitzler, 2015). The grid is finest near the location of bar crest [0.2 m for one cell]. The vertical layers is defined as a percentage of the water depth, which are 1%, 1.3%, 1.6%, 2%, 2.4%, 3.1%, 3.8%, 4.8%, 5.8%, 7%, 8.2%, 9%, 9%, 8.2%, 7%, 5.8%, 4.8%, 3.8%, 3.1%, 2.4%, 2%, 1.6%, 1.3% and 1%(Schnitzler, 2015).

4.2.2. Initial and boundary conditions

The water level is set uniform to 0 m and sediment concentration in the water column is set to 0 kg/m^3 at the start of the model run [t=0 s](Schnitzler, 2015).

An open boundary in the model is at location X=0 m. Waves are generated at this open boundary with 0.85 m wave height and 4 s wave period(Schnitzler, 2015).

4.2.3. Model settings

On the basis of SINBAD measurements, the median grain size (d_{50}) is 246 µm. The 10 percentile grain size (d_{10}) and the 90 percentile grain size (d_{90}) are 154 µm and 372 µm(Schnitzler, 2015).

The bottom roughness, the Chezy roughness value, is listed in

Table 11 Bed roughness set-up along the entire wave flume, values are taken from Schnitzler(2015).

X	[0 m – 38 m]	[38 m – 68 m]	[68 m – end]
Bed roughness set-up	85 [m$^{0.5}$/s]	Predicted by Van Rijn(2007a)	45 [m$^{0.5}$/s]

In Table 11, the bed roughness between X=38 m and X=68 m is predicted by *Van Rijn(2007a)*, which includes effects of ripples. The morphodynamic updating was switched off in the model. Therefore, the bottom is fixed in the Delft3D model of SINBAD wave flume experiment(Schnitzler, 2015).

4.2.4. Adapted wave height prediction for regular wave conditions

According to Baldock, et al.(1998), the default parameterization model of wave energy dissipation [Equation (2-5)] was developed for irregular wave conditions. It was adjusted later by Van Rijn and Wijnberg(1996), which is applicable for regular wave conditions(Walstra, et al., 2012).

$$D_w = \frac{1}{4}\alpha_{rol}\rho_w g \frac{1}{T} H_{max}^2 Q_b \tag{4-1}$$

In Equation (4-1), Q_b is a parameter indicating wave breaking, with the value 1 in waves breaking conditions and 0 in wave nonbreaking conditions(Schnitzler, 2015). A criterion had been added to the source code that waves continue breaking as long as the wave height during the next spatial step is higher than a relative depth of 0.35 m, on the basis of measurements(Schnitzler, 2015).

$$\begin{aligned} Q_b &= 1 \quad if \quad \frac{H_{rms}}{h} > \gamma \\ Q_b &= 1 \quad if \;\; Q_{b(x-1)} = 1 \; and \; H_{rms(x+1)} > reldep \\ Q_b &= 0 \quad otherwise \end{aligned} \tag{4-2}$$

γ is a manually defined index to justify whether waves break. This adaption was implemented by *Schnitzler (2015)* only for regular wave conditions.

4.3. hydrodynamic model sensitivity study and re-calibration

In the wave breaking region, the wave height is critical as it influences turbulence production, roller energy production, wave-related sediment transport and etc. Undertow controls current-related offshore-directed suspended sediment transport. Most importantly, according to Chapter 3, the selected reference concentration models are Hsu and Liu(2004)'s adaption combined with default model and Van der Zanden, et al.(2017)'s model. Both of them take near bed turbulent kinetic energy as an input. Under this circumstance, the vertical turbulent kinetic energy distribution in the water column and near bed turbulence were investigated in order to ensure an accurate input for these implemented models.

Therefore, a sensitivity analysis in terms of wave height, undertow and turbulent kinetic energy was conducted to look into the room for re-calibration. Five user input parameters in Delft3D hydrodynamic model are listed in Table 12 and have been calibrated in sensitivity analysis. Roller energy dissipation is in Equation (2-5), roller slope parameter in Equation (2-7) and bottom friction factor in Equation (2-6). The wave breaking index is in Equation (4-2) for regular wave conditions. The breaker delay parameter is in Equation (2-8). As the breaker delay parameter only influences the undertow prediction(Walstra *et al.*, 2012), it is noted the breaker delay parameter was calibrated in sensitivity analysis of undertow. The Range of these parameters in sensitivity analysis was empirically set-up. In this sensitivity analysis, while one of parameters is being tested, other parameters remain the same as in Schnitzler (2015)'s set-up model.

Table 12 Five user input parameters in Delft3D model.

User input parameters	Schnitzler(2015)'s set up	Range for sensitivity analysis
Roller energy dissipation α_{rol}	6	[2-10]
Roller slope parameter β_{rol}	0.2	[0.05-0.30]
Wave breaking index γ	0.58	[0.54-0.62]
Bottom friction factor f_w	0	[0-0.08]
Wave breaker delay parameter λ	0	[0-10]

Noticeably, to exclude the time dependency of measurements in 6 experimental runs, only measurements in the 4th run was used to be compared with modelled results.

4.3.1. Sensitivity analysis of wave height

In this section, different effects of parameters on the wave height are shown and discussed in order to find the finest agreement between the predictions of Delft3D and measurements. In this part of analysis, the prediction calibrated by Schnitzler (2015) is included as well, which indicates the room for improvements.

In this sensitivity analysis, pressure transducers (PTs) underestimated measured wave heights in the region (X=50 m-54 m) due to exclusion of various effects, such as air bubbles. Therefore, a dimensionless Root-Mean-Square-Error [RMSE] analysis was conducted only on the basis of measurements in the breaking region and inner surf zone (X=54 m-62 m).

- **Roller energy dissipation**

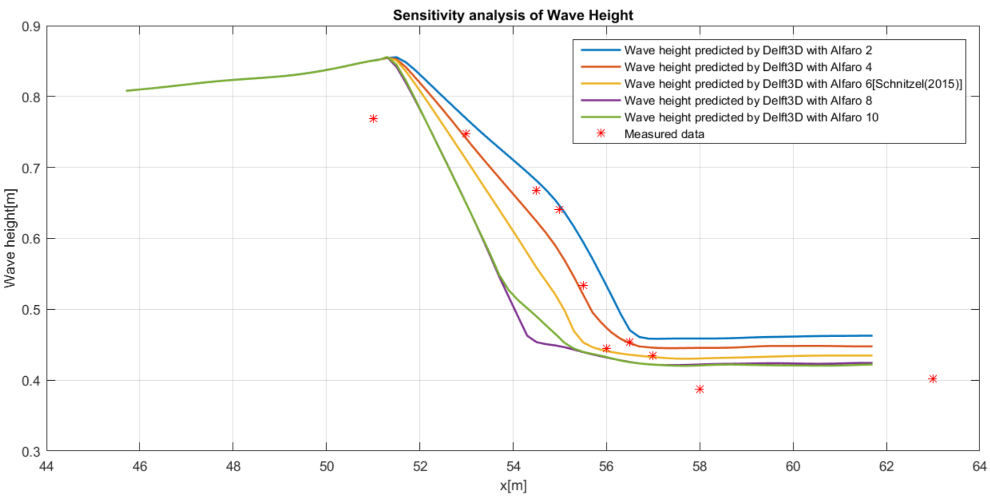

Figure 15 Sensitivity analysis of roller energy dissipation effect on wave height.

According to Equation (2-5), the roller energy dissipation *(Alfaro)* indicates dissipation rate of wave energy, which is shown in Figure 15 as well.

Table 13 RMSE analysis in terms of different values of Alfaro.

Alfaro	2	4	6	8	10
RMSE	0.1463	0.1079	0.1048	0.1104	0.1065

When the roller energy dissipation α_{rol} *(Alfaro)* is 2, the modelled wave height agrees generally well with measurements, while it overestimates the wave height in the inner surf zone (X=58 m-62 m). When the roller energy dissipation α_{rol} *(Alfaro)* is 4, it underestimates the wave height at the plunging point. When the roller energy dissipation α_{rol} *(Alfaro)* is 6, the model underestimates the wave height in the breaking region (X=53 m-56 m), while it shows the best dimensionless Root-Mean-Square-Error [RMSE] in this sensitivity analysis. When the roller energy dissipation α_{rol} *(Alfaro)* comes to 8 and 10, the wave height prediction is similar, with significant underestimations in the breaking region (X=53 m-56 m). In this case, it is observed that roller energy dissipation α_{rol} *(Alfaro)* influences the rate of wave height decreasing. Based on the observation and dimensionless RMSE, roller energy dissipation α_{rol} *(Alfaro)* 6 is preferable.

- **Roller slope parameter**

According to Equation (2-7), the roller slope parameter β_{rol} *(Betaro)* barely has influence on the wave height as it controls roller energy transformation. Thus, the parameter was not used to calibrate the wave height and is not discussed here.

- **Wave breaking index**

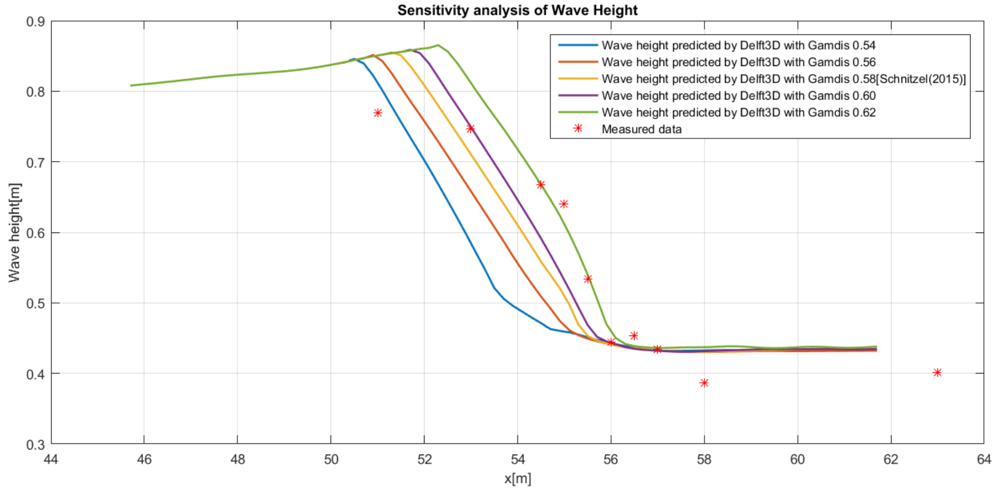

Figure 16 Sensitivity analysis of wave breaking index effect on wave height.

The wave breaking index γ *(Gamdis)* controls cross-shore locations of the breaking point in this case. As the breaker index γ *(Gamdis)* increases, the breaking point is moved shoreward, which is observed from Figure 16. Additionally, it slightly increases the wave height around the breaking point.

Table 14 RMSE analysis in terms of different values of Gamdis.

Gamdis	0.54	0.56	0.58	0.60	0.62
RMSE	0.1143	0.1120	0.1048	0.0974	0.0856

When the wave breaking index γ *(Gamdis)* is 0.54, the breaking point is shifted offshore-ward, which underestimates the wave height in the breaking region. On the contrary, when the wave breaking index γ *(Gamdis)* comes to 0.62, the predicted wave height agrees with measurements well, with the smallest dimensionless RMSE 0.0856.

- **Bottom friction**

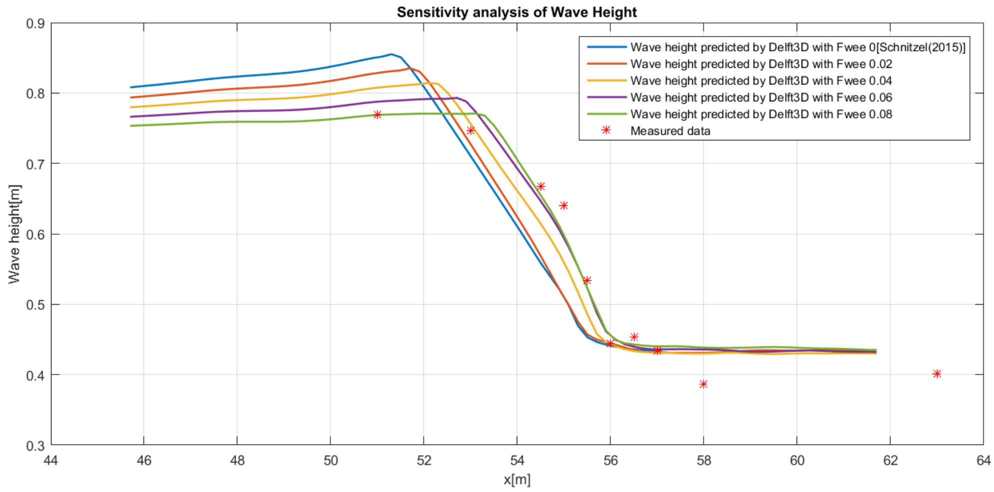

Figure 17 Sensitivity analysis of bottom friction effect on wave height.

According to Equation (2-7), it's obvious that bottom friction *(f_w)* decreases the wave height as wave energy dissipates due to bottom friction. Additionally, the bottom friction slightly shifts the breaking point shoreward.

Table 15 RMSE analysis in terms of different values of f_w.

f_w	0	0.02	0.04	0.06	0.08
RMSE	0.1048	0.1043	0.0831	0.0797	0.0868

From Table 15, the bottom friction *(f_w)* gives the smallest RMSE of 0.036, which is mainly because the location of the breaking point in the case of bottom friction 0.08 is shifted onshore-ward by 2 m compared to Schnitzler (2015)'s set-up. Taking effects of the wave breaking index γ *(Gamdis)* 0.62 into consideration, the bottom friction 0.08 would overly contribute to this onshore shift. Under this circumstance, the bottom friction 0 is preferable.

- **Breaker delay parameter**

According to Walstra *et al.*(2012), the breaker delay parameter λ has no effect on the wave height. Therefore, the sensitivity analysis of wave height in terms of breaker delay parameter λ is shown in Appendix C for reference and not discussed here.

4.3.2. Sensitivity analysis of undertow

In this section, the sensitivity analysis of modelled undertow regarding all five user input parameters is investigated.

- **Roller energy dissipation**

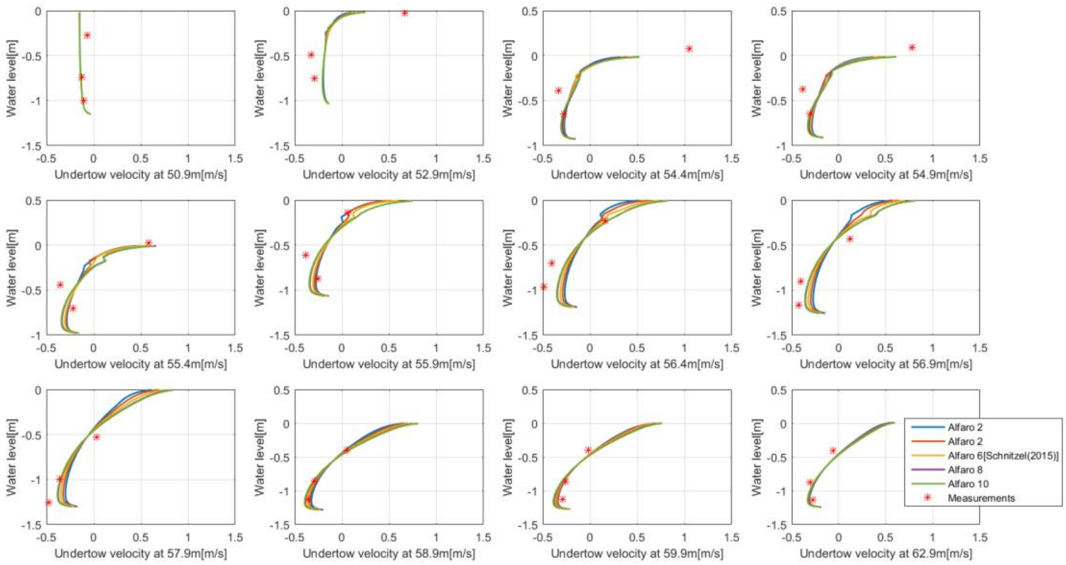

Figure 18 Sensitivity analysis of roller energy dissipation effect on vertical undertow distribution in the water column.

Generally, the modelled undertow is predicted by Schnitzler (2015)'s set-up well. From Figure 18, the roller energy dissipation α_{rol} *(Alfaro)* has little effect on vertical distribution of undertow in the water column. With the roller energy dissipation α_{rol} *(Alfaro)* increasing, vertical undertow profile is more inclined to the bottom, which is beneficial to improve default reference concentration model and Hsu and Liu(2004)'s adaption combined with default model in the breaking region. However, the roller energy dissipation α_{rol} *(Alfaro)* can improve the vertical undertow distribution in the water column with a very limited capability. Further effects on turbulence is necessary to be looked into.

- **Roller slope parameter**

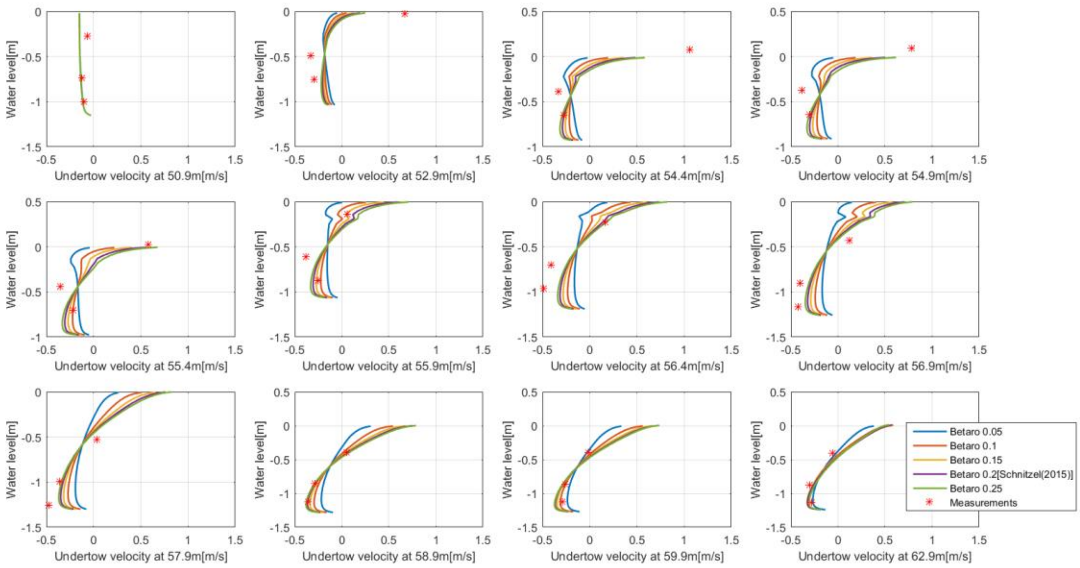

Figure 19 Sensitivity analysis of roller slope parameter effect on vertical undertow distribution in the water column.

From Figure 19, the roller slope parameter strongly affects vertical undertow distribution in the water column. With the increasing values of roller slope parameter β_{rol} *(Betaro)*, near bed undertow increases and current velocity near the water surface decreases, which means the vertical undertow profile is more inclined to the bottom. Additionally, Figure 19 indicates strong undertow only appears in the breaking region and the inner surf zone (X=52.9 m- 62.9 m). In summary, higher values of roller slope parameter β_{rol} *(Betaro)* are preferable in terms of undertow prediction, although the investigation of turbulence prediction is still needed.

- **Wave breaking index**

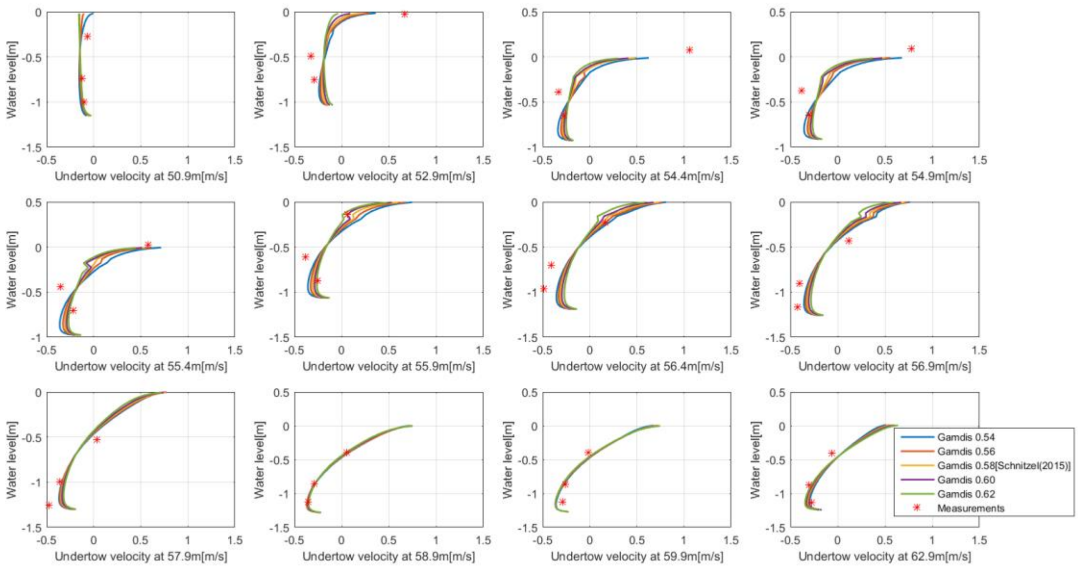

Figure 20 Sensitivity analysis of wave breaking index effect on vertical undertow distribution in the water column.

From Figure 20, the wave breaking index γ *(Gamdis)* influences on vertical undertow profiles in shoaling and breaking regions. With the increasing wave breaking index γ *(Gamdis)*, the vertical undertow profiles in the water column is more evenly distributed. Therefore, lower values of the wave breaking index γ *(Gamdis)* are preferable in this case.

- **Bottom friction**

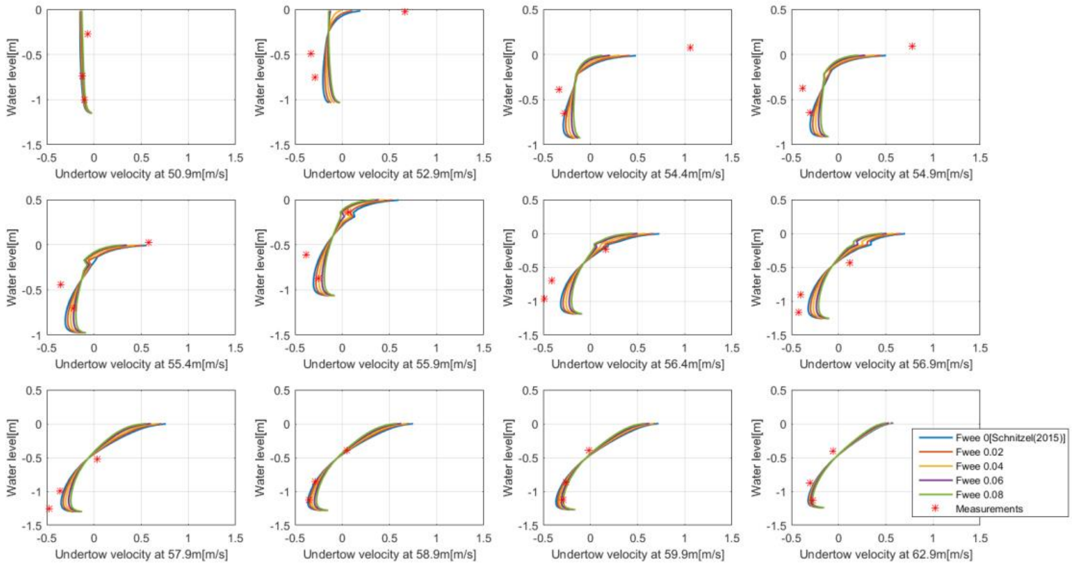

Figure 21 Sensitivity analysis of wave breaking index effect on vertical undertow distribution in the water column.

Apparently, larger bottom friction *(f_w)* significantly decreases the near bed offshore-directed current velocity, resulting in more evenly distributed vertical undertow profiles in the entire surf zone. When bottom friction become smaller, the near-bed offshore-directed current velocity is better predicted along the entire surf zone. Therefore, bottom friction 0 is preferable in this case.

- **Breaker delay parameter**

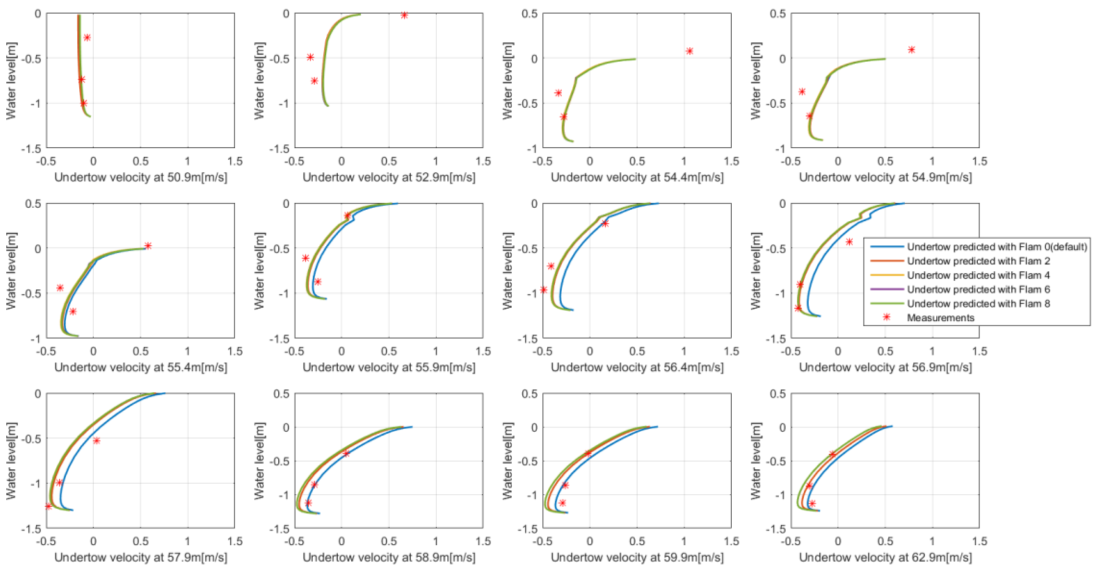

Figure 22 Sensitivity analysis of breaker delay effect on vertical undertow distribution in the water column.

The breaker delay parameter only influences the undertow prediction in the water column(Walstra *et al.*, 2012). In Figure 22, with the increasing breaker delay parameter, undertow increases from the plunging point to the inner surf zone (X=55.4 m-62.9 m). Significant difference between breaker delay parameter 0-2 is noted.

4.3.3. Sensitivity analysis of turbulent kinetic energy

In this section, the sensitivity analysis of modelled turbulent kinetic energy regarding five user input parameters was conducted and investigated.

- **Roller energy dissipation**

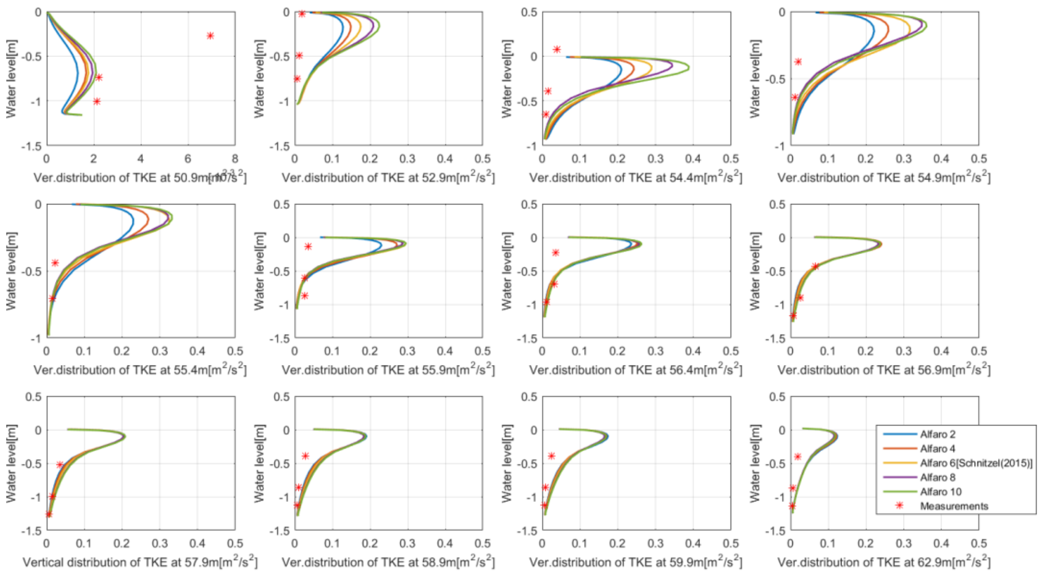

Figure 23 Sensitivity analysis of roller energy dissipation effect on vertical turbulent kinetic energy distribution in the water column.

Generally, the near surface turbulent kinetic energy production is highly overestimated by Schnitzler (2015)'s set-up model. From SINBAD measurements at the plunging point in Figure 23, it indicates the turbulent kinetic energy is more evenly vertically distributed in the water column for regular wave conditions due to waves constantly breaking at the same cross-shore location. However, Delft3D predicts that near surface turbulent kinetic energy produced by wave energy dissipation transfers downward as a triangle with ½ significant wave height injection depth.

From Figure 23, the roller energy dissipation α_{rol} *(Alfaro)* significantly influences on vertical turbulence profiles in the water column from shoaling region to the plunging point (X=50.9 m-55.9 m), where short wave energy dissipates. It is proved that the roller energy dissipation α_{rol} *(Alfaro)* influences short wave energy dissipation in Equation (2-5).

With the increasing roller energy dissipation α_{rol} *(Alfaro)*, the near surface turbulent kinetic energy significantly increases in the region where waves dissipate. Considering the turbulent kinetic energy in the water column is already overestimated, the higher values of roller energy dissipation α_{rol} *(Alfaro)* is non-preferable.

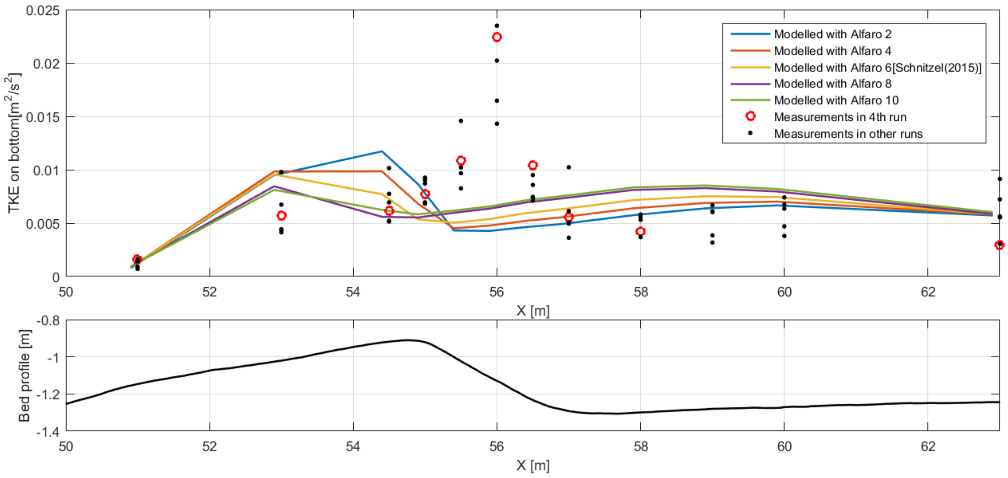

Figure 24 Sensitivity analysis of roller energy dissipation effect on near bed turbulent kinetic energy in reference of bed profile, measurements in 4th run is highlighted.

Additionally, as an important input for implemented models of Van der Zanden, et al.(2017) and Hsu and Liu(2004), near bed turbulent kinetic energy is looked into as well. From Figure 24, near bed turbulent kinetic energy is significantly underestimated by Schnitzler (2015)'s set-up model with a factor 2.5. With a decreasing roller energy dissipation α_{rol} *(Alfaro)*, the maximum near bed cross-shore turbulent kinetic energy increases and is shifted shoreward. In this case, the roller energy dissipation α_{rol} *(Alfaro)* 2 or 4 is preferable.

- **Roller slope parameter**

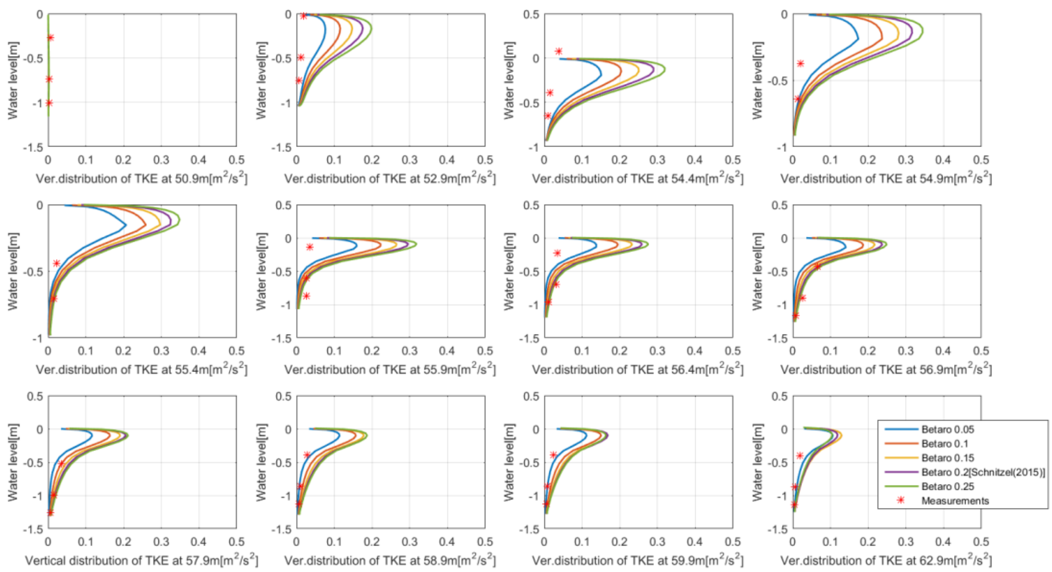

Figure 25 Sensitivity analysis of roller slope parameter effect on vertical turbulent kinetic energy distribution in the water column.

From Figure 25, it is obvious that increasing value of roller slope parameter β_{rol} *(Betaro)* amplifies vertical turbulence distribution in the water column along the entire surf zone. When the roller slope parameter β_{rol} *(Betaro)* comes to 0.2 or 0.25, turbulent kinetic energy from the plunging point to splash point is better modelled (X=55.4 m-57.9 m), while it significantly overestimates turbulent kinetic energy from shoaling region to the plunging point (X=50.9 m-55.4 m) and slightly overestimates turbulent kinetic energy in the inner surf zone (X=58.9 m-62.9 m). In this case, low values of roller slope parameter β_{rol} *(Betaro)* are preferable.

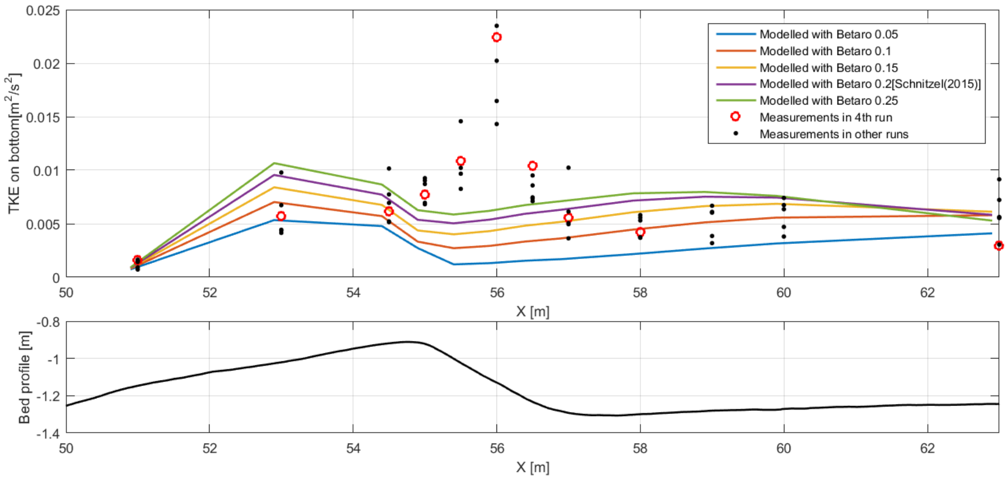

Figure 26 Sensitivity analysis of roller slope parameter effect on near bed turbulent kinetic energy in reference of bed profile, measurements in 4th run is highlighted.

Similarly, according to Figure 26, the increasing value of roller slope parameter β_{rol} *(Betaro)* amplifies the near bed cross-shore turbulent kinetic energy distribution along the entire surf zone. However, a 3 m mismatch between the maximum modelled near bed cross-shore turbulence and measurements is noted. This mismatch is due to the small wave breaking index γ (Gamdis) in Schnitzler (2015)'s set-up model.

- **Wave breaking index**

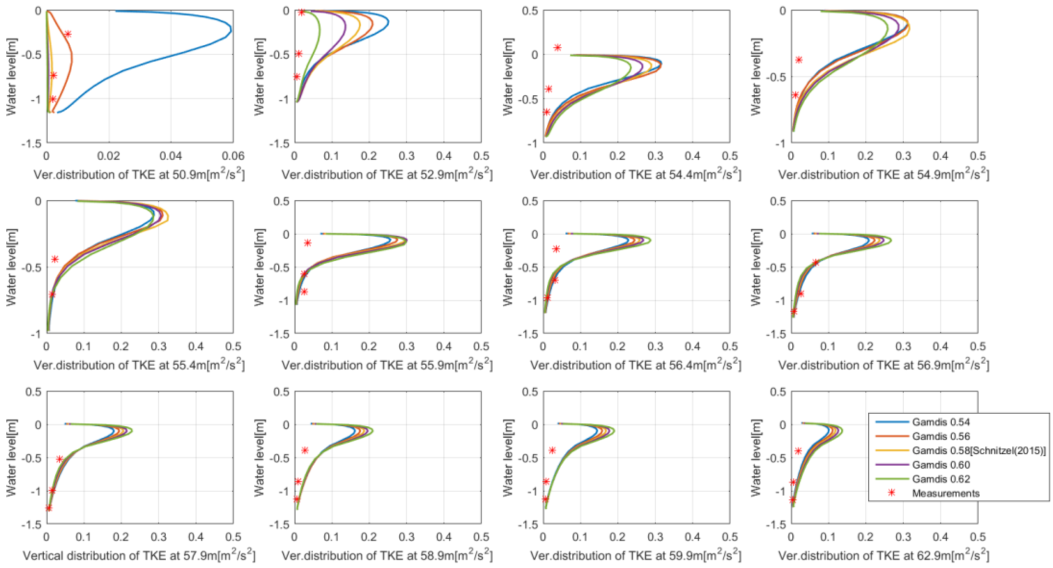

Figure 27 Sensitivity analysis of wave breaking index effect on vertical turbulent kinetic energy distribution in the water column.

As discussed above, the wave breaking index γ *(Gamdis)* significantly controls the cross-shore location of the breaking point. With different values of wave breaking index γ *(Gamdis)*, the cross-shore location of the breaking point is moved shoreward and backward. From Figure 27, it shows that maximum turbulence near the water surface occurs in different water columns when wave breaking index γ *(Gamdis)* is different. In the breaking and inner surf region (X=52.9 m-62.9 m), the turbulent kinetic energy near the water surface is overestimated anyway. Therefore, the wave breaking index γ *(Gamdis)* has limited effects on vertical turbulence profiles in the water column.

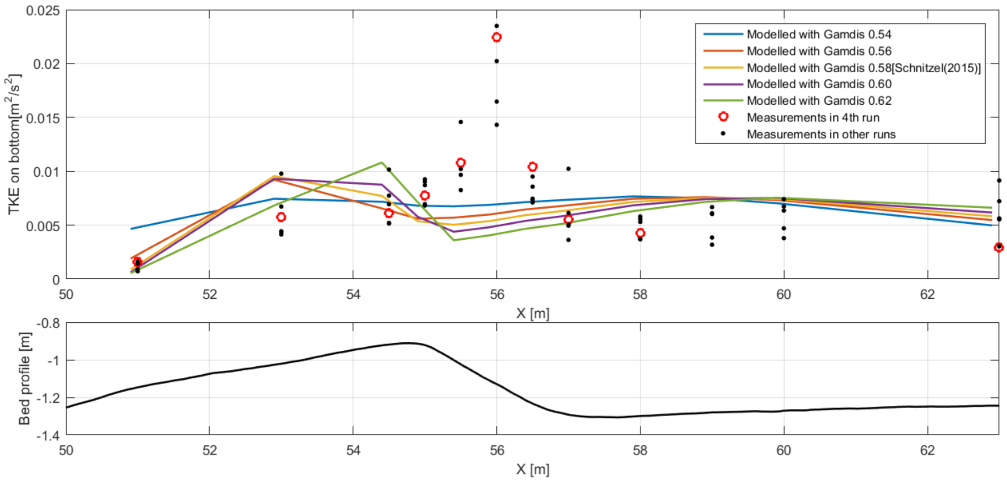

Figure 28 Sensitivity analysis of wave breaking index effect on near bed TKE in reference of bed profile, measurements in 4th run is highlighted.

Apparently, the wave breaking index *γ (Gamdis)* significantly influences the location of the maximum near bed cross-shore turbulence. When the wave breaking index *γ (Gamdis)* is 0.62, the mismatch between measurements and predictions is improved. In this case, a larger value of wave breaking index *γ (Gamdis)* is probably necessary to improve the mismatch.

- **Bottom friction**

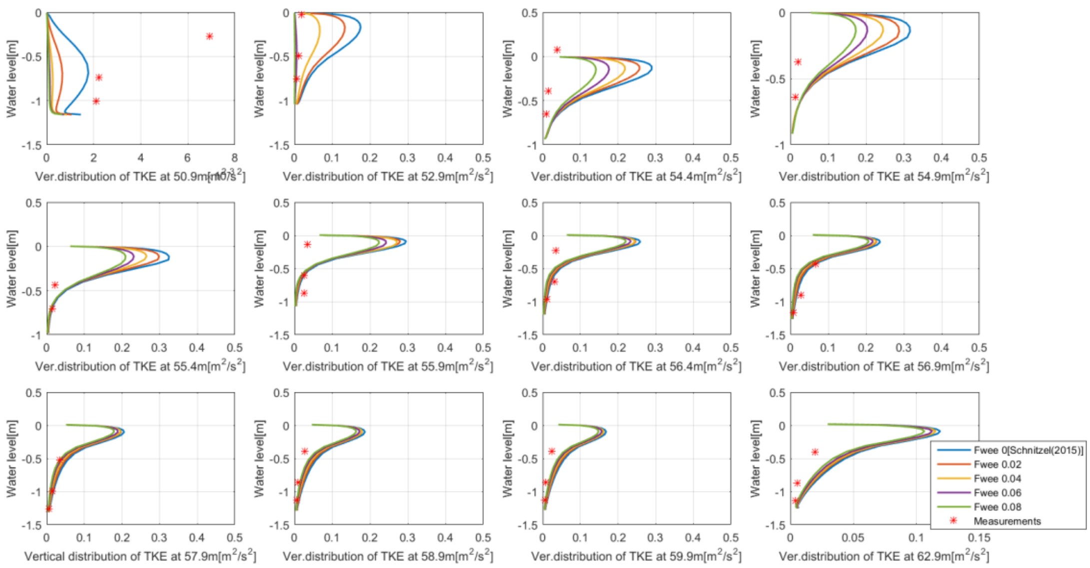

Figure 29 Sensitivity analysis of bottom friction effect on vertical TKE distribution in the water column.

In Figure 29, with increasing bottom friction, turbulent kinetic energy in the water column decreases along the entire surf zone, especially in shoaling region and the breaking region. According to Equation (2-2), more short wave energy is transferred to heat due to bottom friction, the less turbulence is produced. In this case, bottom friction significantly decreases turbulence near the water surface from shoaling region to the plunging point (X=52.9 m-55.4 m), while it has limited effects from plunging point to the inner surf zone (X=55.9 m-62.9 m). Considering the turbulent kinetic energy is overestimated near the water surface, the larger value of bottom friction is preferable in this case.

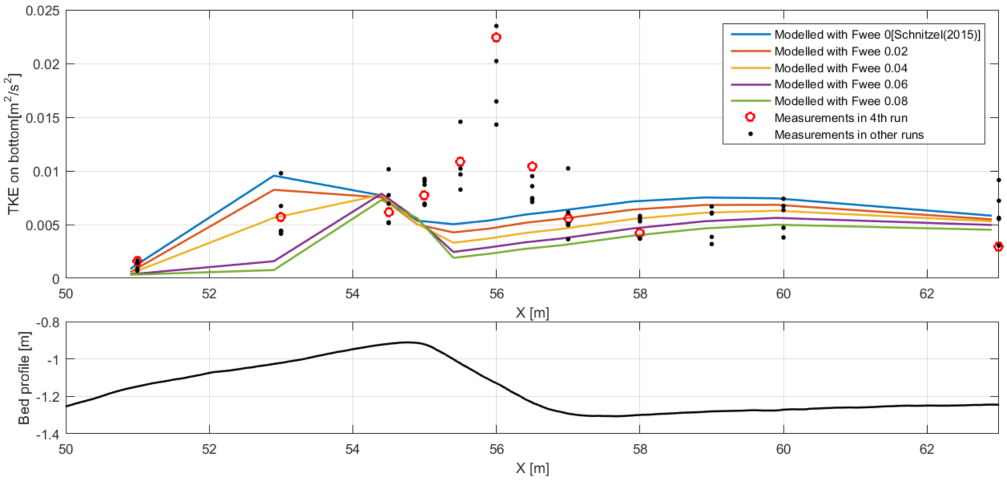

Figure 30 Sensitivity analysis of bottom friction effect on near bed turbulent kinetic energy in reference of bed profile, measurements in 4th run is highlighted.

From Figure 30, the bottom friction decreases near bed turbulent kinetic energy along the entire surf zone. Additionally, the maximum near bed cross-shore turbulence is shifted shoreward by 1.5 m. Taking the cross-shore mismatch between measurements and predictions into account, bottom friction 0.04 is preferable in this case.

- **Breaker delay parameter**

According to Walstra *et al.*(2012), the breaker delay parameter λ barely has effect on the turbulent kinetic energy. Therefore, the sensitivity analysis of turbulent kinetic energy in terms of breaker delay parameter λ is shown in Appendix C for reference and not discussed here.

4.3.4. Summary of the re-calibration

In summary, the preferable parameter settings are listed in the Table 16.

Table 16 Preferable values in terms of five user input parameters for hydrodynamic model calibration

User input parameters	α_{rol}	β_{rol}	γ	f_w	λ
Wave height	6	N/A	0.62	0	N/A
Undertow	6-10	0.2-0.25	0.54-0.58	0	2-10
Turbulence	2-4	0.05-0.1	N/A	0.04	N/A
Near bed turbulence	2-4	0.2-0.25	0.62	0.04	N/A
Re-calibrated values	6	0.25	0.62	0	2

In this re-calibration, the model was locally optimized based on one of five variables. It is very difficult to guarantee the optimized combination of five parameters agrees with global optimization. Therefore, re-calibrated parameters are empirically selected on the basis of Table 16, in order to obtain a better hydrodynamic prediction.

In terms of roller energy dissipation α_{rol} *(Alfaro)*, larger values are beneficial for predicting wave height and undertow, while smaller values improve the overestimation of vertical turbulence profile in the water column and the mismatch between the maximum near bed cross-shore turbulence and measurements. Therefore, value 6 was selected to achieve a balance between wave height, undertow and turbulence. In terms of the roller slope parameter β_{rol} *(Betaro)*, only the vertical turbulence profile in the water column prefers smaller values of β_{rol}. Considering the turbulence near the water surface is overestimated anyway, in order to better predict undertow and near bed turbulence, a value 0.25 was selected. In terms of wave breaking index γ *(Gamdis)*, it is significantly related to the cross-shore location of the breaking point and has limited effects on undertow. Therefore, a value 0.62 was selected. Regarding the bottom friction, considering the well-predicted wave height and undertow when f_w is 0, bottom friction is set to 0. When the breaker delay parameter is 2, the undertow prediction was already significantly increased in the breaking region and inner surf zone. Therefore, a value 2 of breaker delay parameter was selected for improving undertow prediction.

The re-calibrated results are shown below.

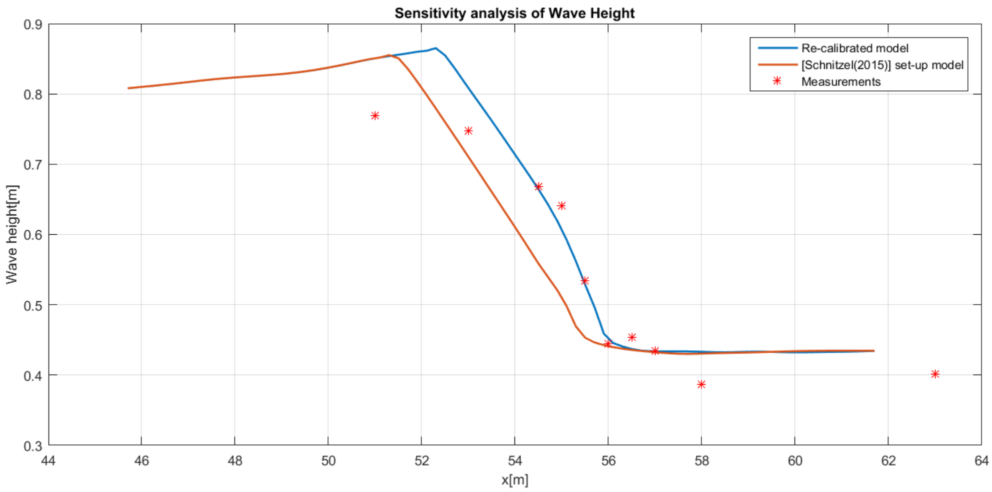

Figure 31 Re-calibrated wave height compared to Schnitzler (2015)'s set-up model.

In Figure 31, the re-calibrated wave height agrees better with measurements in the breaking region, with a slightly higher wave height at the breaking point (X=54 m-57 m). Both Schnitzler(2015)'s set-up model and re-calibrated model overestimate wave height in the inner surf zone (X=58 m-62 m).

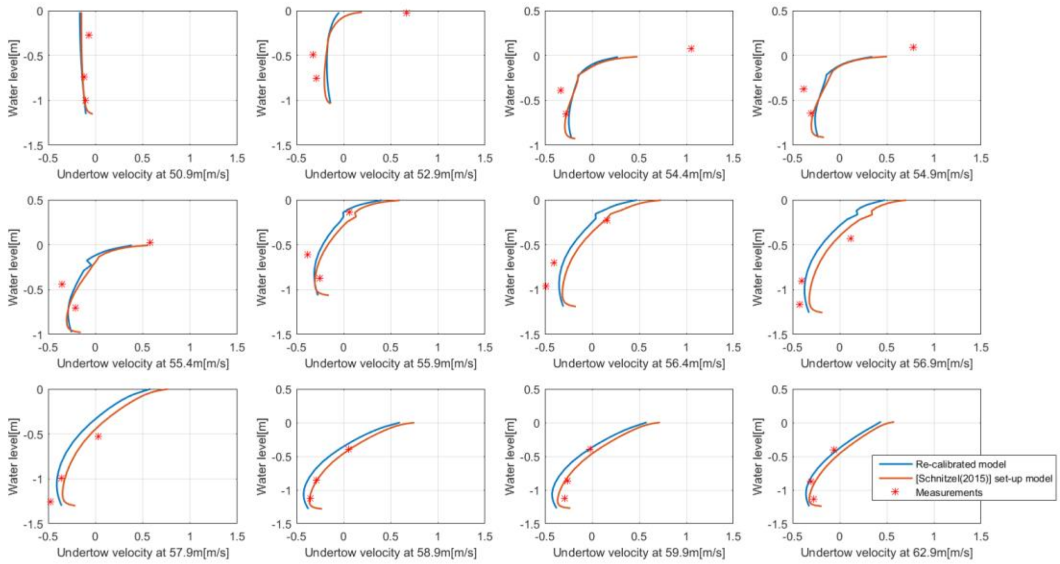

Figure 32 Re-calibrated undertow compared to Schnitzler (2015)'s set-up model.

From Figure 32, the re-calibrated model predicts slightly better than in Schnitzler (2015)'s set-up model, with more evenly distributed undertow profiles in the breaking region (X=54.4 m-56.9 m). However, the re-calibrated model slightly overestimates undertow in the inner surf zone (X=57.9 m-62.9 m). According to the insight in sensitivity analysis of undertow in Section 4.3.2, the large value of *Gamdis* 0.62 worsens the undertow prediction, while large value of roller slope energy β_{rol} *(Betaro)* 0.25 and breaker delay parameter 2 were applied to compensate the effect of large wave breaking index and improve the undertow profile in the water column.

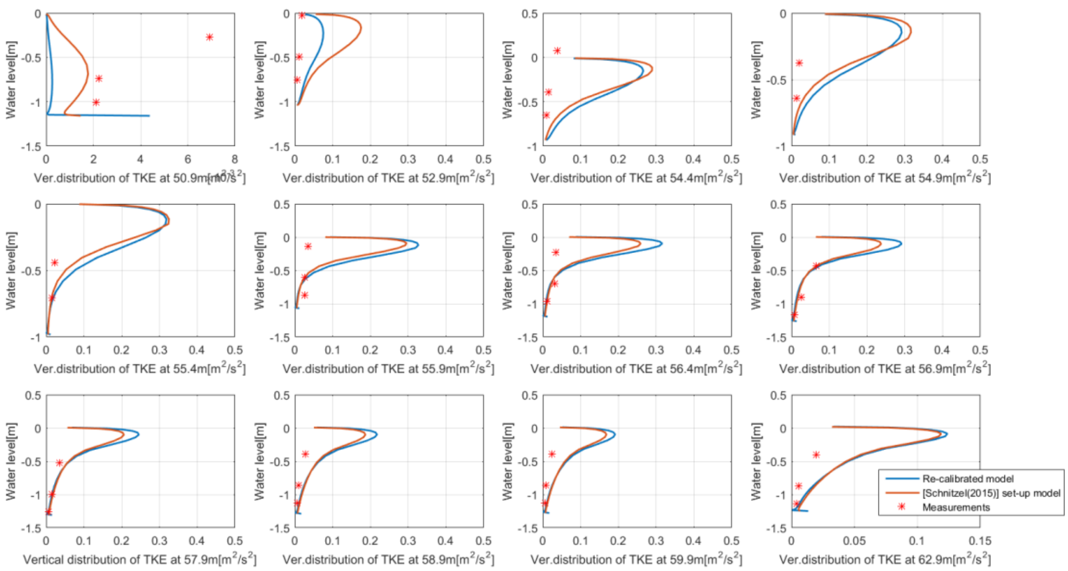

Figure 33 Re-calibrated vertical turbulence profiles in the water column compared to Schnitzler (2015)'s set-up model.

According to sensitivity analysis of turbulent kinetic energy in Section 4.3.3, large value of roller slope parameter β_{rol} *(Betaro)* 0.25 increases the vertical turbulent kinetic energy distribution in the water column along the entire surf zone, especially from the plunging point to splash point (X=55.9 m-57.9 m). Besides, some differences in vertical turbulence profiles in the water column are induced by a different cross-shore location of the breaking point.

It is obvious that the turbulence is significantly overestimated near the water surface and little turbulence injects into the lower half of water column by both models [Schnitzler (2015)'s set-up model and re-calibrated model].

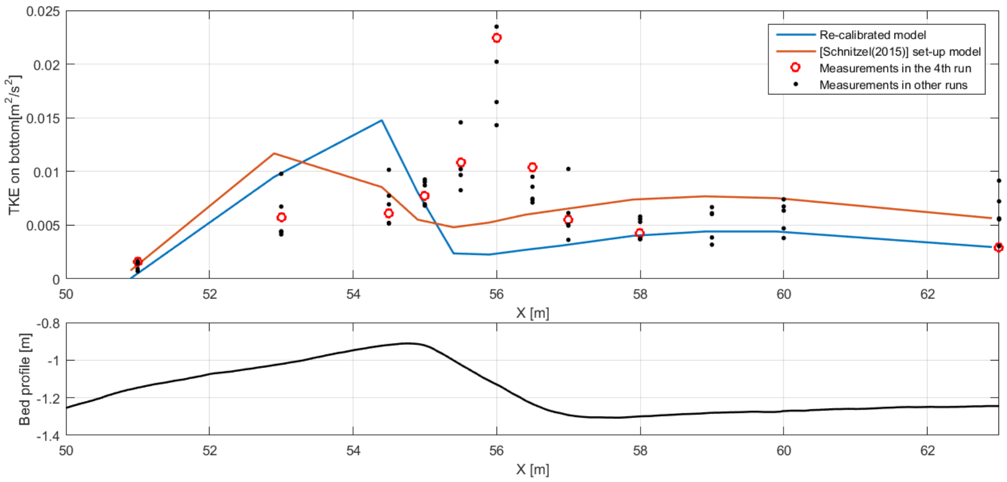

Figure 34 Re-calibrated near bed cross-shore TKE distribution compared to Schnitzler (2015)'s set-up model, the measurements in the 4th run are highlighted.

From Figure 34, the re-calibrated model improves the mismatch between the maximum near bed cross-shore turbulence distribution and measurements. Additionally, the re-calibrated model agrees better with measurements than in Schnitzler (2015)'s set-up model in the inner surf zone.

In conclusion, the wave height was improved by re-calibration, while the undertow prediction is slightly worse than in Schnitzler (2015)'s set-up model to an acceptable extent. The vertical turbulence distribution in the water column, and near bed cross-shore turbulence are poorly modelled due to short injection depth and large production term in Equation (2-17), which will be adapted in the next section.

4.4. Additional adaption for breaking-induced turbulence production

In this section, an additional adaption is applied for regular wave conditions in order to better predict vertical turbulent kinetic energy distribution.

4.4.1. Implementing adaptions

After the sensitivity analysis, the re-calibration of five user input parameters even gives a worse prediction of turbulent kinetic energy. Therefore, besides the recalibration, the surface production formula of breaking induced turbulent kinetic energy [Equation (2-17)] was re-evaluated. It is argued that in the assumption of Walstra et al.(2001), half significant wave height of linear vertical distribution of turbulent kinetic energy might not be sufficient under regular wave conditions. It is explained that turbulence was massively generated beneath the front of the waves, where the plunging jets of the breaking waves inject turbulence deeper into the water column(Brinkkemper, et al., 2014).

The Equation (2-17) is rewritten to,

$$P_k = \frac{0.1D_w}{H_{rms}}\left(1 - \frac{z\prime}{4H_{rms}}\right) \qquad for\ z' \leq 4H_{rms} \tag{4-3}$$

Which assumes that ½ significant wave height linear injection depth of turbulent kinetic energy production is insufficient in this case, replaced with 4 times of significant wave height injection depth. Accordingly, in order to remain the same depth-averaged turbulence in the water column, the factor in front of D_w should be changed to 0.5. Additionally, under regular wave conditions, the factor was changed to 0.1, assuming 80% of turbulence surface production is transformed to heat. The new vertical distribution of surface turbulent kinetic energy production is shown in Figure 35.

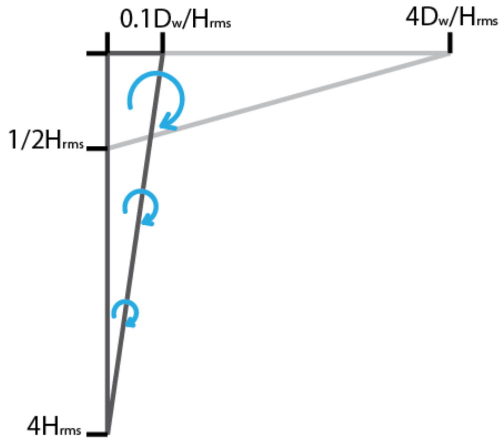

Figure 35 Re-distributed surface turbulent kinetic energy production.

Noticeably, the re-distribution of the injection depth and surface production term was purely data driven.

4.4.2. Results of the additional adaption

In this part, as the adaption does not influence the wave height prediction, it is not shown in this section. According to Equation (2-27), undertow is critical to suspended sediment transport and turbulent kinetic energy is evident for implemented reference concentration models. Therefore, undertow and turbulent kinetic energy are investigated in the case of implementing the additional adaption.

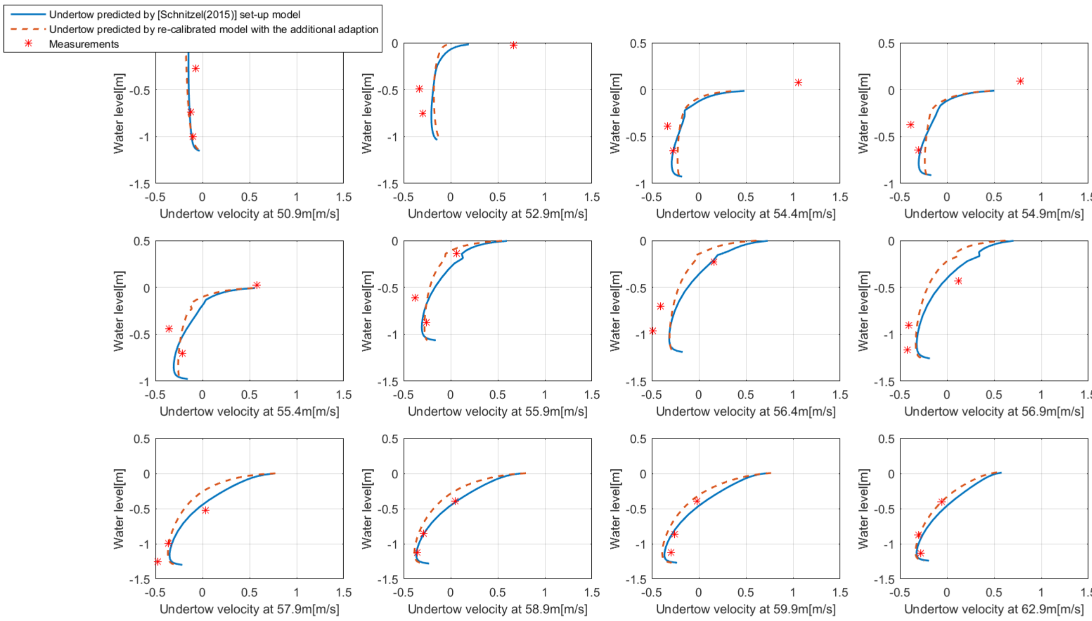

Figure 36 Vertical undertow profiles predicted by re-calibrated model with the additional adaption and Schnitzler (2015)'s set-up model.

From Figure 36, the undertow predicted by adapted model is more evenly distributed in the water column due to the well-mixed turbulence, while it remains the similar near bed offshore-directed current velocity as in Schnitzler (2015)'s set-up model and increases the near surface offshore-directed current velocity (decreasing onshore-directed current velocity near the water surface) in the breaking region and inner surf zone (x= 54.4 m- 62.9 m). In general, in adapted model, predicted undertow is stronger than in Schnitzler (2015)'s set-up model.

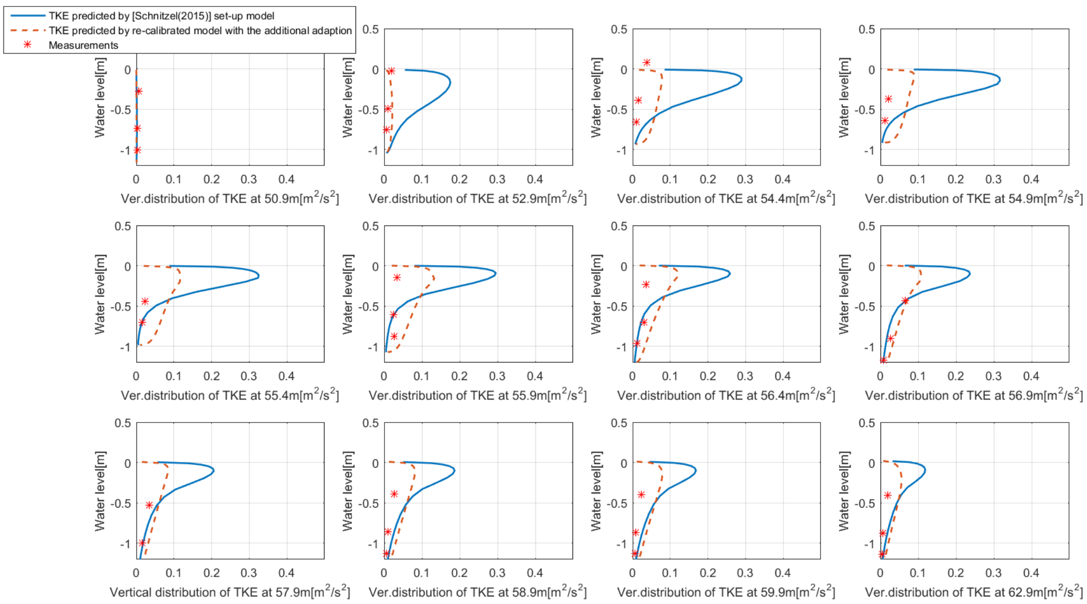

Figure 37 Vertical turbulent kinetic energy profiles in the water column predicted by adapted model and Schnitzler (2015)'s set-up model.

After applying Equation (4-3), turbulent kinetic energy in the water column is more evenly vertically distributed, which means more turbulent kinetic energy is transferred to the bottom. From Figure 37, the vertical turbulent kinetic energy in the water column is significantly improved by the adaption, especially around the plunging point (X=55.9 m-57.9 m). In this region, the near bed turbulent kinetic energy is critical as an input for implemented models. Therefore, it is investigated here as well.

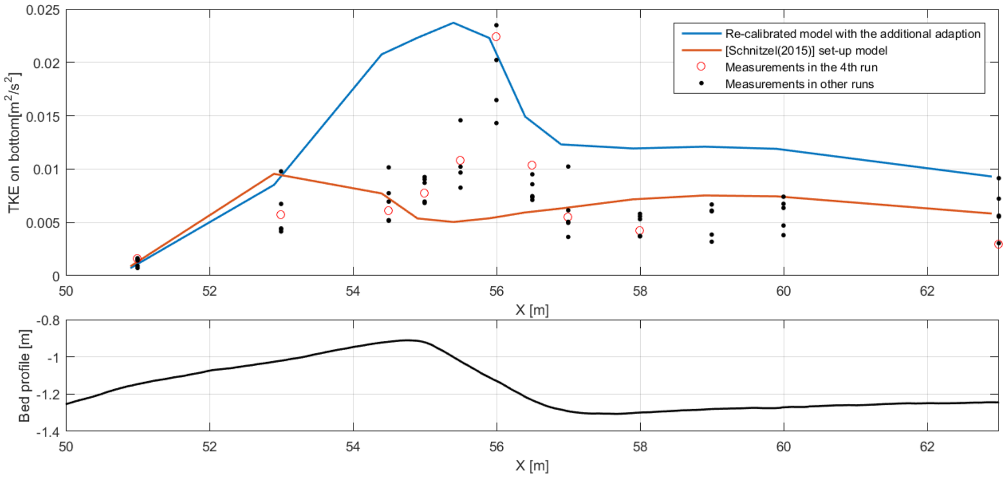

Figure 38 Near bed cross-shore turbulent kinetic energy predicted by adapted model and Schnitzler (2015)'s set-up model.

From Figure 38, the re-calibrated model with the additional adaption significantly improves the near bed turbulence. With the adaption for regular wave conditions, the maximum near-bed cross-shore turbulent kinetic energy has the same order of magnitude with the maximum measurement. Besides, the maximum predicted turbulence is moved shoreward by 2 m relatively to Schnitzler (2015)'s set-up model. Even though, an 1 m offshore mismatch compared to measurements still remains. Based on the insights from the sensitivity analysis in Section 4.3, a re-calibration in terms of the wave breaking index γ *(Gamdis)* was conducted in order to improve the mismatch between the predicted near-bed turbulence and measurements.

4.4.3. 2nd Calibration

As discussed above, the turbulent kinetic energy production is induced by the dissipation of short wave energy. In order to improve the near bed cross-shore turbulence distribution, the waves breaking index γ*(Gamdis)* was tested from 0.62-0.74.

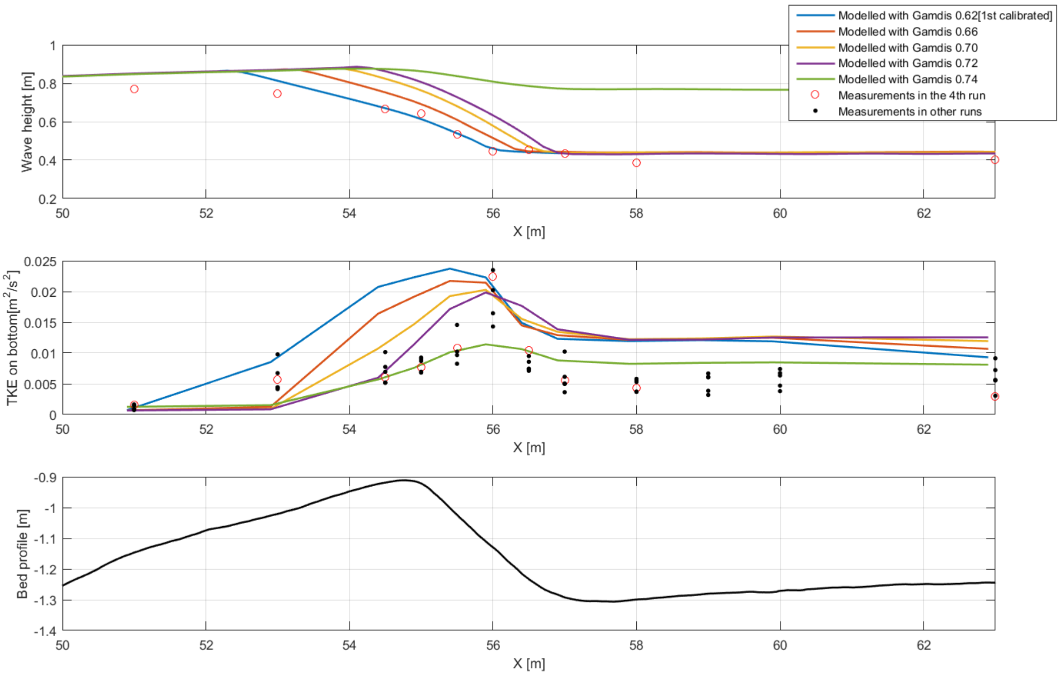

Figure 39 2nd Sensitivity analysis in terms of the wave breaking index (Gamdis) in reference to wave height and bed profiles, measurements in 4th run are highlighted.

According to Equation (4-2), with the increasing wave breaking index γ*(Gamdis)*, the near bed turbulent kinetic energy decreases as less short wave energy dissipates around the plunging point (X=56 m), which can be observed in Figure 39.

From Figure 39, it is obvious that the model with the wave breaking index γ*(Gamdis)* 0.72 gives the best prediction. When the wave breaking index γ*(Gamdis)* is 0.72, the near bed cross-shore turbulent kinetic energy distribution is improved and generally agrees with measurements, except for the overestimation in the inner surf zone (X=58 m-62 m) and slight underestimations in shoaling region (X=50 m-53 m). This underestimation in shoaling region seems to be induced by weak advection and diffusion of turbulence in Delft3D. As waves have not broken yet in shoaling region (X=50 m-53 m), little breaking induced turbulence is generated.

In this case, the accurate wave height prediction was sacrificed for a better near bed cross-shore turbulence prediction. Considering near bed turbulence is the only extra input for two implemented reference concentration models in this case, it was prior to be taken into consideration and re-calibrated. Apparently, when wave breaking index γ*(Gamdis)* comes to 0.74, waves do not break due to the large water depth at the trough of the breaker bar. Without waves' energy dissipation, no turbulence would be produced near the water surface. It indicates the value 0.74 is beyond the upper limit of the wave breaking index.

After the 2nd calibration, the turbulence prediction in Delft3D hydrodynamic model is better, which ensures the generally accurate input for improved reference concentration models.

Beside the near bed turbulence prediction, undertow is evident in current-related suspended sediment transport, as shown in Equation (2-27). Therefore, significant attentions have been paid to effect of this larger wave breaking index *(Gamdis)* on undertow prediction.

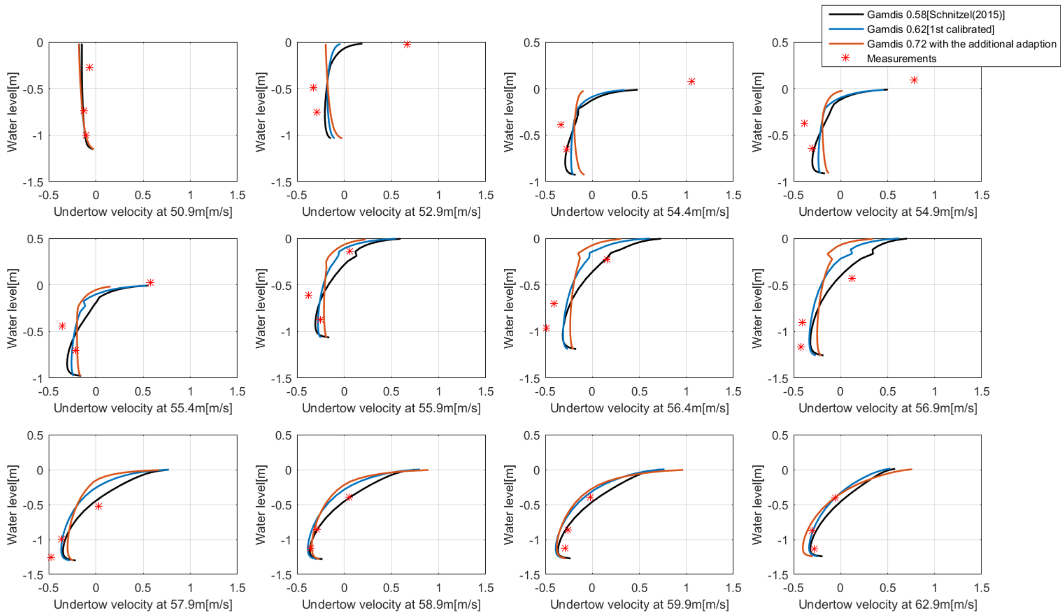

Figure 40 Undertow comparison between Schnitzler(2015)'s set-up model [Black line], adapted model with Gamdis 0.62 [Blue line], adapted model with Gamdis 0.72 [orange line] and measurements [Red dots].

In Figure 40, compared to Schnitzler(2015)'s set-up model, the vertical undertow profile in the water column predicted by adapted model is more evenly distributed, especially in the breaking region (X=54.4 m-57.9 m). It is because of the deeper injection implemented in Equation (4-3), which leads to well-mixed turbulence in the water column around the plunging point (X=55.4 m-56.9 m). However, due to applied breaker delay parameter 2, a slightly stronger undertow is predicted by the adapted model with wave breaking index 0.72 compared to Schnitzler(2015)'s set-up model.

In this case, it is still unclear that how much the worse predicted undertow will influence the suspended sediment transport, which will be discussed in Chapter 5.

4.5. Summary of Delft3d hydrodynamic model validation

In summary, based on the Delft3D model of SINBAD wave flume experiment set-up by Schnitzler(2015), a sensitivity analysis was conducted for hydrodynamics re-calibration. This re-calibration improves the wave height and undertow predictions.

Then, an additional adaption for regular wave conditions was implemented into Delft3D source code, which increases the near surface turbulence injection depth and decreases the near surface turbulence production. With this adaption, the breaking induced turbulent kinetic energy was significantly improved. After the application of the adaption, the large value 0.72 of the wave breaking index was used in order to improve the predicted near bed cross-shore turbulent kinetic energy distribution. Besides, under this circumstance, the undertow profile in the water column is more evenly vertically distributed, which influences the suspended sediment transport discussed in Chapter 5.

Eventually, the calibrated five user input parameters are listed in Table 17.

Table 17 Calibrated five user input parameters in test against SINBAD wave flume experiment.

User input parameters	α_{rol}	β_{rol}	γ	f_w	λ
Re-calibrated values	6	0.2	0.72	0	2

Therefore, the re-calibrated parameters and the additional adaption were applied to the test of implemented reference concentration models against SINBAD wave flume experiment in Delft3D environment. The performances of implemented models in Delft3D environment will be shown in the Chapter 5, with a better predicted turbulent kinetic energy.

Chapter 5 Implementation and validation of new reference concentration models in Delft3D

After the stand-alone tests of existing reference concentration models against the SINBAD measurements, two models were determined to be implemented into Delft3D environment, which are Hsu and Liu(2004)'s adaption combined with default model and Van der Zanden, et al.(2017)'s model. Both of these two models relate reference concentration to breaking induced turbulence kinetic energy, agreeing with the measurements in SINBAD wave flume experiment(Van der Zanden 2016).

5.1. Introduction of Implementation and validation of new models

In this chapter, a general introduction of the implementation and validation of new models is given in Section 5.1.

Then, the simplified wave boundary layer was numerically implemented into Delft3D source code. The simplification and implementation is briefly introduced in Section 5.2 and detailedly documented in Appendix A.

After the implementation, Hsu and Liu(2004)'s adaption combined with default model and Van der Zanden, et al.(2017)'s model were tested against measurements in SINBAD wave flume experiment in terms of suspended sediment concentration and transport in surf zone. In this test, the hydrodynamic validation in Chapter 4 was applied into both models which were tested under the regular wave condition. These tests are discussed in Section 5.3.

In Section 5.4, in order to test the implemented models under irregular wave conditions, LIP 1B case was selected as it shows more similarities with SINBAD wave flume experiment due to strong waves and undertow. Then, the implemented models were tested against measurements in LIP 1B case in terms of suspended sediment concentration and transport. Noticeably, as the Delft3D hydrodynamic validation in Chapter 4 was only developed for regular wave conditions, the tests against LIP 1B case were conducted with default Delft3D hydrodynamic model.

In Section 5.5, the tests against both SINBAD and LIP 1B wave flume experiments are summarized.

5.2. Numerical Implementation

In order to implement these two models into Delft3D, the near bed turbulent kinetic energy was introduced to reference concentration models as an input. As discussed in Section 3.1, both implemented models take a 2 cm wave boundary layer along the entire surf zone into account. Therefore, turbulent kinetic energy at 2 cm above the bed [Boundary layer] was implemented into the Delft3D source code as well.

As discussed above, Delft3D is a process-based numerical modelling system based on time-averaged input and output. For Sigma-layers calculation, the water column is divided into *k (integer)* layers with the bottom layer (the lowest layer) `'kmax'` in vertical direction. In two horizontal directions of x- and y-axis, the spatial step is divide into `'nm'` spatial steps. In each layer, the hydrodynamic and morphodynamic output is depth-averaged. Thus, the turbulent kinetic energy on the boundary layer which is at 2 cm above the bed was simplified to,

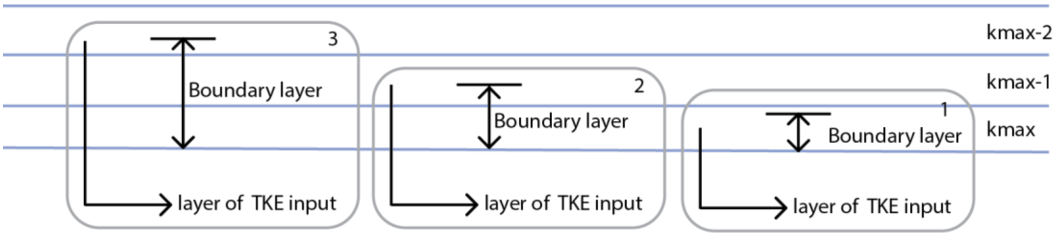

Figure 41 The brief explanation of the implemented conditional judgement in Delft3D source code.

In Figure 41, it assumes that the thickness of lowest three layers are highly possibly thicker than 2 cm of the boundary layer. When the level of 2 cm above the bed is in 'kmax-2' layer, the turbulent kinetic energy generated in this layer would be used as input. Similarly, when it is in 'kmax' or 'kmax-1' layer, turbulence in these layers would be used.

Then, Hsu and Liu(2004)'s adaption combined with default model and Van der Zanden, et al.(2017)'s model are implemented into Delft3D environment. Noticeably, for implementing critical bed shear stress in Van der Zanden, et al.(2017)'s model [Equation (3-59)], the settling velocity for non-cohesive materials in Delft3D environment was used as a input.

5.3. Test against SINBAD wave flume experiment

In this part, results of two implemented reference concentration models are shown and discussed. In this test, the re-calibrated five user input parameters and the additional adaption in Chapter 4 for the regular wave conditions were applied.

5.3.1. Suspended sediment concentration test

Suspended sediment concentration in surf zone is discussed in terms of reference concentration and suspended sediment concentration profiles in the water column

In order to exclude the time dependency of measurements in 6 runs of the experiment, measurements in the 4th run are taken as the representative run and is highlighted as red circles in Figure 42. Regarding the suspended sediment concentration in the water column, only measurements in the 4th run are shown in Figure 43. As the modelled reference level in both implemented models is same as in default model, Hsu and Liu(2004)'s adaption, Van der Zanden, et al.(2017)'s model and measurements are compared to each other in one figure.

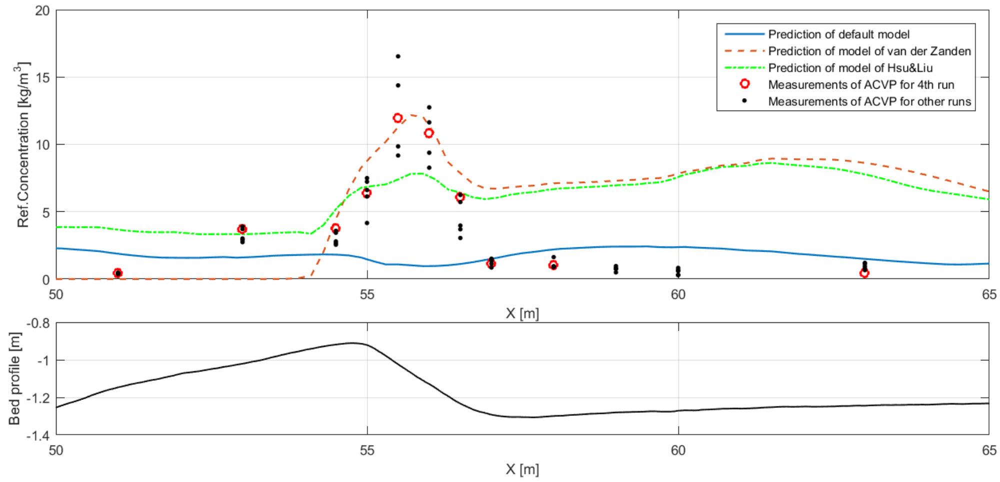

Figure 42 Reference concentration predicted by default model [Blue solid], Hsu & Liu(2004)'s adaption combined with default mode [Green dash lines], Van der Zanden, et al.(2017)'s model [Orange dash lines] and measurements of ACVP at reference level [Black dots], measurements in 4th run are highlighted [Red circles].

Beside the reference concentration, the suspended sediment concentration profile in the water column is shown and looked into in Figure 43.

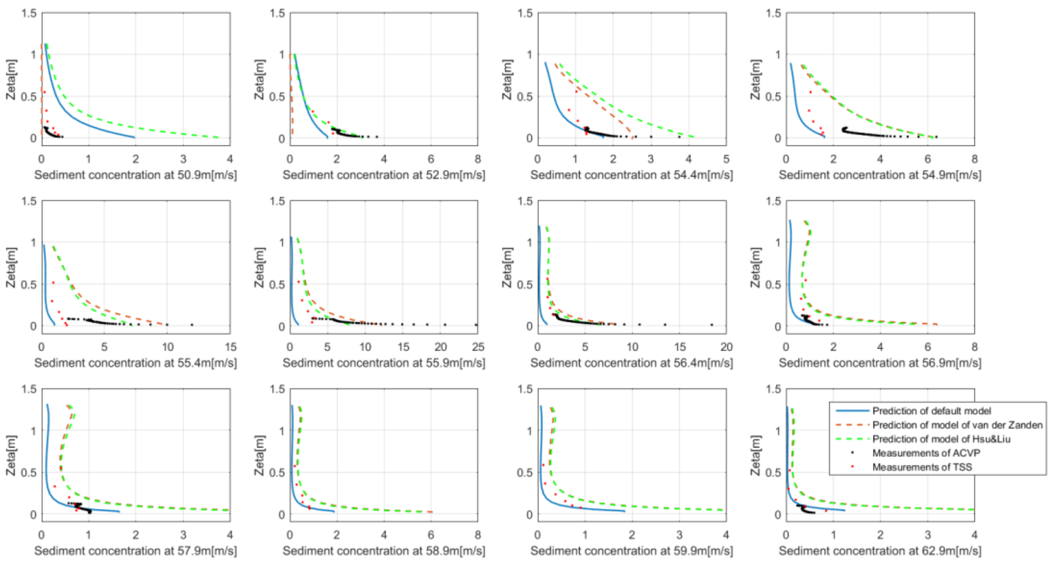

Figure 43 Suspended sediment concentration in water columns predicted by default model [Blue solid], Hsu & Liu(2004)'s adaption combined with default mode [Green dash lines], Van der Zanden, et al.(2017)'s model [Orange dash lines], measurements of ACVP in 4th run [Black dots] and measurements of TSS in 4th run[Red dots].

From Figure 43, near-bed measurements of ACVP in 4th run generally agrees with measurements of TSS in 4th run.

- **Hsu and Liu(2004)'s adaption combined with default model**

In terms of reference concentration in Figure 42, Hsu and Liu(2004)'s adaption combined with default model improves cross-shore reference concentration distribution in the breaking region (X=50 m-57 m), compared to default model. In shoaling region (X=50 m-53 m), the reference concentration is overestimated by Hsu and Liu(2004)'s adaption compared to measurements with a factor of 8, while it is overestimated by default model with a factor of 4. It indicates near bed turbulent kinetic energy increases the reference concentration in non-breaking wave region (X=50 m-53 m). In Hsu and Liu(2004)'s adaption, it is probably due to the near bed turbulence generated by wave orbital velocity and strong undertow, which is a potential risk of double counting combined wave-current effects.

In the breaking region (X=53 m-58 m), the reference concentration is underestimated by Hsu and Liu(2004)'s adaption compared to measurements with a factor of 0.5, while it is significantly underestimated by the default model. The increase of reference concentrations in the breaking region (X=53 m-58 m) is due to implemented breaking induced near bed turbulence, while the underestimation is explained the predicted near bed undertow in the adapted model is slightly weaker than measured undertow due to the well-mixed turbulence. Therefore, the smaller near bed current-velocity plays as an offset for increasing reference concentration due to turbulence.

Moreover, this underestimation in the breaking region is similar to the stand-alone test of Hsu and Liu(2004)'s adaption with Matlab. Considering the near bed turbulent kinetic energy is well modelled, it indicates sediment suspension efficiency coefficient e_k could be re-calibrated against measurements of SINBAD wave flume experiment.

In the inner surf zone (X=58 m-65 m), the adapted model significantly overestimates the reference concentration compared to measurements with a factor of 7. It is explained that massive turbulent kinetic energy is produced in shallow water near the end of the flume and it was advected backward by strong undertow.

In terms of suspended sediment concentration in Figure 43, Hsu and Liu(2004)'s adaption significantly overestimates suspended sediment concentration along the entire water column in shoaling region (X=50.9 m-52.9 m). Noticeably, at the breaking point (X=52.9 m), the predicted suspended sediment concentration profile by adapted model agrees well with measurements accidentally. In the SINBAD wave flume experiment, near-bed suspended sediment concentration is advected backward from high concentration at the plunging point (X=56 m) due to relatively strong measured undertow. However, in Delft3D, advection of sediment concentration are weak as undertow is underestimated by the model in this region. Moreover, as waves have not broken yet in shoaling region, little breaking induced turbulence is produced. The near bed turbulence that increases the predicted reference concentration in the model is probably induced by wave orbital flow and current flow, it explains the accidental agreement between prediction and measurements.

Around the breaking point in the model (X=54.4 m), the adapted model overestimates the concentration profiles with the increasing breaking induced turbulent kinetic energy. Around the plunging point (X=55.4 m-56.4 m), the near bed suspended sediment concentration is modelled well by the adapted model, while the concentration along the entire water column is slightly overestimated by the adapted model. It is induced that near bed measurements of ACVPs are much larger than measurements of TSS, which indicates the near bed suspended sediment concentration is very sensitive to the elevation above the bottom. Besides, the mixing coefficient of suspended sediment concentration can be further validated against measurements of SINBAD wave flume experiment.

In the inner surf zone (X=56.9 m-62.9 m), the adapted model overestimates suspended sediment concentration in the water column. It is due to the mismatch between low measured and high modelled turbulent kinetic energy in this region.

- **Van der Zanden, et al.(2017)'s model**

Regarding the reference concentration in Figure 42, Van der Zanden, et al.(2017)'s model predicts zero reference concentration in shoaling region (X=50 m-53 m), which generally agrees with measurements. With the same input of turbulent kinetic energy as in Hsu and Liu(2004)'s adaption, the predicted zero reference concentration is due to adapted critical bed shear stress in Equation (3-59), as mobilisation strength of the near bed wave- and current-generated turbulent kinetic energy does not exceed the critical bed shear velocity(Van der Zanden 2017).

In breaking region (X=53 m-58 m), Van der Zanden, et al.(2017)'s model significantly improves the predicted reference concentration compared to default model. However, it underestimates the reference concentration compared to measurements with a factor of 0.67. According to Van der Zanden(2017), with the wave-averaged turbulent kinetic energy forcing the model, the distribution of turbulent kinetic energy is negatively skewed, resulting in a significantly lower reference concentration by 15%(Van der Zanden 2017).

In the inner surf zone (X=58 m-65 m), Van der Zanden, et al.(2017)'s model highly overestimates the reference concentration with a factor of 8. Similarly, it is due to massive turbulent kinetic energy produced in shallow water, as explained above.

Regarding the suspended sediment concentration in Figure 43, Van der Zanden, et al.(2017)'s model gives nearly zero suspended sediment concentration in shoaling region (X=50.9 m-52.9 m). Similarly, as little breaking induced turbulence is produced in this region, with weak offshore-directed advection of turbulent kinetic energy due to underestimated undertow in Delft3D, this model underestimates suspended sediment concentration.

With waves start breaking in the breaking region (X=54.9 m-57.9 m), Van der Zanden, et al.(2017)'s model gives the very similar prediction as in Hsu and Liu(2004)'s adaption. Although the near bed turbulent kinetic energy is taken as the only input in Van der Zanden, et al.(2017)'s model, it indicates that the near bed turbulence combined with coefficient 0.3 takes combined wave- and current-related effects into account.

In the inner surf zone (X=58.9 m-62.9 m), Van der Zanden, et al.(2017)'s model significantly overestimates the suspended sediment concentration along the water column as well due to the overestimation of near-bed turbulence in this region.

5.3.2. Suspended sediment transport test

Eventually, the suspended sediment transport is investigated as it is evident for engineering practice. In this case, only current-related suspended sediment transport is shown and discussed in terms of suspended sediment concentrations and undertow predictions on the basis of Equation (2-27).

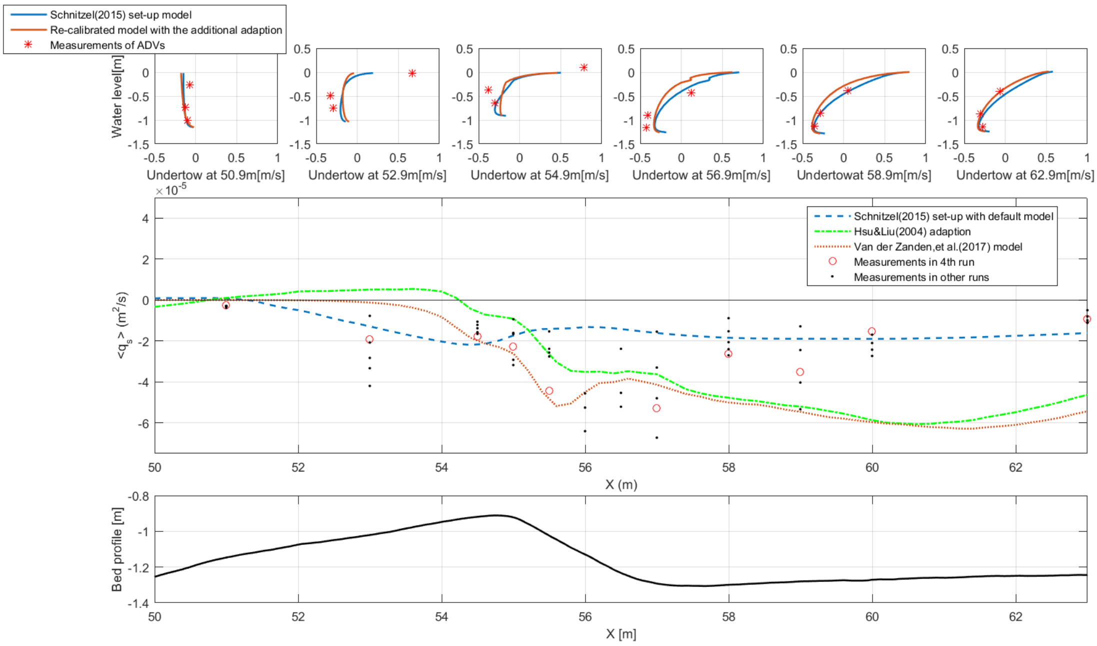

Figure 44 Current-related suspended sediment transport in Schnitzler(2015)'s set-up model [Blue dash line], Van der Zanden, et al.(2017)'s model [Red dash line], Hsu & Liu(2004)'s adaption [Green dash line] and measurements [Black dots]. Measurements in 4th run are highlighted as red circles.

- **Hsu and Liu(2004)'s adaption combined with default model**

According to Figure 44, in shoaling region (X=50 m-52.9 m), Hsu and Liu(2004)'s adaption combined with default model underestimates the current-related suspended sediment transport, especially around the breaking point (X=52.9 m). With the accidentally well modelled suspended sediment concentration, the suspended sediment transport is underestimated due to underestimation of undertow at the breaking point. Noticeably, suspended sediment transport is onshore-directed, indicating onshore current is modelled near the water surface. Around this point, the default model gives a better prediction of suspended load.

Around the breaking point (X=54.9 m-55.4 m), Hsu and Liu(2004)'s adaption reasonably well predicts the offshore suspended load transport due to the overestimated suspended sediment concentration along the water column and the underestimated undertow. The underestimated undertow plays an offset to the suspended concentration overestimation. In this region, the default model gives a slightly better prediction. However, from the plunging point to splash point (X=55.4 m-57.9 m), Hsu and Liu(2004)'s adaption significantly improves, but still underestimates the offshore-directed suspended load transport compared to measurements. In the SINBAD wave flume experiment, strong near bed turbulent kinetic energy stirs up sediment at the trough of the breaker bar. The suspended sediment is brought to the bar crest by the strong undertow in the region, while Delft3D model underestimates near bed undertow, leading to this underestimation.

Around the splash point (X=57.9 m-59 m), the modelled suspended load transport gives overestimations with a factor of 2 because of the overestimated suspended sediment concentration. Behind the splash point (X=59 m-63 m), the suspended load transport was significantly overestimated by Delft3D model due to overestimations of suspended sediment concentration in the inner surf zone.

- **Van der Zanden, et al.(2017)'s model**

In terms of Van der Zanden, et al.(2017)'s model, it gives a similar prediction of suspended load. In shoaling region (X=50 m-52.9 m), the underestimation of predicted suspended sediment transport is due to the zero suspended sediment concentration.

Around the breaking point (X=52.9 m), Van der Zanden, et al.(2017)'s model slightly underestimates the offshore suspended load due to the underestimated undertow in the Delft3D hydrodynamic model along the water column. Similarly, around the plunging point (X=55.4 m-57.9 m), even with the overestimated sediment concentration, the suspended load is significantly underestimated anyway due to the slightly underestimated undertow.

In the inner surf zone (X=57.9 m-63 m), the model overestimates the suspended load transport due to the overestimation of suspended sediment concentration. As discussed above, the overestimated suspended sediment concentration is induced by massive turbulent kinetic energy produced in the shallow water. In this region, undertow is generally well-predicted.

5.4. Test against LIP experiment

In this section, tests of both models [Hsu and Liu(2004)'s and van der Zanden(2017)'s models] were conducted against LIP wave flume experiment in order to investigate whether they could be applied to various experimental conditions or reality. Noticeably, in this test, the re-evaluation of turbulence production [Equation (3-1)] wasn't applied as the large injection depth of turbulence production is only valid under regular wave conditions. Therefore, only two reference concentration models were implemented into Delft3D source code in this case.

5.4.1. Description of LIP experiment

The LIP experiment are detailed measurements of hydrodynamics and morphodynamics in the surf zone (Roelvink, 1995). These experiments were conducted in the 240 m long Delta flume. In this experiment, irregular waves were generated. This study uses LIP cases 1B and 1C, which have already been tested in UNIBEST-TC and Delft3D (J. Van der Werf, et al., 2015). The median sediment size was 220μm. In this experiment, wave heights, wave-averaged and orbital velocities, wave-averaged sediment concentrations and bed profiles were measured.

- **LIP experiment 1B**

LIP 1B is the erosive case, which has a spectral peak period of 5 s and a significant wave height of 1.2 m. In this erosive case, the breaker bar (X=140 m) migrated offshore-ward due to rapid changes of net transport from small onshore rates at the toe of the beach profile to strong offshore transport along the breaker bar(J. Van der Werf, et al., 2015), which is observed in Figure 45.

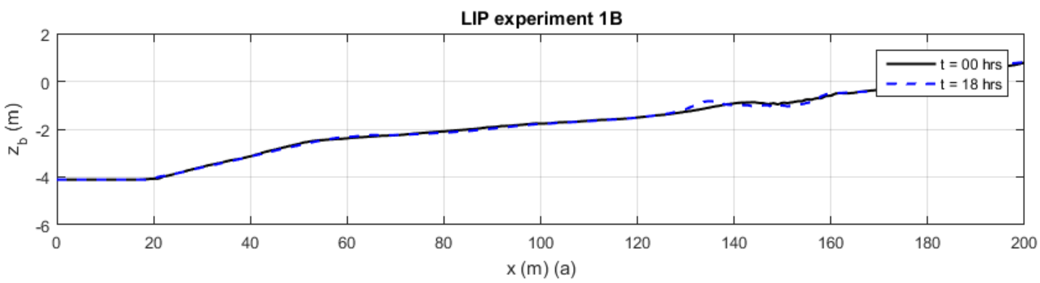

Figure 45 Evolution of bed profile under erosive waves' condition in 18 hours. Taken from J. Van der Werf et al.(2015)

- **LIP experiments 1C**

LIP 1C is the accretive case, which has a spectral peak period of 8 s and a significant wave height of 0.6 m. This mild wave condition generated a shoreward bar migration (X=135 m). The 1C case shows a gradual migration of the breaker bar(J. Van der Werf et al., 2015), which is observed in Figure 46.

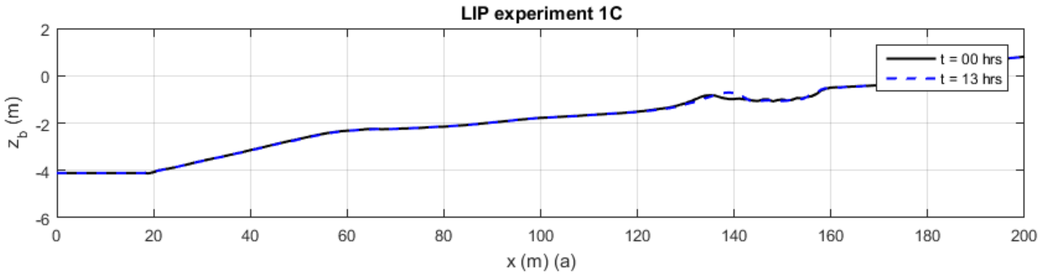

Figure 46 Evolution of bed profile under accretive waves' condition in 13 hours. Taken from J. Van der Werf et al.(2015)

Under this circumstance, in order to test the implemented models in a similar hydrodynamic condition, Iribarren number was calculated according to the wave height, the wave length and the slope of the bed in both SINBAD and LIP wave flume experiments. The Iribarren number is a dimensionless parameter used to model several effects of breaking waves on beaches(Battjes, 1974). It is also known as surf similarity parameter. The Iribarren number is listed in .

Table 18 Similarity comparison between LIP 1B, 1C and SINBAD experiments in terms of Iribarren number.

Experiments	SINBAD	LIP-1B	LIP-1C
Wave height [m]	0.85	1.20	0.60
Wave period [s]	4.00	5.00	8.00
Wave length [m]	24.96	38.99	99.82
Bed slope [-]	0.10	0.07	0.07
Iribarren number ζ_0	0.54	0.38	0.87

According to , the 1B case in LIP wave flume experiment is more similar to the SINBAD wave flume experiment. In LIP 1B case, steeper wave were generated, leading to a strong undertow, breaker bar erosion and offshore migration. In SINBAD wave flume experiment, strong regular waves generated strong undertow and deepened the breaker bar trough.

In order to test the implemented reference concentration models under a similar surf condition [strong waves and undertow], LIP 1B case was selected for testing.

5.4.2. Suspended sediment concentration

As the lowest measuring device of sediment concentration is at 5 cm above the bed, no measured reference concentration could be used. In order to be compared with modelled results, an exponential best fit line was extrapolated on the basis of measured suspended sediment concentrations in the upper water column. The measured reference concentration is extracted from the best fit exponential profile at the reference level, which is approximately at 1 cm above the bed. Therefore, the extrapolated measured reference concentration is not reliable.

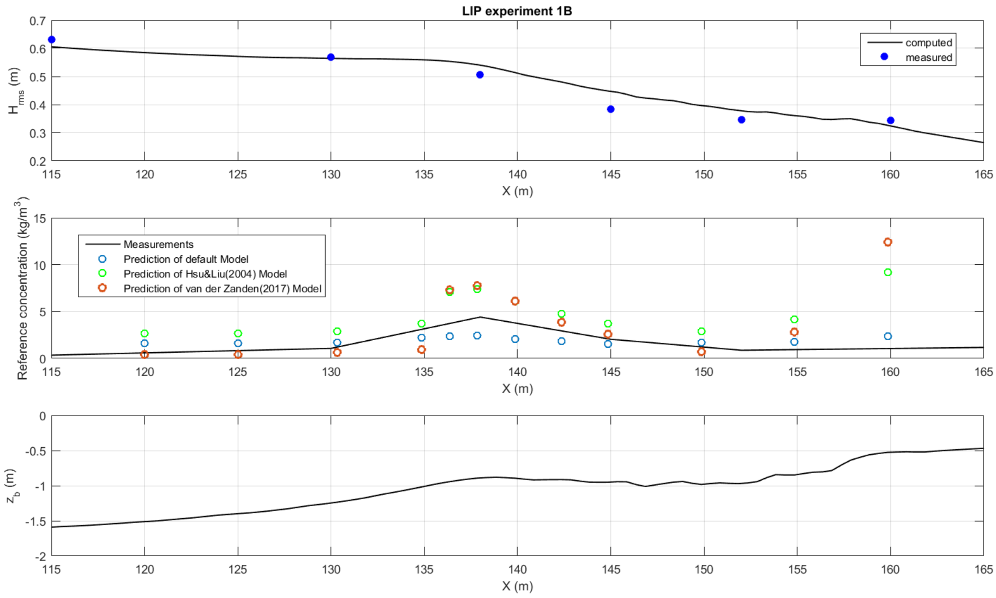

Figure 47 Comparison of measured near bed suspended sand concentration and the near bed suspended sediment concentration modelled by default model, Van der Zanden, et al.(2017) and Hsu & Liu(2004) in reference to the wave height and bed profile.

Different from SINBAD wave flume experiment, LIP wave flume experiment was conducted under the irregular wave conditions. Therefore, waves break along the entire breaking region (X=135m-160m). The modelled reference concentration is shown in Figure 47. Then, offshore directed current velocity and suspended sediment concentration profiles in the water column are shown and discussed in Figure 48. In this test, the hydrodynamic model of LIP 1B case was not re-calibrated and adapted.

In Figure 48, the offshore-directed current velocity is generally modelled well. At X=130 m, the modelled undertow is slightly stronger than measurements along the water column. At the crest of breaker bar (X=138 m), the near bed offshore-directed current is modelled accurately well, while the model slightly underestimates the near surface current. At X=145 m, the model underestimates the near bed offshore-directed current, while it gives accurate predictions in the upper water column. At X=152 m, the near bed offshore-directed current is significantly overestimated by the model.

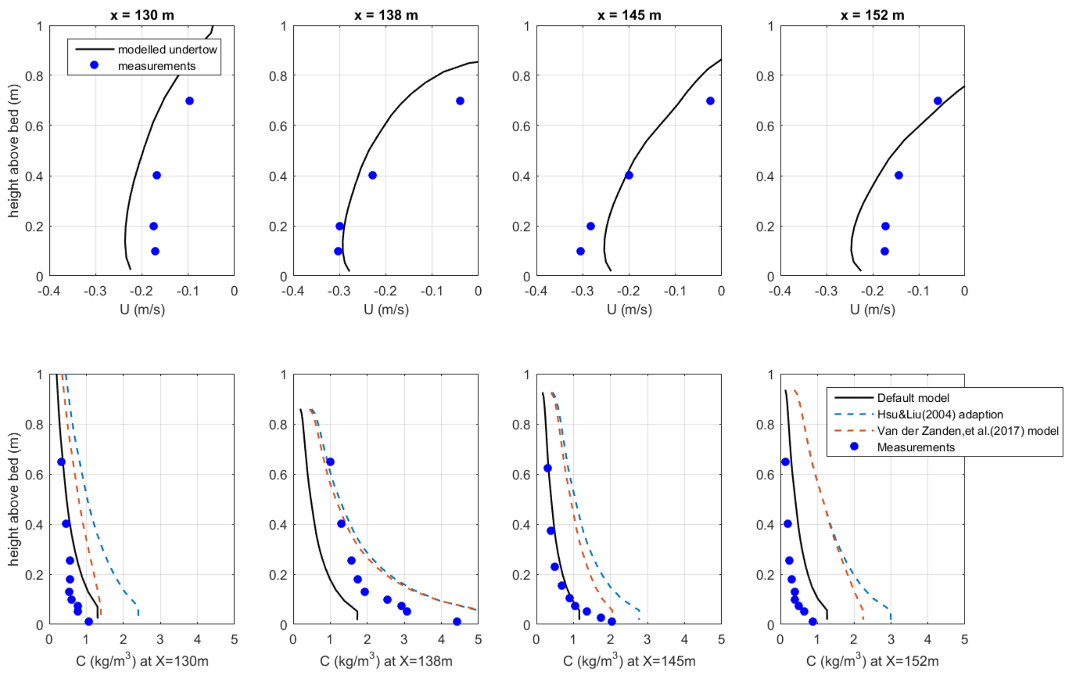

Figure 48 Offshore directed current velocity and suspended sediment concentration profiles at X=130m, 138m, 145m, 152m and 170m. Blue dots are measurements, black solid line is prediction of default model, blue dash line is prediction of Hsu & Liu(2004)'s adaption and red dash line is Van der Zanden(2017)'s model.

- ***Hsu and Liu(2004)'s* adaption combined with default model**

In terms of reference concentration in Figure 47, Hsu and Liu(2004)'s adaption generally gives overestimations along the entire surf zone. From X=120 m to X=130 m, waves have not broken yet and the measured reference concentration is low, while in this region, Hsu and Liu(2004)'s adaption takes the near bed wave- and current-generated turbulence into account, leading to an overestimation of reference concentration compared to the measurements.

Around the first breaker bar (X=130 m-145 m), with breaking induced turbulent kinetic energy produced, Hsu and Liu(2004)'s adaption overestimates the reference concentration along the entire breaking region with a factor of 2. In this test, the cross-shore location of the maximum modelled reference concentration agrees with measurements accurately well.

From X=150 m to X=155 m, Hsu & Liu(2004)'s adaption still overestimates the reference concentration with a factor of 4. Around the secondary breaker bar (X=160 m), another massive production of breaking induced turbulent kinetic energy occurred, resulting in an overestimation of reference concentration with a factor of 10.

In non-breaking region (X=130 m, 145 m and 152 m), the default reference concentration model gives good predictions in non-breaking region, while it underestimates the measured suspended sediment concentration at the breaker bar (X=138 m). Hsu and Liu(2004)'s adaption overestimates the suspended sediment concentration in the entire tested surf zone.

- ***Van der Zanden, et al.(2017)'s* model**

Regarding the reference concentration in Figure 47, from X=120 m to X=130 m, no sand suspension is predicted by the Van der Zanden, et al.(2017)'s model as near-bed wave- and current-generated turbulent kinetic energy does not exceed the critical shear velocity(Van der Zanden 2017).

From X=130 m to X=145 m, the modelled reference concentration increases rapidly, resulting in a similar maximum near-bed reference concentration as in Hsu & Liu(2004)'s adaption.

From X=150 m to X=155 m, the Van der Zanden, et al.(2017)'s model gives a better prediction compared to Hsu and Liu(2004)'s adaption, with slight underestimations and overestimations.

At the secondary breaker bar (X=160 m), the reference concentration is overestimated with a factor of 12.

Regarding the suspended sediment concentration in the water column in Figure 48, Van der Zanden, et al.(2017)'s model gives similar predictions as in Hsu and Liu(2004)'s adaption at the breaker bar. At X=130 m, 145 m and 152 m, Van der Zanden, et al.(2017)'s model improves the near bed suspended sediment concentration compared to Hsu and Liu(2004)'s adaption. It agrees better with the near bed measurements. However, in this region, Van der Zanden, et al.(2017)'s model still overestimates the suspended sediment concentration along the water column, induced by well-mixed sediment concentrations in the upper water column.

In general, both implemented models give similar predictions under the irregular wave condition in the breaking region. Compared to Hsu and Liu(2004)'s adaption, Van der Zanden, et al.(2017)'s model gives a lower modelled results in the non-breaking region. For Hsu and Liu(2004)'s adaption, it might double count the wave- and current-related effects in introduced near bed turbulence, while in Van der Zanden, et al.(2017)'s model, wave-averaged turbulent kinetic energy input tends to underestimate the reference concentration(Van der Zanden, 2017a).

5.4.3. Suspended sediment transport

In LIP 1B case, it's a critical issue that breaking bar was eroded. Therefore, not only the suspended sediment concentration profile, but also the suspended sediment transport is investigated.

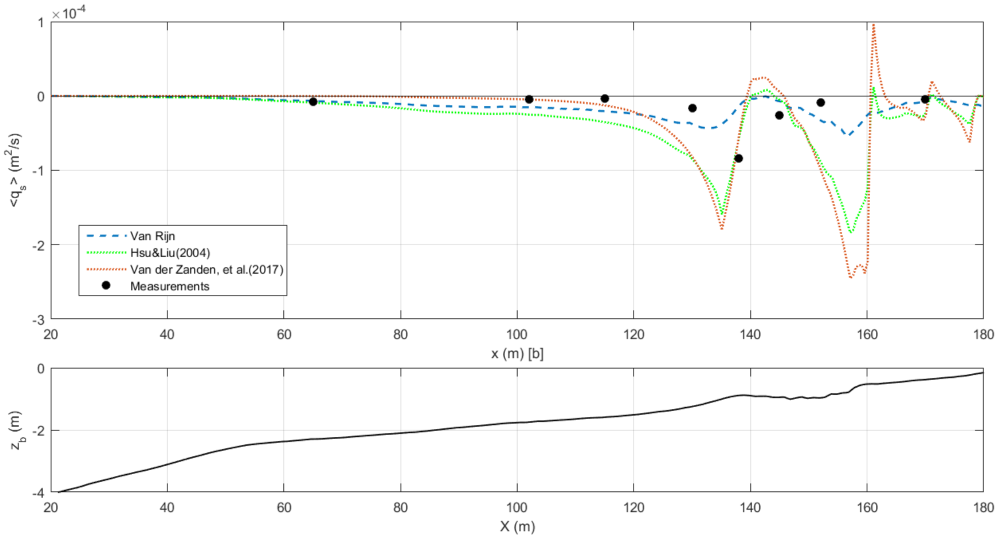

Figure 49 Suspended sediment transport predicted by default model [Blue dash line], Hsu & Liu(2004)'s adaption [Green dash line] and van der Zanden, et al.(2017)'s model [Red dash line].

- **Hsu and Liu(2004)'s adaption combined with default model**

From Figure 49, Hsu and Liu(2004)'s adaption combined with default model overestimates offshore-directed suspended sediment transport generally. Behind the first breaker bar (X=138 m-150 m), the adapted model significantly underestimates the offshore suspended sediment transport due to the underestimated near bed undertow. From X=150 m-160 m, waves broke at a secondary breaker bar, which leads to higher suspended sediment concentrations. Due to the overestimated offshore-directed current velocity in the shallow water, the suspended load is significantly overestimated at the secondary breaker bar.

- **Van der Zanden, et al.(2017)'s model**

Similar to Hsu and Liu(2004)'s adapted model, Van der Zanden, et al.(2017)'s model gives lower predictions of offshore-directed suspended load transport in non-breaking region (X=60 m-130 m) due to lower predicted near bed suspended sediment concentration. However, in breaking regions (X=130 m-170 m), this model gives higher overestimations of suspended load transport compare to Hsu and Liu(2004)'s adapted model. It is because the model is more sensitive to breaking induced turbulent kinetic energy than Hsu and Liu(2004)'s adapted model.

Noticeably, an onshore-directed suspended load occurs at X=145 m. It is probably explained that the strong near bed undertow generates a circulation flow at the lee side of the first breaker bar, resulting in onshore-directed suspended sediment transport.

5.5. Summary of tests against SINBAD and LIP wave flume experiments

In the test against SINBAD wave flume experiment, with the additional adaption in re-calibrated hydrodynamic model of SINBAD experiment, the reference concentration is significantly improved by both implemented models in the breaking region. *Van der Zanden, et al.(2017)'s* model gives a slightly better prediction of reference concentration in breaking region. However, both model highly overestimates the reference concentration in the inner surf zone as massive turbulent kinetic energy is produced in shallow water and advected backward by strong undertow.

In terms of offshore-directed suspended sediment transport, two implemented models improve the order of magnitude of predicted suspended load compared to default model. *Van der Zanden, et al.(2017)'s* model gives a higher prediction of suspended load in the breaking region due to a higher predicted suspended sediment concentration. Both models fail to predict the high suspended load around the splash point due to underestimated near bed undertow.

Regarding the test against LIP wave flume experiment, LIP 1B case was selected as it shows more similarities to SINBAD experiment. Both implemented models similarly overestimates the reference concentration at the breaker bar under the irregular wave conditions. In non-breaking region, *Van der Zanden, et al.(2017)'s* model performs better as *Hsu and Liu(2004)'s* adapted model overestimates the reference concentration along the surf zone.

In terms of offshore-directed suspended load in LIP case, both models overestimates the suspended sediment transport in breaking regions. Similarly, near the breaker bar trough, high suspended load was significantly underestimated by both implemented models, probably due to the underestimated near bed undertow as well.

Chapter 6 Discussion

In this chapter, results of the research project are discussed. It addresses four parts, Measurements, Stand-alone tests of existing models, hydrodynamic validation of Delft3D model and implementation and validation of new reference concentration models. The last three parts are corresponding to three research questions.

• Measurements in SINBAD and LIP 1B wave flume experiments

Due to the bed profile evolution in the SINBAD wave flume experiment, the measured reference concentration at the reference level show strong time-dependency. In SINBAD experiment, the near bed suspended sediment concentration is measured by the Acoustic Concentration and Velocity Profiler (ACVP), which is at a fixed level. However, the bed profile was changing, resulting in relative differences between levels of ACVPs and the bottom. As the near bed suspended sediment concentration is very sensitive to the measurement elevation above the bed, this bed profile evolution gives many uncertainties in measured reference concentrations.

Besides, in SINBAD wave flume experiment, the turbulent kinetic energy in the upper water column was only measured by three vertically aligned Acoustic Doppler Velocimeters (ADVs). It also gives many uncertainties in interpolation of turbulent kinetic energy over the water column. In stand-alone test of Steetzel(1993)'s reference concentration model, the depth-averaged turbulent kinetic energy derived from ADV measurements is uncertain.

In LIP 1B wave flume experiment, the near-bed suspended sediment concentration was not measured with a high resolution. The lowest device for measuring suspended sediment concentration was at 5 cm above the bed, which is higher than the typical reference concentration level. Thus, the near-bed measured reference concentration was extrapolated with an exponential profile on the basis of measurements in the upper water column. In this case, 'measured' reference concentrations used for comparison are not very solid.

• Stand-alone tests of existing models

In these stand-alone tests, the thickness of the wave boundary layer is simplified to 2 cm, which excludes the effects of ripples from the plunging point to the inner surf zone. These ripples could have increased the thickness of wave boundary layer, resulting in lower hydrodynamic inputs for tested models.

With testing various existing reference concentration models with Matlab, it is possible that potentially applicable models weren't selected to be implemented into Delft3D environment. In these stand-alone tested models, many empirical parameters were calibrated against various measurements in different experimental conditions. In *Mocke and Smith(1992)*'s model, it relates the reference concentration to the rate between the wave height and the water depth, which also indicates the wave breaking. By calibrating the empirical exponents against SINBAD measurement, it is possible this model could have been implemented into Delft3D. In Spielmann, et al.(2004b)'s reference concentration model, by moving the maximum roller energy dissipation shoreward, this model is applicable as well. Due to the time limitation, this work had not been done in this project.

• Hydrodynamic validation of Delft3D model

In sensitivity analysis in terms of five user input parameters, with the interactive effects of these parameters, only local optimized values were suggested. In order to find the global optimized combination of these five parameters, lots of computations will be necessary. This work had not been done within the project.

In terms of the additional adaption discussed in Section 4.4, the modification of turbulent kinetic energy production term was purely data-driven. It was roughly estimated by trials and errors. Further detailed validation of this modification under regular wave conditions is necessary.

In general, without adaptions in Delft3D source code, it is impossible to obtain accurate wave height, undertow and turbulent kinetic energy predictions at the same time in Delft3D model. When the wave height is well predicted, the maximum near bed turbulent kinetic energy is shifted offshore-ward. When the undertow is well predicted, the turbulent kinetic energy is overestimation along the water column. In this regular wave condition, the undertow prediction was ensured by a large value of the roller slope parameter β and applied breaker delay parameter. Then, by implementing the additional adaption, the turbulent kinetic energy production was improved. However, this adaption also leads to a slightly depth-uniformed undertow prediction in the breaking region.

• Implementation of selected models

In this implementation, turbulent kinetic energy on the boundary layer (2 cm above the bed) should have been taken as input. In this circumstance, an interpolation of turbulent kinetic energy between layers is necessary in order to compute an accurate turbulent kinetic energy input on the boundary layer. As different modules in Delft3D are interactively related, it is difficult to introduce a new global variable into reference concentration model. Therefore, a simplified adaption was implemented and briefly explained in Section 5.1. The detailed implementation is documented in Appendix A. It results in limited uncertainties in predicting reference concentration compared to stand-alone tested models.

In terms of test against LIP wave flume experiment, LIP 1B case was selected for this test due to a similar Iribarren number to SINBAD wave flume experiment. However, according to the classification of breaker types(Battjes, 1974), LIP 1C shares the same type of breaking wave (plunging) with SINBAD wave flume experiment, while LIP 1B case has spilling of breaker type. Due to the time limitation, test against LIP 1C had not been done within this project.

Chapter 7 Conclusions and recommendations

In this chapter, conclusions are drawn on the basis of three research questions mentioned in Chapter 1. Then, recommendations are given.

7.1. Conclusions

RQ 1) With input of SINBAD measurements, how well do existing models predict reference concentrations in the wave breaking region.

In SINBAD wave flume experiment, the time-averaged measurements in terms of suspended sediment concentration, undertow, wave orbital velocity, water depth, wave height and turbulent kinetic energy were used for testing potentially applicable reference concentration models.

With SINBAD measurements input, Van Rijn(2007b)'s model gives reasonably good prediction in non-breaking region, while it underestimates the reference concentration in the breaking region with a factor of 0.5. Nielsen(1986)'s model and Okayasu(2009)'s adaption give poorly predicted reference concentration along the entire surf zone. Mocke & Smith(1992)'s model underestimates the reference concentration in the breaking region and the maximum reference concentration is shifted offshore-ward compared to measurements. Hsu and Liu(2004)'s adaption and Van der Zanden, et al.(2017)'s model introduce turbulent kinetic energy into the calculation of reference concentration, which give well-modelled results in the breaking region. Spielmann, et al.(2004b)'s model significantly underestimates the reference concentration along the entire surf zone. However, after the re-calibration of a non-dimensional coefficient in the model, the order of magnitude of the predicted maximum reference concentration is improved, while the cross-shore reference concentration distribution is shifted offshore-ward. Steetzel(1993)'s model underestimates the reference concentration along the entire surf zone with both Delft3D input and measurements input due to the empirical function of breaking behaviours.

Therefore, it is concluded that Hsu and Liu(2004)'s adaption and Van der Zanden, et al.(2017)'s model are most suitable to be implemented into Delft3D environment, supported by small values of dimensionless Root-Mean-Square-Error [RMSE] or Pearson correlation coefficient. It is concluded that reference concentration models taking turbulence into account work well in the wave breaking region.

RQ 2) How well are the hydrodynamics of regular plunging breaking waves simulated by Delft3D and how could it be improved?

The model of SINBAD wave flume experiment was set-up by Schnitzler(2015). This model gives a slightly offshore shifted wave height prediction, well-modelled undertow and significantly overestimated turbulent kinetic energy near the water surface, while it significantly underestimates the near bed turbulent kinetic energy.

In order to investigate the room for improving Delft3D hydrodynamic model under the regular wave condition, a sensitivity study in terms of wave height, undertow and turbulent kinetic energy was conducted. In this sensitivity study, the cross-shore location of the breaking point is controlled by wave breaking index. The undertow is significantly influenced by roller slope parameter and breaker delay parameter. The turbulent kinetic energy cannot be directly calibrated well under regular wave conditions. Later on, the Delft3D hydrodynamic model was calibrated on the basis of the insights obtained from sensitivity analysis. The wave height was significantly improved by a larger value of wave breaking index and the undertow was slightly improved by breaker delay parameter and roller slope parameter.

After the calibration, the turbulent kinetic energy was still poorly predicted. An additional adaption was implemented into Delft3D source code, which decreases turbulence production near the water surface and increases the turbulence injection depth. With the adaption, the turbulent kinetic energy is significantly improved under regular breaking wave conditions, while the mismatch between the maximum near bed turbulent kinetic energy and measurements remains. In order to improve this mismatch, the breaking point is shifted shoreward by 2 m, sacrificing the well-predicted wave height. At last, the near bed turbulent kinetic energy is well modelled.

RQ 3) To what extent does the implemented reference concentration models into Delft3D contribute to better simulations of suspended sediment concentrations and transport in the surf zone?

With an accurate near bed turbulent kinetic energy input from the Delft3D hydrodynamic model, the reference concentration predicted by the implemented models (Hsu and Liu(2004)'s adaption and Van der Zanden, et al.(2017)'s model) generally agrees with SINBAD measurements. Hsu and Liu(2004)'s adaption underestimates the reference concentration in the breaking region and overestimates it in shoaling region. Van der Zanden, et al.(2017)'s model gives better predictions in shoaling and breaking region. However, both models significantly overestimates the reference concentration in the inner surf zone, due to massive turbulent kinetic energy is produced in shallow water and advected backward by strong undertow.

In terms of suspended sediment transport, both implemented models underestimate the offshore-directed suspended load transport at the breaker bar trough with a factor of 2, which is induced by underestimated near bed undertow.

In test against LIP wave flume experiment, LIP 1B case was selected as it is more similar to SINBAD wave flume experiment in terms of Iribarren number (Surf Similarity Number). Under the irregular wave condition of LIP 1B case, both Hsu and Liu(2004)'s adaption and Van der Zanden, et al.(2017)'s model overestimate the maximum reference concentration at the breaker bar crest with a factor of 2. However, Hsu & Liu(2004)'s adaption overestimates the reference concentration along the entire surf zone, while Van der Zanden, et al.(2017)'s model gives closer predictions in non-breaking region compared to Hsu & Liu(2004)'s adaption. Additionally, both model significantly overestimate the reference concentration at a secondary breaker bar in shallow water.

In this test, the offshore-directed suspended sediment transport is overestimated by both implemented models due to the significantly overestimated reference concentration in the breaking region.

7.2. Recommendations

In this section, recommendations are given in order to further improve the suspended sediment transport modelling.

In stand-alone tests of existing reference concentration models with Matlab, the wave boundary condition can be better modelled in the surf zone, taking the effect of ripples into account. Besides, the Spielmann, et al.(2004b)'s reference concentration model can be further validated by calibrating Delft3D roller model.

As the hydrodynamics in SINBAD wave flume experiment were only detailedly measured near the bottom, the further high-resolution measurements of undertow and turbulent kinetic energy over the water column is recommended to be conducted.

Against this high resolution measured undertow and turbulence, the Delft3D hydrodynamic model can be further calibrated and validated. In this case, the additional adaption in Section 4.4 for regular wave conditions can be further calibrated and justified with this detailedly measured turbulent kinetic energy over the water column. Furthermore, the significantly overestimated turbulent kinetic energy in the shallow water is recommended to be further improved.

In the implementation of new reference concentration models into Delft3D, the interpolation of turbulent kinetic energy on the boundary layer is recommended in order to give more accurate inputs. Moreover, the implemented models can be tested against LIP 1C case, which shares plunging breaker type with SINBAD wave flume experiment under the irregular wave condition.

Reference

Baldock, T. E. *et al.* (1998) 'Cross-shore hydrodynamics within an unsaturated surf zone', *Coastal Engineering*, 34(3–4), pp. 173–196. doi: 10.1016/S0378-3839(98)00017-9.

Battjes, J. A. (1974) 'Surf Similarity', *Coastal Engineering Proceedings*, 1(14). doi: 10.9753/ICCE.V14.%P.

Brinkkemper, J. A. *et al.* (2014) 'Observations of turbulence within the surf and swash zone of a field-scale sandy laboratory beach', *Coastal Engineering*. Elsevier B.V., 113, pp. 62–72. doi: 10.1016/j.coastaleng.2015.07.006.

Deltares (2014) 'Delft3D Flow User Manual-3D/2D modelling suite for integral water solutions', p. 710.

Drake, D. E. and Cacchione, D. A. (1989) 'Estimates of the suspended sediment reference concentration (Ca) and resuspension coefficient (γ0) from near-bottom observations on the California shelf', *Continental Shelf Research*, 9(1), pp. 51–64. doi: 10.1016/0278-4343(89)90082-4.

Engelund, F. and Hansen, E. (1967) 'A monograph on sediment transport in alluvial streams', *Monografia*, p. 65. doi: 10.1007/s13398-014-0173-7.2.

Feddersen, F. and Williams, A. J. (2007) 'Direct Estimation of the Reynolds Stress Vertical Structure in the Nearshore', *Journal of Atmospheric and Oceanic Technology*, 24(1), pp. 102–116. doi: 10.1175/JTECH1953.1.

Giardino, A., Brière, C. D. E. and Van der Werf, J. J. (2011) *Morphological modelling of bar dynamics with Delft3D*.

Henderson, S. M. and Allen, J. S. (2004) 'Nearshore sandbar migration predicted by an eddy-diffusive boundary layer model', *Journal of Geophysical Research C: Oceans*, 109(6), pp. 1–15. doi: 10.1029/2003JC002137.

Hsu, T. and Liu, P. L. F. (2004) 'Toward modeling turbulent suspension of sand in the nearshore', *Journal of Geophysical Research C: Oceans*, 109(6), pp. 1–14. doi: 10.1029/2003JC002240.

Jones, W. and Launder, B. (1972) 'The prediction of laminarization with a two-equation model of turbulence', *International Journal of Heat and Mass Transfer*, 15(2), pp. 301–314. doi: 10.1016/0017-9310(72)90076-2.

Jonsson, I. (1966) 'Wave boundary layers and friction factors', *Coastal Engineering Proceedings*, pp. 127–148. doi: 10.1111/joms.12088.

Lesser, G. R. *et al.* (2004) 'Development and validation of a three-dimensional morphological model', *Coastal Engineering*, 51(8–9), pp. 883–915. doi: 10.1016/j.coastaleng.2004.07.014.

Mocke, G. P. and Smith, G. G. (1992) 'Wave breaker turbulence as a mechanism for sediment suspension', *Coastal Engineering Proceedings*, 1(23).

Nielsen, P. (1986) 'Suspended sediment concentrations under waves', *Coastal Engineering Journal*, 10(1986), pp. 23–31. doi: 10.1016/0378-3839(86)90037-2.

Okayasu, A., Keiichiro, F. and Masahiko, I. (2009) 'EFFECT OF EXTERNAL TURBULENCE ON SEDIMENT PICKUP RATE', *Coastal Engineering*, pp. 4–5.

Phillips, O. M. and Miles, J. W. (1960) 'On the dynamics of unsteady gravity waves of finite amplitude Part 1. The elementary interactions', *Journal of Fluid Mechanics*. Cambridge University Press, 9(2), p. 193. doi: 10.1017/S0022112060001043.

Van Rijn, L. C. (1984) 'Sediment transport: bed load transport.', *Journal of Hydraulic Engineering--ASCE*, 110(10), pp. 1431–1456. doi: 10.1061/(ASCE)0733-9429(1987)113:9(1187).

Van Rijn, L. C. (2007) 'Unified View of Sediment Transport by Currents and Waves. I: Initiation of Motion, Bed Roughness, and Bed-Load Transport', *Journal of Hydraulic Engineering*, 133(6), pp. 649–667. doi: 10.1061/(ASCE)0733-9429(2007)133:6(649).

Van Rijn, L. C. (2007) 'Unified View of Sediment Transport by Currents and Waves. II: Suspended Transport', *Journal of Hydraulic Engineering*, 133(6), pp. 668–689. doi: 10.1061/(ASCE)0733-9429(2007)133:7(776).

Van Rijn, L. C. and Kroon, A. (1992) ‘Sediment transport by currents and waves’, *Coastal Engineering Proceedings*, pp. 2613–2628. doi: 10.9753/icce.v23.%25p.

Van Rijn, L. C. and Wijnberg, K. M. (1996) ‘One-dimensional modelling of individual waves and wave-induced longshore currents in the surf zone’, *Coastal Engineering*, 28(1–4), pp. 121–145. doi: 10.1016/0378-3839(96)00014-2.

Rodi, W. (1984) Turbulence models and their application in hydraulics : a state of the art review. The Netherlands : International Association for Hydraulic Research. Available at: https://ut.on.worldcat.org/search?queryString=no%3A7159107 (Accessed: 12 August 2017).

Roelvink, J. (1995) *LIP 11D delta flume experiments : a dataset for profile model validation*. Rotterdam: WL / Delft Hydraulics.

Schnitzler, B. (2015) *Modeling sand transport under breaking waves*. University of Twente.

Spielmann, K., Astruc, D. and Thual, O. (2004) ‘Analysis of some key parametrizations in a beach profile morphodynamical model’, *Coastal Engineering*, 51(10), pp. 1021–1049. doi: 10.1016/j.coastaleng.2004.07.020.

Steetzel, H. J. (1993) *Cross-shore Tramsport during Storm Surges*. Delft University of Technology.

Stive, M. J. F. (1980) ‘Velocity and pressure field of spilling breakers.’, *Proc. 17th Int. Conf. Coastal Eng.*, pp. 547–566.

Swart, D. H. (1974) ‘Offshore sediment transport and equilibrium beach profiles’, p. 302.

Ting, F. C. K. and Kirby, J. (1995) ‘Dynamics of surf-zone turbulence in a strong plunging breaker’, *Coastal Engineering*, 24(3–4), pp. 177–204. doi: 10.1016/0378-3839(94)00036-W.

Du Toit, C. G. and Sleath, J. F. A. (1981) ‘Velocity measurements close to rippled beds in oscillatory flow’, *Journal of Fluid Mechanics*, 112, pp. 71–96. doi: http://dx.doi.org/10.1017/S002211208100030X.

Walstra, D. J. R. *et al.* (2012) ‘On bar growth and decay during interannual net offshore migration’, *Coastal Engineering*. Elsevier B.V., 60(1), pp. 190–200. doi: 10.1016/j.coastaleng.2011.10.002.

Walstra, D. J. R., Roelvink, J. A. and Groeneweg, J. (2001) ‘Calculation of Wave-Driven Currents in a 3D Mean Flow Model’, *Coastal Engineering*, pp. 1050–1063. doi: 10.1061/40549(276)81.

Van der Werf, J. J. (2013) ‘Review coastal sand transport modelling in Delft3D’.

Van der Werf, J. J. *et al.* (2015) ‘Testing of the New Santoss Transport Formula in the Delft3D Morphological Modeling System’, *Coastal Sediments 2015, At San Diego*, (June), pp. 1–14.

Yoon, H. D. and Cox, D. T. (2012) ‘Cross-shore variation of intermittent sediment suspension and turbulence induced by depth-limited wave breaking’, *Continental Shelf Research*. Elsevier, 47, pp. 93–106. doi: 10.1016/j.csr.2012.07.001.

Van der Zanden, J. (2017a) ‘Inclusion of Wave Breaking Turbulence in Reference Concentration Models’, *Coastal Dynamics*, (188), p. 13.

Van der Zanden, J. (2017b) *Sand Transport Processes in the Surf and Swash Zones*. University of Twente.

List of Tables

List of Figures

Appendix

Appendix A – Implementations in Delft3D source code

In this project, an implementation was conducted in Delft3D source code. The adaptions of source code are introduced in this Appendix.

Within Delft3D source code, the turbulent kinetic energy near the bottom is given by,

$$rtur0(nm, kref, ltur)$$

With the turbulent kinetic energy when `rtur0 = 1` and its dissipation rate when `rtur0 = 2`.

In turbulent kinetic energy in the Delft3D source code, `'kref'` is defined by,

```
thickbt  =  thick(kmax) * h0

thichbt1 =  [thick(kmax-1) + thick(kmax)] * h0
```

The variables `'thickbt'` and `'thickbt1'` are the thicknesses of lowest layer and lowest two layers.

```
If (thichbt>0.02) then

    kref = kmax

elseif (thickbt1>0.02) then

     kref = kmax-1

else

    kref = kmax-2

endif
```

As the reference concentration model of *Van Rijn*(2007b) is modelled with parameters and input of scalars, the turbulent kinetic energy `rtur0(nm,kmax,1)` should be passed through the file *'erosed.f90'* and defined as an array. Then `rtur0(nm,kmax,1)` was passed through '*eqtran.f90*' and '*tram2.f90*' as a scalar in order to be introduced into '*bedbc2004.f90*' to calculate the reference concentration based on the Equation (3-57) in *Hsu & Liu(2004)'s* adaption.

The source code in '*bedbc2004.f90*' is rewritten into,

```
taubcw = alfacw*muc*tauc + muw*tauwav + 0.05_fp*rhowat*rtur0
```

Similarly to *Hsu & Liu(2004)'s* model, *van der Zanden(2017)'s* model introduces TKE into the default model of reference concentration with a different coefficient 0.3. In this case, the effective current- and wave-related bed shear stress is only related to TKE and rewritten in the source code of Delft3D as in Equation (3-58).

```
taubcw = 0.3_fp*rhowat*rtur0
```

Additionally, the critical bed shear stress is rewritten as in Equation (3-59),

```
taucr1 = fpack * fch1 * fclay * rhowat * (4.0_fp*ws0/dstar)**2.0_fp
```

Where '`taucr0`' is recalculated as Equation (3-59). `'fpack'`, `'fch1'` and `'fclay'` is calibration factor for cohesive materials like mud and clay. In the expression above, `'_fp'` is accuracy defined within the model, `'dstar'` is the dimensionless sediment diameter and `'ws0'` is settling velocity for non-cohesive materials(Deltares, 2014),

Where D_s is representative diameter of sediment fraction and ν is kinematic viscosity coefficient of water [m^2/s].

Appendix B – Wave height investigation in non-breaking region

In Appendix B, the wave height predicted by Schnitzler(2015), 1st calibrated model [with 0.62 wave breaking index] and 2nd calibrated model [with 0.72 wave breaking index] were compared to measurements along the entire wave flume in order to see whether the wave height in the offshore region is well predicted.

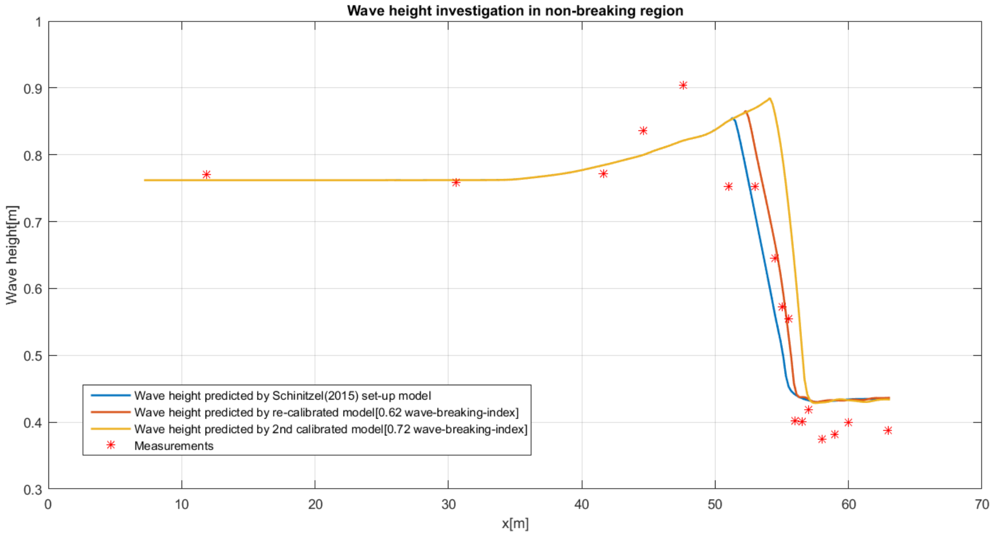

Appendix-Fig 1 Wave height comparison between wave breaking index 0.58, 0.62 and 0.72 along the wave flume, measurements are in 4th SINBAD experimental run.

According to Appendix-Fig 1, different values of the wave breaking index do not influence the wave height prediction in the offshore region. In this circumstance, the measurements in 4th experimental run was used in order to exclude the time-dependency effect. Noticeably, the modelled wave heights at X=44.6 m and X=47.6 m are significantly underestimated compared to measurements. It is probably due to the underestimated wave shoaling effect, which is out of the scope of the project.

In summary, the offshore wave height is reasonably well predicted compared to measurements in 4th SINBAD experimental run.

Appendix C – Effect of wave breaker delay parameter on wave height and turbulent kinetic energy

According to Walstra et al.(2012), the wave breaker delay parameter only influences the undertow prediction in Delft3D hydrodynamic model. Therefore, a sensitivity analysis was conducted in order to see whether the wave height and turbulent kinetic energy predictions could be improved by wave breaker delay parameter. This sensitivity analysis is documented here for reference.

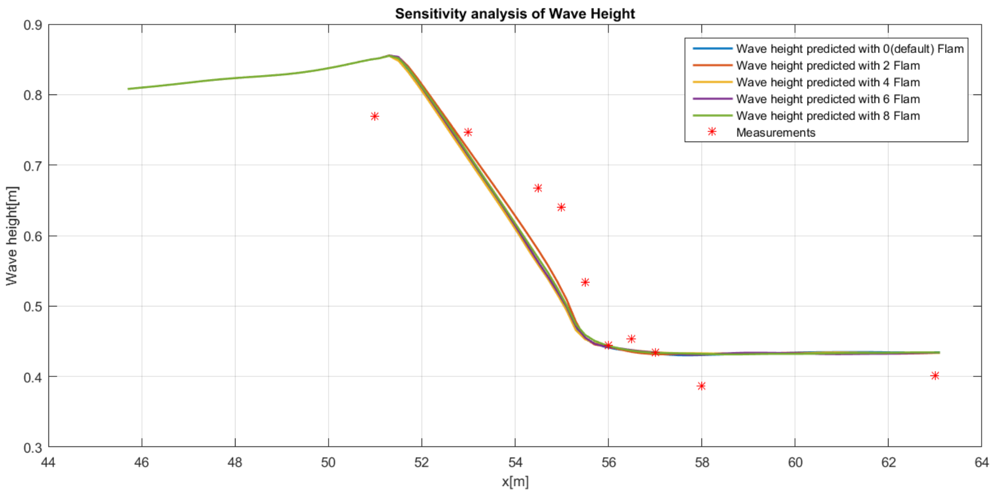

Appendix-Fig 2 Sensitivity analysis of wave breaker delay effect on wave height.

From Appendix-Fig 2, the wave breaker delay parameter hardly has effect on wave height prediction.

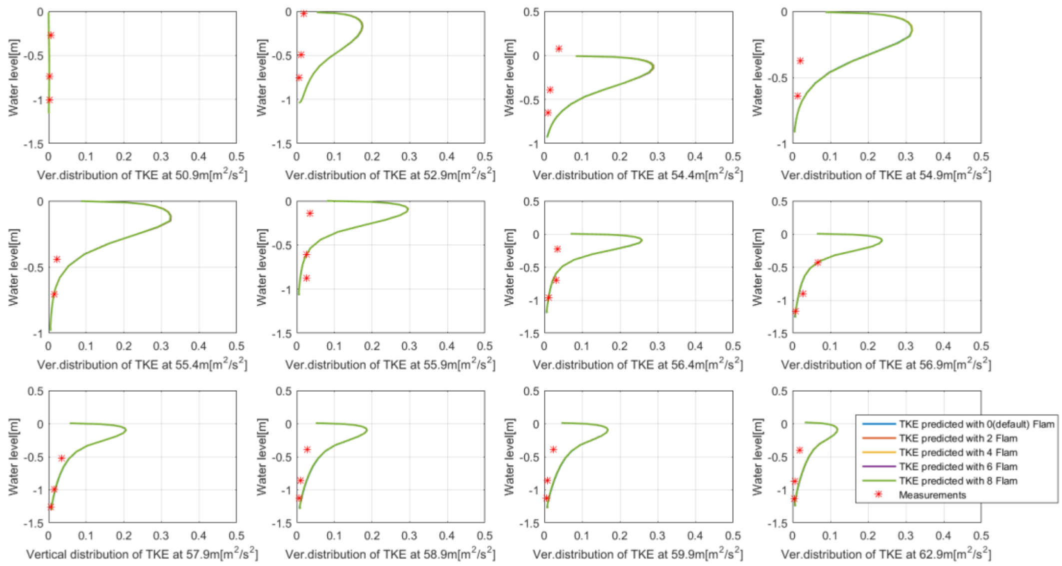

Appendix-Fig 3 Sensitivity analysis of wave breaker delay effect on turbulent kinetic energy distribution in the water column.

Similarly, from Appendix-Fig 3, the wave breaker delay parameter has no effect on turbulent kinetic energy prediction.